Journal of the European Ceramic Society

Bioactivity Enhancement by a Ball Milling Treatment in Novel Bioactive Glass-Hydroxyapatite Composites produced by Spark Plasma Sintering

--Manuscript Draft--

Manuscript Number:	JECESOC-D-22-01944R1
Article Type:	Full Length Article
Keywords:	bioactive glass; Hydroxyapatite; Composites; Ball milling; spark plasma sintering (SPS)
Corresponding Author:	Roberto Orru', PhD University of Cagliari: Universita degli Studi Di Cagliari Cagliari, ITALY
First Author:	Damiano Angioni, PhD student
Order of Authors:	Damiano Angioni, PhD student
	Roberto Orru', PhD
	Giacomo Cao, PhD
	Sebastiano Garroni, PhD
	Devis Bellucci, PhD
	Valeria Cannillo, PhD
Abstract:	Hydroxyapatite (HA) and a lab-made bioactive glass (BGMS10) are combined (50/50 wt.%) in this work, where the effect produced by a ball milling (BM) treatment (0-120 min) prior SPS consolidation on the characteristics of the resulting products is investigated. An extraordinary improvement of the apatite-forming ability during in-vitro test on SPS samples (800°C/70MPa/2min) is obtained using the 30 min BMed mixture. Superior Young's Modulus (122 GPa) and Vickers Hardness (675) were also found compared to unmilled samples (95 GPa and 510, respectively). Microstructural changes induced by BM, with 90 nm HA crystallites size in the bulk composite, and the intimate HA/BGMS10 interfaces established, are the factors mainly responsible for such result. When milling was prolonged to 120 min, samples with relatively lower density, mechanical properties, and in-vitro bioactivity, were produced under the same SPS conditions. The formation of crystalline SiO 2 during SPS might be responsible for such behaviour.

Bioactivity Enhancement by a Ball Milling Treatment in Novel Bioactive Glass-Hydroxyapatite Composites produced by Spark Plasma Sintering

Damiano Angioni[1], Roberto Orrù[1,*], Giacomo Cao[1],
Sebastiano Garroni[2], Devis Bellucci[3], Valeria Cannillo[3]

[1]*Dipartimento di Ingegneria Meccanica, Chimica, e dei Materiali, Unità di Ricerca del Consorzio Interuniversitario Nazionale per la Scienza e Tecnologia dei Materiali (INSTM), Università degli Studi di Cagliari, via Marengo 2, 09123 Cagliari, Italy*

[2]*Dipartimento di Scienze Chimiche, Fisiche, Matematiche e Naturali, Università degli Studi di Sassari, Via Vienna 2, 07100 Sassari,*

[3]*Dipartimento di Ingegneria "Enzo Ferrari", Università di Modena e Reggio Emilia, Via P. Vivarelli 10, 41125 Modena, Italy*

Corresponding author: Roberto Orrù (roberto.orru@unica.it)

Abstract

Hydroxyapatite (HA) and a lab-made bioactive glass (BGMS10) are combined (50/50 wt.%) in this work, where the effect produced by a ball milling (BM) treatment (0-120 min) prior SPS consolidation on the characteristics of the resulting products is investigated. An extraordinary improvement of the apatite-forming ability during in-vitro test on SPS samples (800°C/70MPa/2min) is obtained using the 30 min BMed mixture. Superior Young's Modulus (122 GPa) and Vickers Hardness (675) were also found compared to unmilled samples (95 GPa and 510, respectively). Microstructural changes induced by BM, with 90 nm HA crystallites size in the bulk composite, and the intimate HA/BGMS10 interfaces established, are the factors mainly responsible for such result. When milling was prolonged to 120 min, samples with relatively lower density, mechanical properties, and in-vitro bioactivity, were produced under the same SPS conditions. The formation of crystalline SiO_2 during SPS might be responsible for such behaviour.

Keywords

Bioactive glass; Hydroxyapatite; Composites; Ball milling; Spark Plasma Sintering (SPS)

1. Introduction

The availability of innovative bioceramics able to stimulate the repair of biological tissues, in particular for the treatment of bone defects, represents a current need in regenerative medicine **[1-4]**. To this aim, a useful contribution could be provided by the combination of Hydroxyapatite (HA) with suitable Bioactive Glass (BG) formulations. Due to its similarity to human bone mineral composition, the related biocompatibility and osteoconductivity, HA is the most widely exploited ceramic for orthopaedic applications **[5-7]**. As a drawback, it displays scarce mechanical strength as well as an excessively slow reactivity and interaction with biological fluids and tissues, so that biodegradability and osteoinductivity properties are not adequate for regenerating tissues at the required rate. The latter characteristics could be improved when HA is coupled with bioactive glasses (BGs), which bond tissue to bone more rapidly than other bioceramics **[8-11]**; specific BG compositions are also able to bond to soft tissues. Moreover, molecular biology studies have demonstrated that BGs can stimulate new bone formation, i.e., osteogenesis, through the release in the physiological environment of critical concentration of dissolution products, acting as chemical stimuli which activate the osteoprogenitor cells **[12]**. The higher reactivity of such materials, due to their intrinsic amorphous character, is expected to promote both the bioactivity and the biological responsiveness of the resulting composite material and, in turn, the growth rate of the new natural tissue. The use of glasses can be further exploited to introduce specific ions of biological interest – such as strontium, magnesium, or fluorine – into the HA lattice, in order to mimic the composition of the biological apatite, which is characterized by several ion substitutions **[13,14]**. Finally, the addition of suitable amounts of BG also facilitates the consolidation of HA powders, so that the temperature conditions required to obtain bulk products are correspondingly lowered.

Along this line, several studies reported in the literature have been addressed to the fabrication and characterization of HA-BG composites **[15-27]**. In most of these investigations, the two constituents are homogeneously distributed across the volume **[15-18,20-25,27]**. However, the possibility to combine HA and BG to form Functional Graded

Materials was also explored **[19,26]**. For many years, the main focus of these works was the mechanical improvement of HA through the addition of calcium phosphate glasses **[16]**, which were preferred by virtue of their chemical similarity to HA. Only later, the opportunity of tuning the HA degradation or enhance its bone bonding ability have begun to be investigated, together with the production of porous composites (i.e., scaffolds) for bone tissue regeneration and repair. In this context, silicate glasses (in particular, 45S5 Bioglass®, i.e., the first bioactive glass, whose excellent bioactivity was due to its finely tuned composition) were mostly employed on account of their high bioactivity. In fact, silicon seems to be essential for bone formation, as it favours the adhesion, proliferation, and differentiation of osteoblast-like cells; silicon supplementation is reported to reduce bone fragility and to increase bone mineral density in several animal models **[28,29]**. On the other hand, thermal treatments necessary to sinter and properly densify HA/BG composites may induce the glassy phase to crystallize, thus slowing down, or even inhibiting, both the bioactivity and ion release of the final system **[30]**. For these reasons, in recent years different works have been devoted to the production of new silicate BGs with low tendency to crystallize **[31,32]**; such glasses have been combined with HA to obtain a new generation of ceramic composites, whose biological responsiveness, degradation and mechanical performance can be designed as a function of the given clinical requirement **[20,21]**.

In this contest, the effect produced by a ball milling (BM) treatment of the composite powder mixture on the densification, mechanical and bioactivity behavior of the resulting bulk product is totally unexplored, to the best of our knowledge. BM is a well-known and versatile mechanical treatment route able to induce structural transformations in the processing powders, thus allowing for the synthesis of non-equilibrium phases, the formation of nanostructured alloys, increasing mixture reactivity, degradation of toxic species, etc. **[33]**. The extent of the produced effects depends on the system, the employed devices (planetary ball mills, attritors, etc.), the related operating conditions (rotational speed, milling time, ball to powder or charge ratio, CR, etc.), and it is basically due to the combination of impact and attrition actions involving milling tools and processing powders **[33-36].**

Apart from HA-BG composite systems, the influence of a ball milling treatment on BG or other bioceramics was also barely investigated **[37-39]**. Ibrahim et al. **[37]** examined the effect produced when different milling media made of WC or ZrO_2 were used for the treatment of BG powders (Na_2O-CaO-SiO_2-P_2O_5 system) obtained by melt quenching. Milling was carried out for 18 min using a planetary mill at 500 rpm and negligeable effects were correspondingly noted on the amorphous silica network glass structure. Similarly, no beneficial effects were observed with an increase of the milling time from 20 to 50 h (planetary ball mill, 300 rpm, CR=10, Argon) when processing Ti-HA composite powders, based on SBF (Simulated Body Fluid) assay and wettability test results conducted on the corresponding sintered samples **[38]**.

Sol-gel derived bioactive nanomaterials based on the quaternary MgO-CaO-CuO-SiO_2 system were mechanically processed for 6h at different rotational speeds, in the range 300-500 rpm, using a S100 centrifugal ball mill **[39]**. Bioactivity test results in SBF revealed that apatite formation occurred earlier (after 1 day) when using unmilled powders instead of the milled ones (HA was detected after 3 days). No specific explanation was provided by the authors to justify such negative effect of the mechanical treatment on powder bioactivity.

In this work, the effect produced by a ball milling treatment of HA-BG composite powders on the densification, mechanical, and in vitro biological behaviour is investigated for the very first time in the literature. A mixture consisting of commercial HA and a recently developed Sr- and Mg-containing BG named BGMS10, with low tendency to crystallize **[32,40]**, is first ball milled for different times. The resulting powders are consolidated by Spark Plasma Sintering (SPS) to provide bulk samples to be characterized. Composition, microstructure, mechanical properties, and the bioactivity behaviour in a SBF solution of the sintered composite products are analysed and compared.

2. Materials and methods

2.1 Composite powders

Commercial hydroxyapatite (CAPTAL® Hydroxylapatite, Cod. CAPTAL 60-1, Ca/P ratio equal to 1.67, 99% purity, 99% crystallinity) supplied by Plasma Biotal Ltd. (UK) was selected as one of the composite constituents. The second one is the lab-made BGMS10 bioactive glass with nominal composition (mol%): 2.3% Na_2O, 2.3% K_2O, 25.6% CaO, 10.0% MgO, 10.0% SrO, 2.6% P_2O_5, and 47.2% SiO_2. The glass has been prepared according to a melt-quenching procedure and subsequently ground to obtain powders with grain size < 63 μm, as described elsewhere **[32]**.

50 wt.% HA and 50 wt.% BGMS10 powders (about 16 g total) were mildly mixed in a SPEX 8000 (SPEX CertiPrep, USA) shaker mill using plastic vials and small agata balls (7 mm diam.). The corresponding ball-to-powder weight or charge ratio (CR) was maintained very low, about 0.2. The obtained powders will be considered as unmilled (t_{BM} = 0 min).

Approximately 2.4 g of the latter composite mixture was subsequently mechanically treated at different times (t_{BM}= 30 and 120 min) still using the SPEX 8000 device, but with agata vial and two larger agata balls (12 mm diam.) as milling tools, and by setting a CR value equal to 2.

Particle size distribution was measured using a laser light scattering analyser (CILAS 1180, France).

N_2 sorption isotherms were collected with a Sorptomatic 1990 instrument (Fisons Instruments, Milan, Italy) and the corresponding superficial areas were calculated according to the BET method. 800 mg of each sample were placed in a quartz tube and degassed under mild conditions (100 Pa at 180 °C for 24 h) to prevent any structural evolution. The dead volume of the quartz tube was evaluated through helium adsorption measurements.

Phases identification and structural characteristics of mixed and milled powders were first investigated by X-ray diffraction analysis (Philips PW 1830, Netherlands) using Cu Kα radiation, over a range of scattering angles 2ϑ from 20 to 130, in steps of 0.05° with 15 s acquisition time per angle. The Rietveld method (MAUD program) was used for the

analysis of XRD patterns to determine phases amount and the corresponding microstructural parameters **[41]**.

For TEM observations, a FEI TECNAI 200 operating at 200 kV was used, while samples were prepared by dispersing a few milligrams in absolute ethanol using an ultrasonic bath. Finally, one or two drops of the as-obtained suspension were dispersed on a holey carbon supported grid.

2.2 Bulk composite samples

About 1.56 g of either the unmilled (t_{BM}=0 min) or milled (t_{BM}=30 and 120 min) composite mixture were first placed inside a die cylinder (35 mm external diameter; 15 mm inside diameter; 40 mm height) equipped with two plungers (14.7 mm diameter, 30 mm height), consisting of AT101 graphite (ATAL Srl., Italy). The die was then inserted in the sintering chamber of the SPS equipment (515S model, Fuji Electronic Industrial Co., Ltd., Kanagawa, Japan) which was properly evacuated down to about 20 Pa before electric current application. This apparatus was set to operate with a current sequence of 12 ON pulses followed by 2 OFF pulses, and 3.3 ms as characteristic time of single pulse. Temperature was measured using a K-type thermocouple (TC Misure e Controlli S.R.L., Italy) introduced in a small hole drilled on the external surface of graphite dies, about 1-2 mm far from the processing powders. To make sample release easier after SPS, a graphite foil (0.13 mm thick, Alfa Aesar, Karlsruhe, Germany) was placed between the powders and the inner walls of die/plungers. In addition, thermal losses from the die were limited by covering it with a graphite felt (3 mm thick, Atal s.r.l., Italy).

As reported in Supplementary **Fig. S1**, the temperature was firstly increased at a rate of 50°C/min from the room value to 100°C below the maximum level (T_D). Subsequently, to avoid or reduce possible overshooting problems, the final T_D value was reached at a lower rate (10°C/min). The sample was isothermally heated for 2 min at T_D, then the temperature was decreased at a rate of 50°C/min down to 300°C, followed by a natural cooling step. The applied pressure (P) was suddenly raised to the maximum value in about 1 min, then

maintained constant during the non-isothermal and isothermal heating steps, whereas this parameter was gradually reduced during sample cooling (**Fig. S1**).

Bulk composite samples were produced at different dwell temperature and pressure conditions, in the ranges 750-900°C and 16-70 MPa, respectively. Before their subsequent characterization, the opposite sides of the sintered specimens were accurately ground/polished using abrasive paper to remove residual impurities from the graphite tools. Cylindrical samples with approximately 14.7 mm diameter and 2.5-3 mm height were finally obtained. For the sake of reproducibility, each experimental condition was replicated at least twice.

In what follows, sintered samples to be characterized will be also referred to as t_{BM}/T_D-P, to differentiate them depending on the milling (t_{BM}) and sintering (T_D and P) conditions adopted.

The relative density (ϱ) of bulk samples was determined by the Archimedes' method using ethanol as immersing medium. Sintered disks were weighted using a Ohaus Explorer Pro (Ohaus Corporation, NJ, USA) analytical balance (± 0.0005 g precision). Relative densities were calculated by considering 3.062 g/cm^3 as theoretical value of the composite system, determined by means of a rule of mixture **[42],** and using the values of 3.16 and 2.97 g/cm^3 **[40]** for HA and BGMS10, respectively.

2.3 Microstructural characterization and Mechanical testing

Scanning electron microscopy (ESEM – Quanta 2000, FEI Co., Eindhoven, The Netherlands) was employed to investigate the microstructure of the sintered disks. Additional studies were also conducted using a high-resolution scanning electron microscopy (HR-SEM, mod. S4000, Hitachi, Tokyo, Japan) equipped with a UltraDry EDS detector (Thermo Fisher Scientific, Wal-tham, MA, USA).

The mechanical properties of the samples, embedded into resin and mirror polished, were evaluated by micro-indentation technique. Open Platform equipment, with Vickers indenter tip, (CSM Instruments, Peseux, Switzerland) was employed to measure both the hardness and the Young's modulus of the composites. A load of 500 mN was used during

the indentation process, with 1.5 N/min as loading/unloading rate (loading time at maximum load: 15 s). At least fifteen measurements for each sintered disk were obtained. For each indentation, the load–penetration depth curve was automatically recorded. The elastic modulus was then calculated from the indentation load-unloading curves, according to the Oliver and Pharr method **[43]**.

2.4 *In vitro* bioactivity tests

The bioactivity of the obtained composites was investigated by soaking them in a Simulated Body Fluid solution (SBF), according to the Kokubo protocol **[44]**. Before using it, the pH of the solution was adjusted to 7.4, as recommended **[44]**. Each sample was immersed in 25 ml of SBF and stored in plastic flasks at 37 °C; SBF was refreshed every 48 h. The samples were removed from the solution after 7 and 14 days, carefully washed with distilled water and left to dry at room temperature for 24 h. The possible precipitation of HA on the samples' surface was evaluated by means of both ESEM and micro-Raman spectroscopy. The ESEM was equipped with an Energy Dispersive X-ray microanalysis (INCA, Oxford Instruments, U.K) and used in low-vacuum conditions, i.e. ~0.5 Torr. Raman spectra were acquired by using a LabRAM HR Evolution spectrometer (Horiba, France) with a diode laser source emitting at 632.8 nm (output power: 21 mW at the sample). Photons scattered by each sample were dispersed by a 1800 lines/mm grating monochromator and then collected by on a CCD camera (a 100x objective was employed as collection optic). A spectra collection setup of ten acquisitions, each of them taking 30 s, was used.

3 Results and discussion

3.1 Composite powders

First, it should be specified that, as reported in previous studies, particles of commercial HA powders are relatively coarser (d10, d50, d90, and d43: 8.80, 34.0, 52.0, and 32.7 μm, respectively) **[45]** compared to those ones of the glass constituent (d10, d50, d90, and d43: 0.8, 4.9, 26.2, and 9.4 μm, respectively) **[40]**.

As for the HA-BGMS10 system investigated in this work, the effect produced by the ball milling treatment on particle size of the resulting mixture can be deduced from **Fig. 1**. The corresponding d10, d50, d90, and d43 are reported in supplementary **Table S1**.

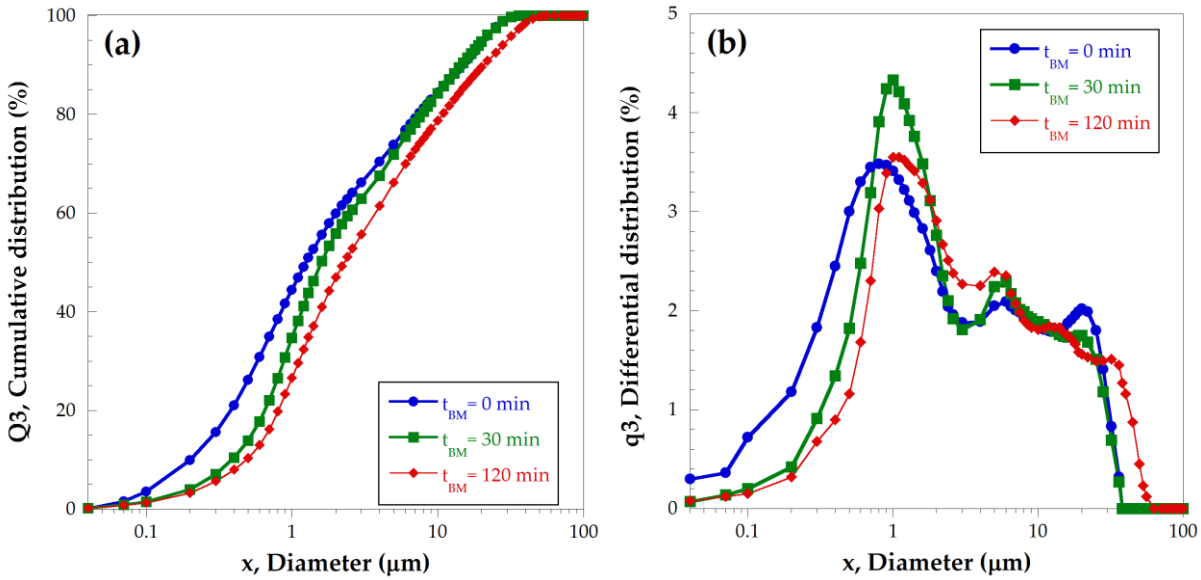

Figure 1 Particles size distribution of unmilled (t_{BM} = 0 min) and milled HA-BGMS10 composite powders: cumulative (a) and differential (b) curves

Both cumulative and differential curves evidence that particles progressively increase their size during milling, to indicate the occurrence of powder agglomeration phenomena. It is likely that the softer HA particles incorporate the glass ones. In addition, the results of this analysis suggest that, when the mechanical treatment is conducted up to 30 min, most of the changes are confined to the lower range of particles size (< 2.5 μm). This is supported by the fact that, the maximum value of the q3 curve at about 1 μm, which represents the higher percent of particles at that size, markedly increases. On the other hands, only small changes in the cumulative and differential curves, compared to the unmilled (t_{BM} = 0 min) mixture, can be observed when considering the larger particles size range. Moreover, the measured average size (d43=4.6 μm) did not vary compared to that of untreated powders (see supplementary **Table S1**).

In contrast, when the milling treatment is prolonged to 2 h, powder agglomeration leads to the formation of coarser particles, as manifested by the shifting of both Q3 and q3 curves on the right side as well as by the decreased intensity of the q3 curve maximum.

Textural properties of the unmilled (t_{BM} = 0 min) and milled (t_{BM} = 30 and 120 min) samples have been then investigated by N_2 physisorption. The isotherms of all the samples are depicted in **Figs. 2(a)-2(c)**. BET (Brunauer, Emmett, Teller) surface areas vary from 5.0 m^2g^{-1} for the unmilled (t_{BM} = 0 min) to 11.7 and 11.1 m^2g^{-1} for the systems milled at 30 and 120 minutes, respectively (see **Table 1**).

Table 1. B.E.T surface area values estimated for the unmilled (t_{BM} = 0 min) and milled (t_{BM} = 30 and 120 min) samples. HA have been measured for comparison.

Sample	**B.E.T Surface Area [m^2g^{-1}]**
HA (commercial)	5.5
t_{BM} = 0 min	5.0
t_{BM} = 30 min	11.7
t_{BM} = 120 min	11.1

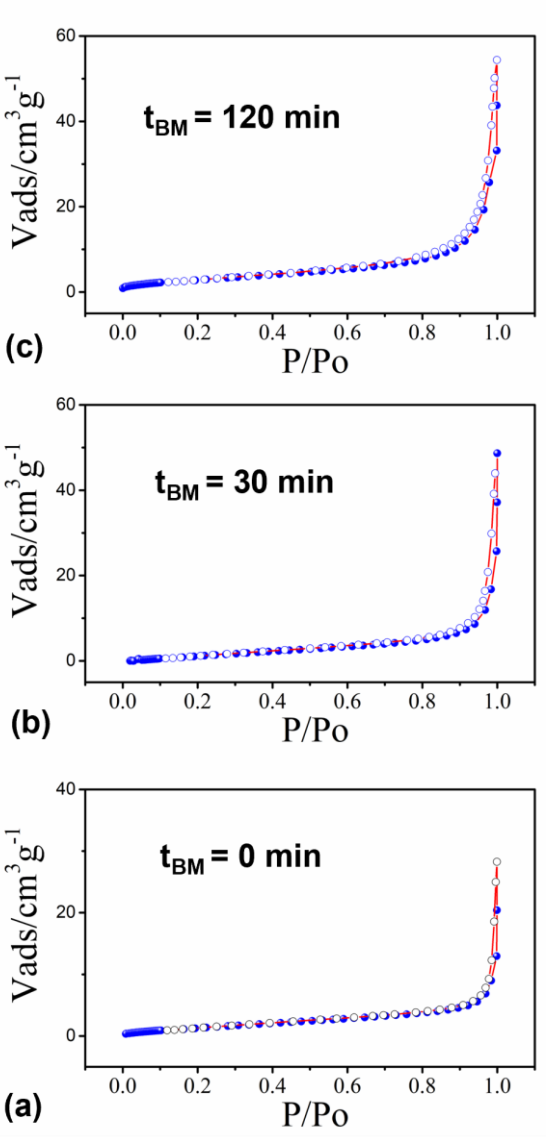

Figure 2. N_2 physisorption isotherms of the (a) unmilled (t_{BM} = 0 min) sample and, milled for 30 (b) and 120 minutes (c) samples.

All the samples show a type II isotherm with a H3 type hysteresis loop typical of macroporous materials. The mechanical processing acts significantly by increasing the specific surface area of the system, thus reaching the maximum value after 30 minutes. The increase of the specific surface area during the first period of milling is the result of the new exposed surfaces correspondingly formed, together with the desorption of physisorbed gases, which typically occlude nanopores. With the extension of the milling treatment, particle fracturing is balanced by the formation of agglomerates, and only minor changes in the specific surface area are observed.

Structural and microstructural characteristics of the three batches of powders are then investigated by XRD analysis (**Fig. 3**).

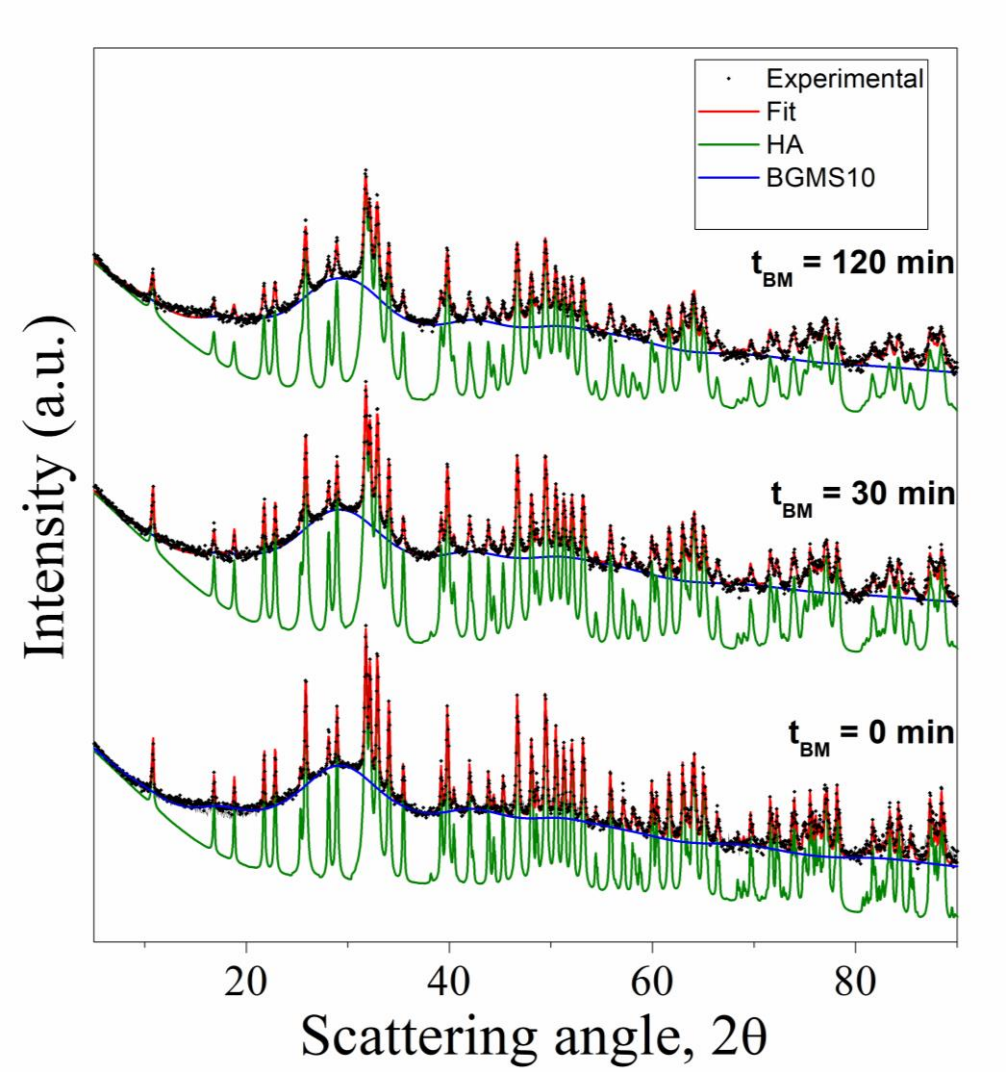

Figure 3. XRD patterns of unmilled (t_{BM} = 0 min) and milled HA-BGMS10 samples. Black dots are experimental data, and the red line is the calculated fit. Deconvoluted amorphous BGMS10 and hydroxyapatite phases are indicated by blue and green full line.

The pattern referred to the unmilled system shows Bragg reflections ascribable to the hydroxyapatite phase (S.G. *P63/m*) together with a typical shape of an amorphous glass related with the BGMS10. The phase, named as $Ca_{1.5}Na_{2.64}Si_9O_3$, has been computed using a pseudo-crystalline structure factor ($Ca_{1.5}Na_{2.64}Si_9O_3$ phase; symmetry: trigonal; space group: R-3 m; crystallite size: 20 Å; microstrain: 0.03) according to the LeBail approach **[46]**.

Relative amount of each phase and microstructural parameters determined by Rietveld refinement, are reported in supplementary **Table S2**. The relative amount of each phase contained in the unmilled (t_{BM} = 0 min) composite (46/54 wt.% - HA/BGMS10) is rather consistent with the initial nominal mixture. This holds also true when considering the milled powders. **Fig. 3** also highlights that the XRD pattern of the sample milled for 30 minutes is still characterized by the halo peak ascribable to the amorphous phase. However, as expected, the hydroxyapatite crystallites size decreased significantly from > 2000 Å to 700 Å (**Table S2**), as a consequence of the mechanical processing. Increasing the milling time up to 120 minutes, both crystalline and amorphous phases are still observed, while the crystallite dimensions of the hydroxyapatite phase further decreased down to 470 Å (**Table S2**). Interestingly, as emerged from the microstructural parameters here estimated, the cell volume associated with the hydroxyapatite phase increases as the milling time was augmented.

The microstructure of unmilled and milled powders was further characterized by TEM. The corresponding images presented in **Fig. 4** suggest that all the three systems analysed are characterized by agglomerates of particles with different shapes which confirms the formation of an intimate mixture already when HA and BGMS10 were just mixed. Crystalline domains decreased, accordingly to the XRD analysis, when the powders were subject to mechanical milling. No new phase emerged both from TEM and XRD characterization, at least up to this stage of milling.

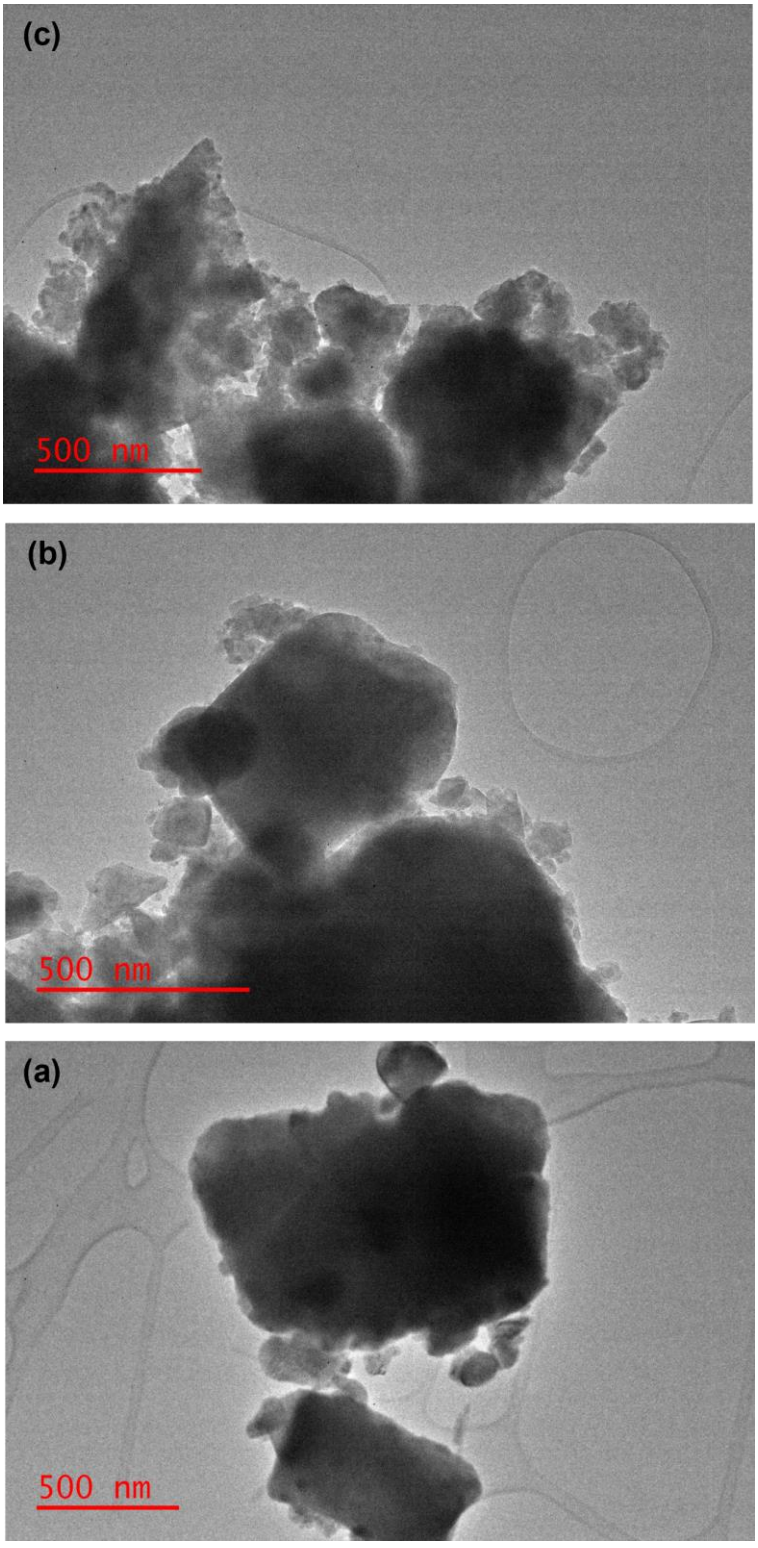

Figure 4. Representative TEM images at comparable magnifications of the (a) unmilled (t_{BM} = 0 min), (b) 30, and (c) 120 min milled powders.

3.2 *Bulk samples*

The effect of the holding temperature (P=16 MPa) and the applied pressure (T_D=800°C) on the densification of the sintered products was investigated for the case of t_{BM} = 0 min, i.e. unmilled composite powders. The obtained results are reported in **Fig. 5a-5b**. **Fig. 6** shows the corresponding compositional/structural changes.

Powders are scarcely consolidated at 750°C (about 88.4 % relative density). No evidence of glass crystallization arises from the resulting XRD analysis on the bulk products. The latter statement holds also true when T_D was increased to 800°C, which determined an improvement in sample densification (93%). On the other hand, new peaks ascribed to α- and β-$CaSiO_3$ are detected in the pattern at 850°C, corresponding to a 95.9% dense product. The two crystalline phases formed from the glass are also observed when the holding temperature was raised to 900°C, which also led to a slight decrease in product density (95.6%). The latter feature could be due to the progress of glass crystallization and grain growth caused by the temperature increase.

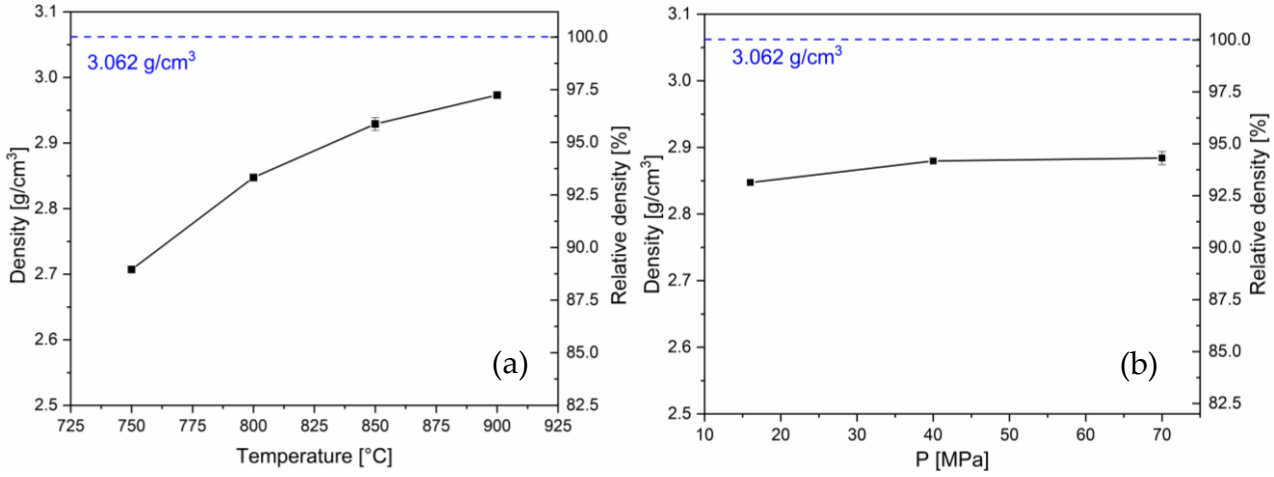

Figure 5. Density of SPS products from unmilled (t_{BM} = 0 min) composite HA-BGMS10 powders as a function of (a) the holding temperature (P=16 MPa) and (b) the applied pressure (T_D=800°C).

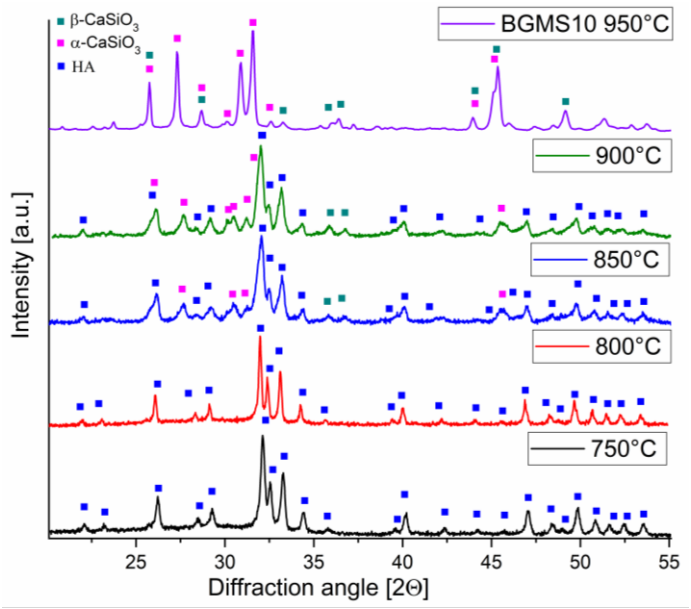

Figure 6. XRD patterns of dense composite samples obtained at different temperatures by SPS from unmilled powders (t_{BM} = 0 min). The pattern corresponding to the sintered glass-ceramic product obtained at 950°C from pure BGMS10 **[40]** is also reported for comparison.

Fig. 5(b) shows that an increase of the mechanical pressure from 16 to 40 MPa at T_D=800°C provided an improvement of sample density from 93 to 94%, whereas only modest changes (94.2%) were observed when this processing parameter was further raised to 70 MPa. No modifications in product composition were correspondingly obtained (supplementary **Fig. S2**), being hydroxyapatite the only crystalline phase detected under such conditions.

The effect produced by a mechanical treatment of the composite powders before their consolidation by SPS was then investigated. As evidenced in **Fig. 7**, a beneficial outcome was obtained after 30 min ball milling, with an increase of the relative density from 94.2 to 94.7%. The interfaces between the two constituents are enhanced by ball milling, so that sintering phenomena are promoted. In contrast, when such treatment was extended to 2h, sintered sample were relatively less dense (92.4%). A possible motivation for such outcome could be that, is spite of the beneficial effect produced by the interface formation, particles become considerable coarser for t_{BM}=120 min (**Figure 1 and Table S1**), which is expected to hinder powder consolidation. Another supplementary plausible explanation will be provided afterwards, after examining the composition of SPS product.

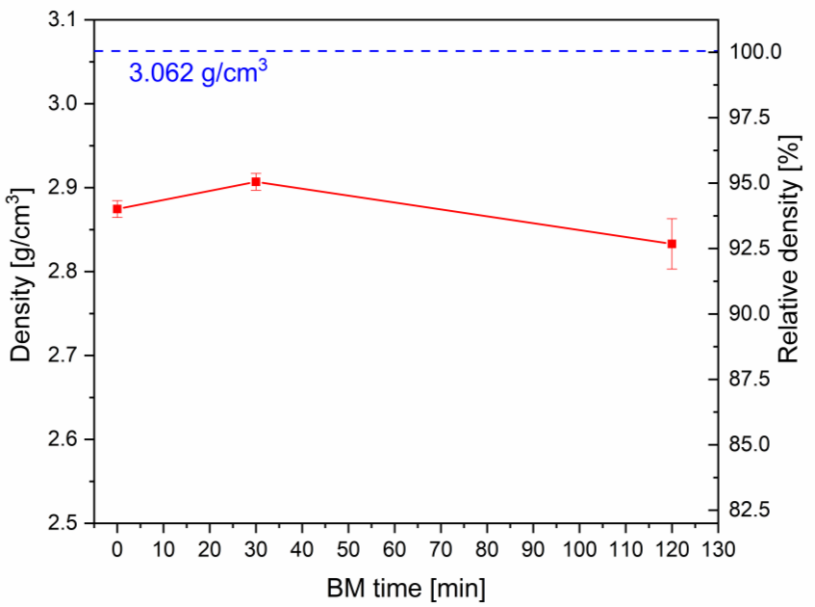

Figure 7. Effect of the milling time (t_{BM}) on the density of products obtained by SPS (T_D=800°C, P=70 MPa).

The XRD experimental patterns (black rhombohedral) and the best fit (red line) relative to the SPS products obtained from unmilled (t_{BM} = 0 min) and milled powders are shown, on a log scale, in **Fig. 8**. Supplementary **Table S3** summarizes the structural and microstructural parameters evaluated from the Rietveld analysis applied to these patterns. The 0/800-70 sample obtained starting from the unmilled powders consists of the amorphous glass and crystalline hydroxyapatite phases, with an estimated relative amount of 53 and 47 wt.%, respectively. Similar values for the HA/BGMS10 weight ratio were also obtained for the milled systems processed by SPS (supplementary **Table S3**). Moreover, when t_{BM}=30 min (sample 30/800-70), the crystallite sizes of HA keep within nanostructured conditions of 900 Å, just slightly higher than those relative to the starting milled powders, i.e. 709 Å (supplementary **Table S2**). Interestingly, similar crystallite dimensions (850 Å) can be achieved for the sintered sample 120/800-70 obtained from the powders milled for 2 hours. This value corresponds roughly twice those of the original milled powders, i.e. 472 Å (supplementary **Table S2**). Along to this significant result, which can be linked to the higher reactivity of this set of mechanically processed powders, it is important to highlight

that the corresponding XRD pattern presents a second crystalline phase ascribable to SiO_2 (5 wt.%). In this regard, it can be postulated that the prolonged ball milling enhanced the reactivity of BGMS10 powders, thus favoring the nucleation and segregation of quartz from the glass phase. This is in accordance with the trend observed for the volume dimension of the hydroxyapatite crystal lattice which can be distorted by the diffusion of alkali metal cations.

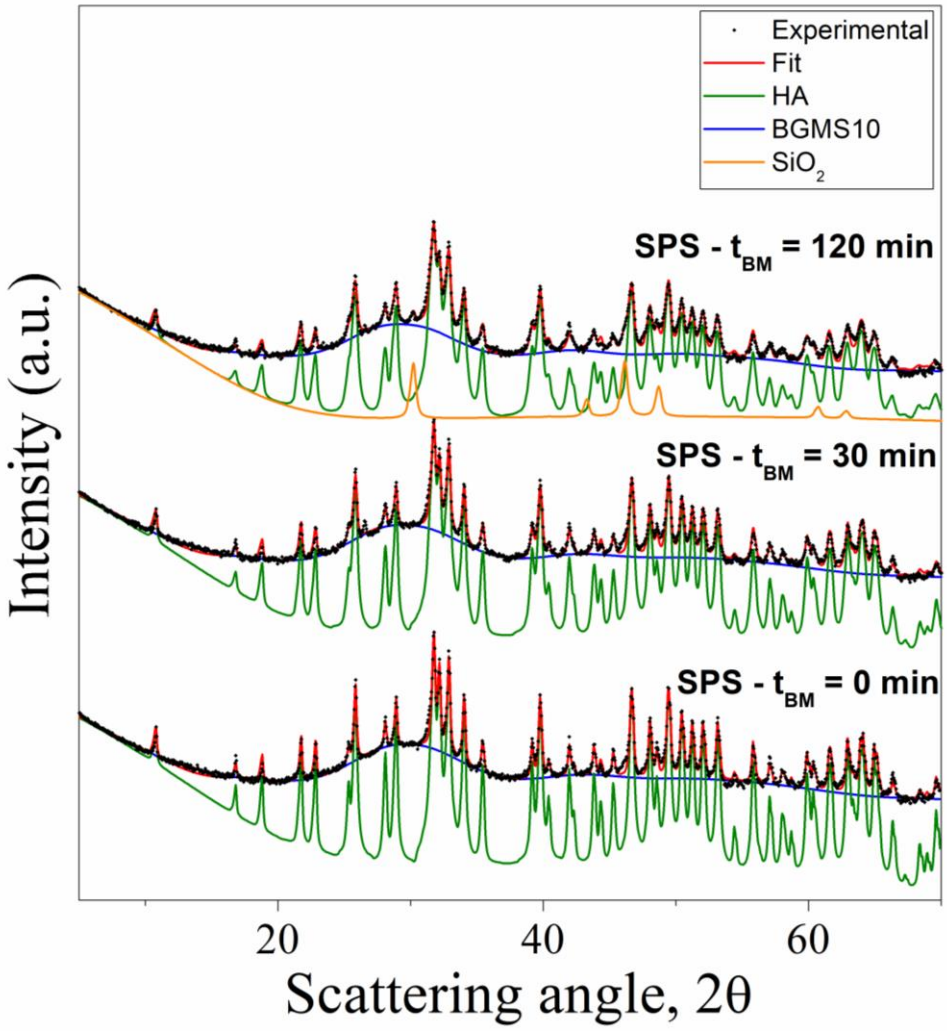

Figure 8. XRD patterns of dense composite samples obtained from the unmilled (t_{BM} = 0 min) and milled powders. Black dots are experimental data, and the red line is the calculated fit. Deconvoluted amorphous BGMS10, hydroxyapatite, and quartz (SiO_2) phases are indicated by blue, green, and orange full lines, respectively.

The formation of a crystalline phase during SPS likely provides a further explanation for justifying the sample density decrease when the milling treatment was extended from 30 to

120 min (**Fig. 7**). Indeed, the occurrence of crystallization phenomena during consolidation of BGMS10 and other glass powders by SPS was found to correspond to relatively less dense products **[40,47]**.

3.3 Microstructural and Mechanical characterization

SEM images of the surface of the sintered composites are shown in **Fig. 9**. The samples appear very similar one to each other, are adequately consolidated, and possess a dense microstructure, apart from some local defects and residual microporosity. This fact confirms the effectiveness of the sintering protocol and is in accordance with the results of the density measurements **(Table 2)**. The more detailed SEM-EDS analysis conducted on the 0/850-16 sample (supplementary **Fig. S3**) evidenced that residual porosity is confined to rounded regions corresponding to the HA constituent. On the other hand, the glassy counterpart in the composite appears to be fully consolidated.

The mechanical properties of the composites (Young's modulus and hardness), as measured by micro-indentation tests, are reported in **Table 2**. In general, the obtained results are analogous or even slightly better than those recently obtained for BGMS10 powders sintered by SPS **[40]**, in particular for 0/850-16 and 30/800-70 samples. This demonstrates the beneficial contribution exerted by the HA phase in the composite; it should be stressed that pure HA, when consolidated by SPS, tends to have better mechanical properties than BGMS10 products obtained by the same technique **[45]**, although it is not straightforward to compare the performance of such samples, given the different processing parameters employed to sinter them, i.e. T_D=1200°C (HA) **[45]**, and T_D=750-950 °C (BGMS10) **[40]**. In addition, it should be also noted that the composite samples investigated in this work possess lower relative densities (in the range 92.4-95.9) compared to those resulting from pure HA (fully dense) **[45]**, and BGMS10 (in the range 98.6-99.6%) **[40]**

The results reported in **Table 2** reveal an increment of both the local elastic modulus and hardness with increasing holding temperature in the set of samples obtained from unmilled powders (i.e., 0/800-70 and 0/850-16). This fact can be ascribed to the increased density of

the samples treated at higher temperature and to the progressive crystallization of their glassy phase, with the concurrent formation of α- and β-$CaSiO_3$ (see **Fig. 6**); in fact, a slight devitrification of the glass phase is expected to increase the mechanical performance of HA/BG composites, as crystalline phases are usually mechanically stronger than their parent glass **[48,49]**. On the other hand, a too wide crystallization should be avoided in this kind of samples, as the development of new phases may also imply non-trivial changes in specific volumes, with a reduction in the final density and compactness of the sintered composite **[40,47]**; in turn, a density reduction is typically associated to a decrease of the mechanical performance. The differences in the Young's modulus of the samples prepared at the same holding temperature (i.e., 800 °C), but with increasing milling times of the starting powders (i.e., 0 min, 30 min and 120 min ball milling), may be also explained in terms of the different degree of density and compactness achieved after sintering (see **Figs. 5** and **7, Table 2**).

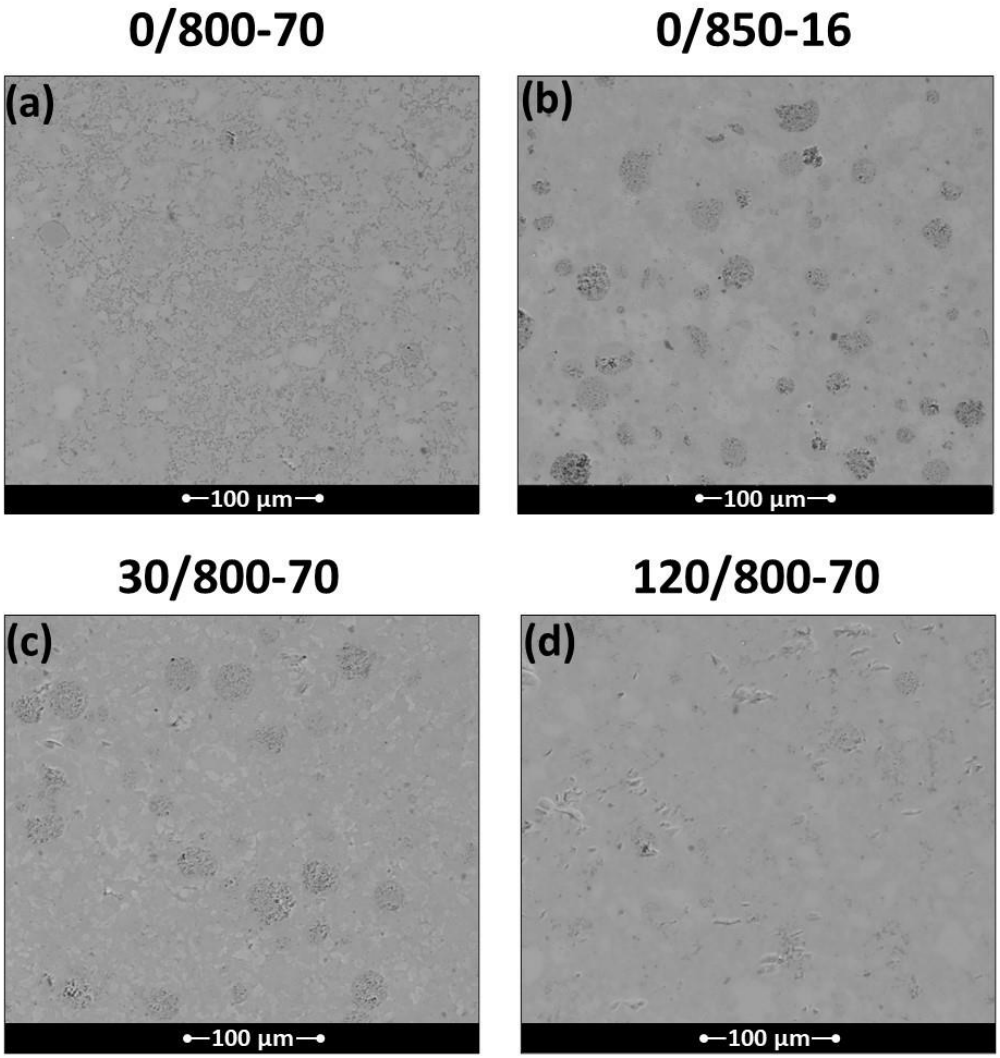

Figure 9. The surface of the sintered disks, showing an excellent densification.

Table 2 Young's modulus and hardness of the investigated samples, as determined by micro-indentation tests. The corresponding relative density values are also reported.

Sample	Relative density (%)	Young's Modulus (GPa)	Hardness (Vickers)
0/800-70	94.2	95.24 ± 2.47	509.88 ± 34.29
0/850-16	95.9	116.39 ± 4.49	697.61 ± 26.89
30/800-70	94.7	122.33 ± 3.58	675.32 ± 38.45
120/800-70	92.4	98.01 ± 4.55	683.22 ± 42.21

3.4 *In vitro* bioactivity

The bioactivity of the produced composites has been evaluated *in vitro* by immersing them in a Simulated Body Fluid solution, which contains an ionic concentration similar to that of human plasma **[44]**. As BGs bond to bone through the formation of a superficial HA film, which mimics the mineral phase of bone tissue, the bone-bonding aptitude of bioactive glasses and bioactive glass-based composites can be easily estimated by studying the ability of HA to form on the samples' surface during their immersion in SBF for different periods of time. These findings are widely employed to preliminary check the reactivity of a potential bioactive material in physiological environment.

The results of the SEM analysis performed on HA/BGMS10 disks after 7 and 14 days in SBF are shown in **Fig. 10**. It is evident that the process parameters – in particular, the milling time of the starting powders and the holding temperature – influence the bioactivity of the samples in a non-trivial way. After one week, the surface of all the produced composites appeared highly degraded, with a widespread porosity due to the dissolution of the samples and their ionic release. After 14 days in SBF, the composites were characterized by different degree of bioactivity; in particular, the sample 0/850-16 showed an almost absence of surface precipitates ascribable to HA. This behaviour can be partially attributed to the crystallization of the glass phase with the concurrent formation of α- and β-$CaSiO_3$, two phases characterized by a slower in vitro reactivity and, therefore, by a less marked bioactivity compared to that of the parent glass **[50]**. All the samples produced with a lower holding temperature (i.e., 800 °C) appeared bioactive after two weeks of soaking, with different degree of reactivity depending on the milling time. It should be noted the extraordinary bioactivity of the 30/800-70 samples, whose surface, already after a week, is highly degraded and completely covered by white precipitates with the typical morphology of *in vitro* formed HA. The X-EDS analysis reported in **Fig. 11** confirms the presence of precipitates rich in calcium and phosphorus, with a Ca/P ratio which gradually approaches that of stoichiometric HA.

The chemical nature of the globular precipitates formed on the sintered disks after immersion in SBF has been further investigated by means of a Raman microscope. In fact,

such technique can be used to locally identify the presence of HA, as the main Raman peaks of the P–O vibrational modes are particularly intense; moreover, since the in vitro grown HA is typically carbonated and the Raman spectroscopy is sensitive to the C–O vibrational modes, the presence of carbonated groups was also verified. **Fig. 12** reports the Raman spectra acquired on the phosphorus and calcium rich precipitates which formed on the 30/800-70 samples after 7 and 14 days in SBF (since the spectra obtained from the other samples are very similar, they are not reported for the sake of brevity). Already after 7 days in SBF, the Raman spectra are dominated by the characteristic peaks of carbonated HA, as reported by the literature [51–53]:

- a very sharp peak at ~960 cm^{-1}, which is related to the symmetric stretching mode of the PO_4 groups;
- two broad peaks at ~430 cm^{-1} and ~590 cm^{-1}, ascribable to the bending modes of the same group;
- a broad peak at about 1070 cm^{-1}, which is imputable to the symmetric stretching mode of the CO_3 groups.

It is then possible to conclude that the precipitates are mainly composed of carbonated HA, thus confirming the marked bioactivity of the produced samples.

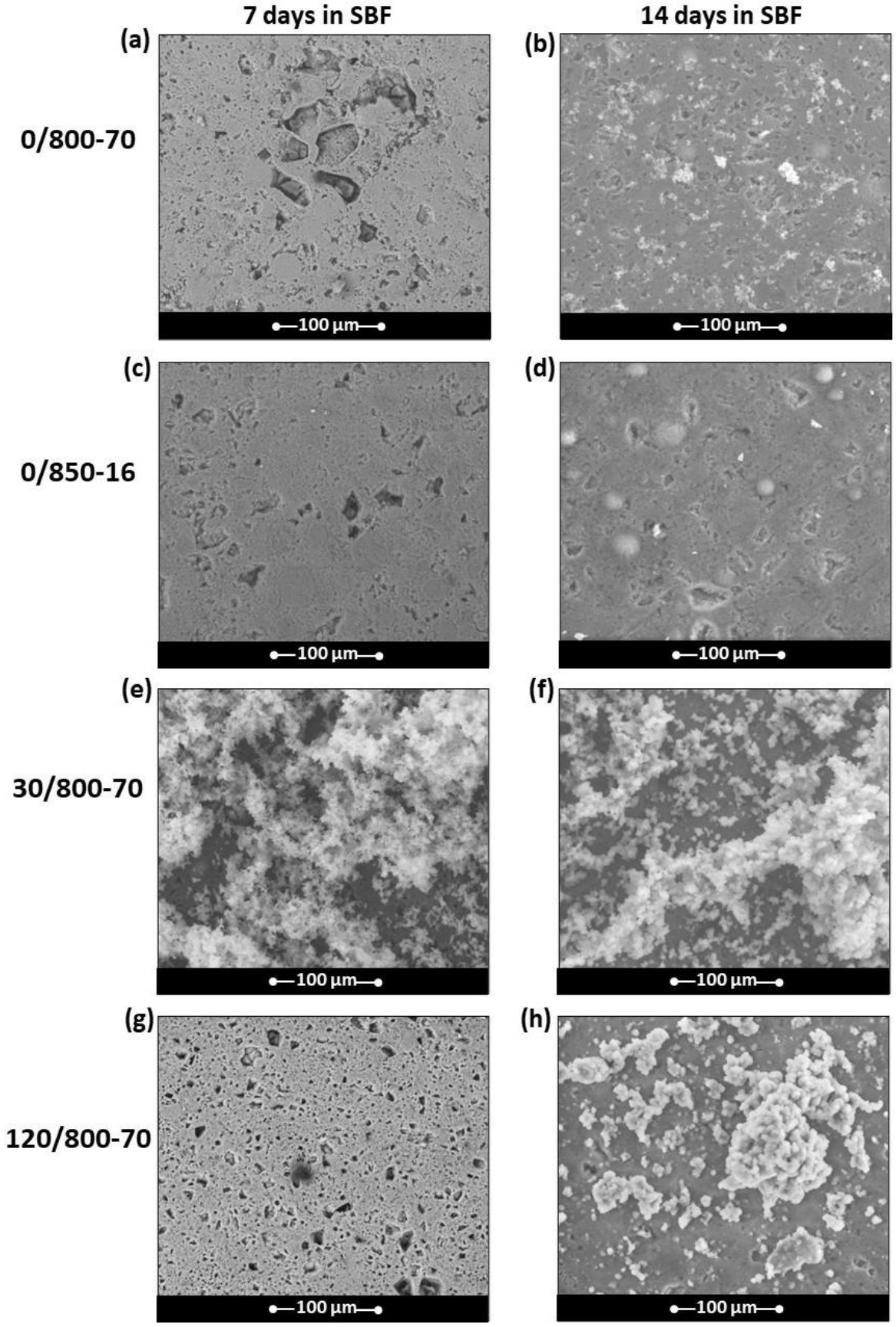

Figure 10. SEM images of the sintered samples after soaking them in SBF for 7 and 14 days. It should be noted the marked HA precipitation on the 30/800-70 samples already after 7 days of immersion.

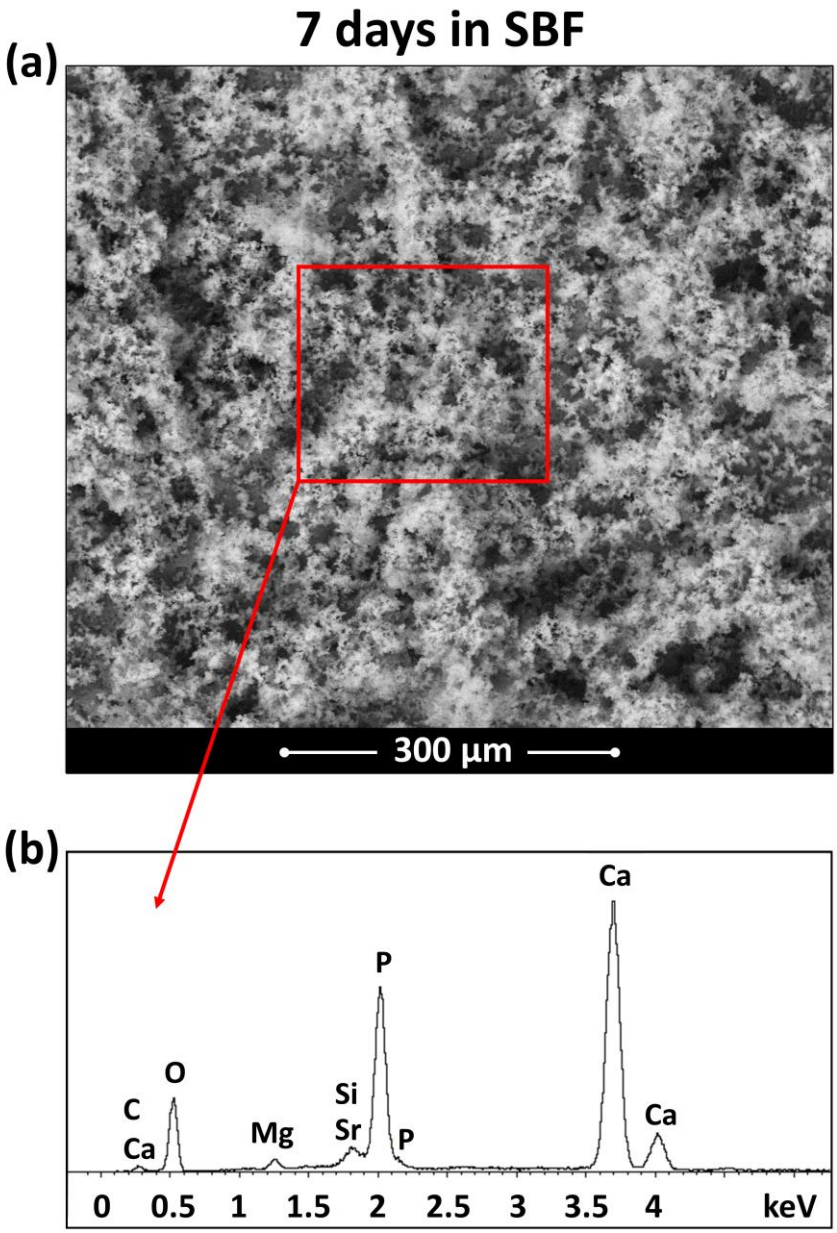

Figure 11. (a) HA formed on the 30/800-70 sample after 7 days in SBF and (b) results of the X-EDS analysis performed on the area shown in (a).

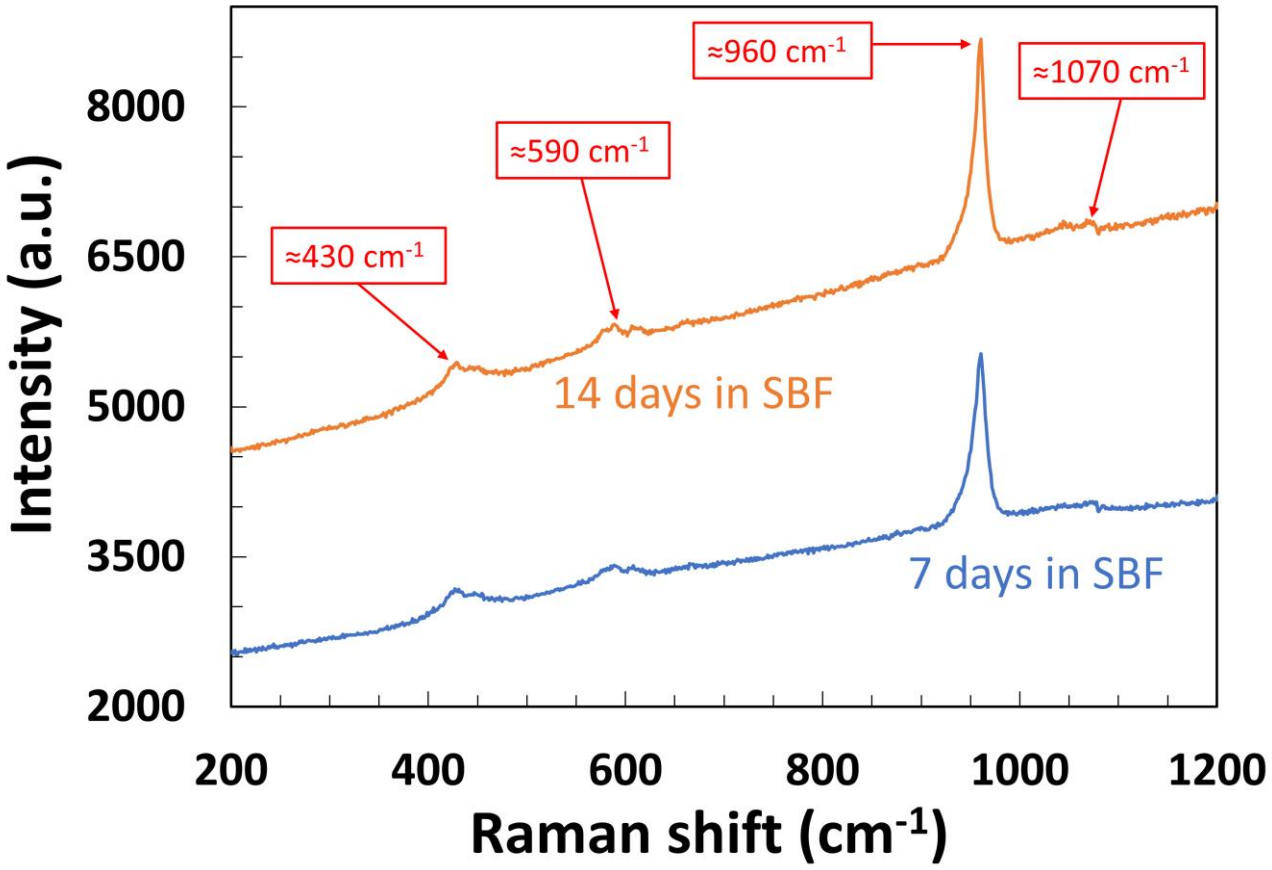

Figure 12. Raman spectra acquired on the calcium and phosphorus rich precipitates formed on the 30/800-70 samples after 7 and 14 days in SBF.

To justify the surprisingly different bioactivity behavior exhibited during in-vitro test by HA/BGMS10 sintered samples when the starting composite powders are mechanically treated prior to SPS, some considerations will be made in what follows. First, as mentioned in the introduction, structural changes, as well as the formation of intimate interfaces among the different processed constituents, are induced by BM. This feature also emerges in this work from the analysis of the three sets of powders. A progressive crystallite size refinement of the HA phase from > 2000 Å (untreated) to 700 Å (t_{BM}=30 min), and 470 Å (t_{BM}=120 min), was correspondingly achieved. Although an unavoidable crystallites growth occurred during their heat treatment by SPS, the samples corresponding to milled powders were still nanostructured, with crystallite size in the range 85-90 nm. Such fine microstructure corresponds to a broader grain boundary area compared to the unmilled sample, so that

composite reactivity, dissolution, and ion-exchange phenomena, as well as the nucleation of the new apatite phase, during SBF test, are expected to be highly promoted.

The formation of intimate composite mixtures induced by the BM treatment, as evidenced by particle size analysis and TEM observation, could also have played a role for the observed enhancement of SPS samples reactivity. The features above could be considered the main factors responsible for the marked bioactivity improvement which came out from SBF test results involving sintered samples prepared using 30 min milled powders. Such considerations are also valid when considering the 2h milled specimen, since the latter one also displays improved HA-forming ability (**Fig.10 (g)-(h)**) with respect to the unmilled (t_{BM} = 0 min) sample (**Fig.10 (a)-(b)**). Nonetheless, product bioactivity was relatively reduced with a prolonged milling treatment. The main structural/compositional difference observed when t_{BM} was increased from 30 to 120 min was the formation of SiO_2 in the bulk SPS products, while very similar HA crystallites size were obtained (90 or 85 nm, respectively). Therefore, the presence of crystalline SiO_2, which is certainly less bioactive than the original glass phase, apparently slows down the apatite-forming ability of the composite.

4 Summary and concluding remarks

The densification behaviour, mechanical properties, and biological response in SBF, of four groups of samples obtained by SPS from unmilled and ball milled (30 and 120 min, CR=2) composite mixture (50/50 wt.%) consisting of HA and BGMS10 glass powders can be briefly summarized in what follows.

a) No crystallization from the glassy phase is observed in bulk samples (93-94.2% dense) obtained by SPS at 800°C from unmilled powders; samples density is improved at 850°C, α- and β-$CaSiO_3$ are formed, Young modulus and Vickers Hardness are higher (from 95 to 116 GPa and from 510 to 698, respectively), whereas the related HA-forming ability during 14 days SBF test is very scarce.

b) HA crystallites size growth is highly retained (from 70 to 90 nm) during SPS of 30 min milled powders; the obtained samples show superior Young's Modulus (122 GPa),

Vickers Hardness (675) and, above all, an extraordinary biological response, being their surface completely covered by HA precipitates just after 7 days immersion in SBF. These findings can be explained by the increased surface area and the significant reduction of HA crystallites size (from above 200 to 70 nm) induced in the powders by the mechanical treatment.

c) The extension to 120 min of the BM process is self-defeating, as it results in less dense products with poorer mechanical properties and lower in-vitro bioactivity. The formation of crystalline SiO_2 during SPS is postulated to be responsible for such outcome.

Based on the results above, it is expected that BM could represent a promising tool, if utilized under proper conditions, for improving the bioactivity of composite systems of potential interest in regenerative medicine.

Future work will be devoted to a comprehensive biological characterization, to further corroborate the findings of this work; specifically other in-vitro tests will be carried out, such as cellular direct and indirect tests. Moreover, an in vivo study will be performed on the most promising products.

Acknowledgements

Damiano Angioni performed his activity in the framework of the International PhD in Innovation Sciences and Technologies at the University of Cagliari, Italy. The authors acknowledge the GAUSS-CeSAR (Centro Servizi d'Ateneo per la Ricerca) of the University of Sassari for TEM analyses. Thanks are due to Dr. Francesco Loy (University of Cagliari) for his technical assistance during SEM-EDS analysis. The authors acknowledge the funding FAR 2021 (Dipartimento di Ingegneria "Enzo Ferrari", Università degli Studi di Modena e Reggio Emilia, Italy).

5 References

[1] Bone Repair Biomaterials. In Woodhead Publishing Series in Biomaterials Editors: J.A. Planell, S.M. Best, D. Lacroix, A. Merolli, Woodhead Publishing, (2009) ISBN 978-1845693855.

[2] A.S. Mao, D.J. Mooney, Regenerative medicine: Current therapies and future directions Proc. Natl. Acad. Sci. U.S.A. 112(47), (2015) pp. 14452-14459 https://doi.org/10.1073/pnas.1508520112

[3] R. Comesaña, F. Lusquiños, J. Del Val, F. Quintero, A. Riveiro, M. Boutinguiza, J.R. Jones, R.G. Hill, J. Pou, Toward smart implant synthesis: Bonding bioceramics of different resorbability to match bone growth rates. Sci. Rep. 5, (2015) 10677 https://doi.org/10.1038/srep10677

[4] E. Saiz, A.R. Boccaccini, J. Chevalier, M. Peroglio, Editorial on Bioceramics for Bone Repair. J. Eur. Ceram. Soc. 38(3), (2018), pp. 821-822. https://doi.org/10.1016/j.jeurceramsoc.2017.11.036

[5] Bioceramics and their Clinical Applications. In Woodhead Publishing Series in Biomaterials, Editor: Tadashi Kokubo, Woodhead Publishing, 2008, ISBN 978-1845692049

[6] S.V. Dorozhkin, Calcium orthophosphate bioceramics Ceram. Int. 41(10), (2015), pp. 13913–13966. https://doi.org/10.1016/j.ceramint.2015.08.004

[7] N.C. Paxton, S.K. Powell, M.A. Woodruff, Biofabrication: The future of regenerative medicine. Tech. Orthop. 31(3), (2016), pp. 190-203 https://doi.org/10.1097/BTO.0000000000000184

[8] A.R. Boccaccini, Q. Chen, L. Lefebvre, L. Gremillard, J. Chevalier, Sintering, crystallization and biodegradation behaviour of bioglass®-derived glass–ceramics, Faraday Discuss. 136, (2007), pp. 27–44. https://doi.org/10.1039/b616539g

[9] L.C. Gerhardt, A.R. Boccaccini, Bioactive Glass and Glass-Ceramic Scaffolds for Bone Tissue Engineering, Materials 3, (2010), 3867. https://doi.org/10.3390/ma3073867

[10] S. Grasso, R.K. Chinnam, H. Porwal, A.R. Boccaccini, M.J. Reece, Low temperature spark plasma sintering of 45S5 Bioglass®, J. Non-Cryst. Solids. 362, (2013), pp. 25-29. https://doi.org/10.1016/j.jnoncrysol.2012.11.009

[11] J.R. Jones Review of bioactive glass: from Hench to hybrids. Acta Biomater. 9, (2013) pp. 4457-4486. https://doi.org/10.1016/j.actbio.2012.08.023

[12] L.L. Hench, Genetic design of bioactive glass. J. Eur. Ceram. Soc. 9, (2009), pp. 1257–1265. https://doi.org/10.1016/j.jeurceramsoc.2008.08.002

[13] J. Kolmas, A. Jaklewicz, A. Zima, M. Bućko, Z. Paszkiewicz, J. Lis, A. Slósarczyk, W. Kolodziejski, Incorporation of carbonate and magnesium ions into synthetic hydroxyapatite: the effect on physicochemical properties, J. Mol. Struct. 987, (2011), pp. 40–50. https://doi.org/10.1016/j.molstruc.2010.11.058

[14] S. Von Euw, Y. Wang, G. Laurent, C. Drouet, F. Babonneau, N. Nassif, T. Azaïs, Bone mineral: new insights into its chemical composition. Sci. Rep. 9(1), (2019), 8456 https://doi.org/10.1038/s41598-019-44620-6

[15] J.C. Knowles, W. Bonfield. Development of a glass reinforced hydroxyapatite with enhanced mechanical properties. The effect of glass composition on mechanical properties and its relationship to phase changes. J. Biomed. Mater. Res. 27 (1993), pp. 1591–1598. https://doi.org/10.1002/jbm.820271217

[16] L.J. Jha, J.D. Santos, J.C. Knowles, Characterization of apatite layer formation on P_2O_5-CaO, P_2O_5-CaO-Na_2O, and P_2O_5-CaO-$Na_2OAl_2O_3$ glass hydroxyapatite composites. J Biomed Mater Res. 31, (1996). pp. 481–486. https://doi.org/10.1002/(sici)1097-4636(199608)31:4%3C481::aid-jbm7%3E3.0.co;2-h

[17] J.D. Santos, R.L. Reis, F.J. Monteiro, J.C. Knowles, G.W. Hastings. Liquid phase sintering of hydroxyapatite by phosphate and silicate glass additions: Structure and properties of the composites. J. Mater. Sci. Mater. Med. 6, (1995), pp. 348–352. https://doi.org/10.1007/BF00120303

[18] J.D. Santos, P.L. Silva, J.C. Knowles, S. Talal, F.J. Monteiro. Reinforcement of hydroxyapatite by adding P2O5-CaO glasses with Na2O, K2O and MgO. J. Mater. Sci. Mater. Med. 7, (1996), pp. 187–189. https://doi.org/10.1007/BF00121259

[19] D. Tanaskovic, B. Jokic, G. Socol, A. Popescu, I.N. Mihailescu, R. Petrovic, Dj. Janackovic, Synthesis of functionally graded bioactive glass-apatite multistructures on Ti substrates by pulsed laser deposition. Appl. Surf. Sci. 254(4), (2007), pp. 1279-1282. https://doi.org/10.1016/j.apsusc.2007.08.009

[20] D. Bellucci, A. Sola, V. Cannillo. Bioactive glass-based composites for the production of dense sintered bodies and porous scaffolds. Mater. Sci. Eng. C 33, (2013), pp. 2138–2151. https://doi.org/10.1016/j.msec.2013.01.029

[21] D. Bellucci, A. Sola, A. Anesi, R. Salvatori, L. Chiarini, V. Cannillo, Bioactive glass/hydroxyapatite composites: Mechanical properties and biological evaluation, Mater. Sci. Eng. C 51, (2015), pp. 196–205. https://doi.org/10.1016/j.msec.2015.02.041

[22] D. Bellucci, L. Desogus, S. Montinaro, R. Orrù, G. Cao, V. Cannillo, Innovative hydroxyapatite/bioactive glass composites processed by spark plasma sintering for bone tissue repair. J. Eur. Ceram. Soc. 37(4), (2017), pp. 1723–1733 https://doi.org/10.1016/j.jeurceramsoc.2016.11.012

[23] D. Bellucci, R. Salvatori, A. Anesi, L. Chiarini, V. Cannillo, SBF assays, direct and indirect cell culture tests to evaluate the biological performance of bioglasses and bioglass-based composites: Three paradigmatic cases. Mater. Sci. Eng. C 96, (2019) pp. 757–764 https://doi.org/10.1016/j.msec.2018.12.006

[24] S. Mondal, G. Hoang, P. Manivasagan, M.S. Moorthy, T.P. Nguyen, T.T. Vy Phan, H.H. Kim, M.H.; Kim, S.Y., Nam, J. Oh, Nano-hydroxyapatite bioactive glass composite scaffold with enhanced mechanical and biological performance for tissue engineering application. Ceram. Int. 44(13), (2018), pp. 15735-15746 https://doi.org/10.1016/j.ceramint.2018.05.248

[25] J.A. Rincón-López, J.A. Hermann-Muñoz, D.A. Fernández-Benavides, A. David, A.L. Giraldo-Betancur, J.M.,Alvarado-Orozco, J. Muñoz-Saldaña, Isothermal phase transformations of bovine-derived hydroxyapatite/bioactive glass: A study by design of experiments. J. Eur. Ceram. Soc. 39(4), (2019), pp. 1613-1624 https://doi.org/10.1016/j.jeurceramsoc.2018.11.021

[26] M. Luginina, D. Angioni, S. Montinaro, R. Orrù, G. Cao, R. Sergi, D. Bellucci, V. Cannillo, Hydroxyapatite/bioactive glass functionally graded materials (FGM) for bone tissue engineering, J. Eur. Ceram. Soc. 40, (2020), pp. 4623-4634. https://doi.org/10.1016/j.jeurceramsoc.2020.05.061

[27] M. Lakrat, M. Jabri, M. Alves, M.H. Fernandes, L.L. Ansari, C. Santos, E.M. Mejdoubi, Three-dimensional nano-hydroxyapatite sodium silicate glass composite scaffold for bone tissue engineering - A new fabrication process at a near-room temperature Mater. Chem. Phys. 260, (2021), 124185 https://doi.org/10.1016/j.matchemphys.2020.124185

[28] D. Reffitt, N. Ogston, R. Jugdaohsingh, H. Cheung, B. Evans, R. Thompson, J.J. Powell, G.N. Hampson, Orthosilicic acid stimulates collagen type I synthesis and osteoblastic differentiation in human osteoblastlike cells in vitro. Bone 32, (2003), pp 127–135. https://doi.org/10.1016/s8756-3282(02)00950-x

[29] M. Dong, G. Jiao, H. Liu, W. Wu, S. Li, Q. Wang, D. Xu, X. Li, H. Liu, Y. Chen, Biological Silicon Stimulates Collagen Type 1 and Osteocalcin Synthesis in Human Osteoblast-Like Cells Through the BMP-2/Smad/RUNX2 Signaling Pathway. Biol Trace Elem Res. 173, (2016), pp. 306-15. https://doi.org/10.1007/s12011-016-0686-3

[30] O. Bretcanu, X. Chatzistavrou, K. Paraskevopoulos, R. Conradt, I. Thompson, A.R. Boccaccini, Sintering and crystallization of 45S5 bioglass® powder, J. Eur. Ceram. Soc. 29, (2009), pp. 3299–3306. https://doi.org/10.1016/j.jeurceramsoc.2009.06.035

[31] D. Bellucci, A. Sola, V. Cannillo, Low temperature sintering of innovative bioactive glasses. J. A. Ceram. Soc. 95 (2012) pp. 1313–1319. https://doi.org/10.1111/j.1551-2916.2012.05100.x

[32] D. Bellucci, V. Cannillo, A novel bioactive glass containing strontium and magnesium with ultra-high crystallization temperature, Mater. Lett. 213, (2018), pp. 67-70. https://dx.doi.org/10.1016/j.matlet.2017.11.020

[33] C. Suryanarayana, Mechanical alloying and milling. Prog. Mater. Sci. 46(1-2), (2001), pp. 1-184. https://doi.org/10.1016/S0079-6425(99)00010-9

[34] D. Maurice, T.H. Courtney, Milling dynamics: Part. II. dynamics of a SPEX mill and a one-dimensional mill. Metall. Mater. Trans. A: Phys. Metall. Mater. Sci. 27(7), (1996), pp. 1973–1979 https://doi.org/10.1007/BF02651947

[35] F. Delogu, M. Monagheddu, G. Mulas, L. Schiffini, G. Cocco, Impact characteristics and mechanical alloying processes by ball milling: experimental evaluation and modelling outcomes. Int. J. Non-Equilib. Process. 11(3), (2000), pp. 235–269

[36] High-Energy Ball Milling, Editor(s): Małgorzata Sopicka-Lizer, Woodhead Publishing, (2010) ISBN 978-1845695316

[37] N.F. Ibrahim, H. Mohamad, S.N.F.M. Noor, Effects of milling media on the fabrication of melt-derived bioactive glass powder for biomaterial application. AIP Conf. Proc. 1791, (2016), 010011. https://doi.org/10.1063/1.4968865

[38] D. Bovand, M. R. Allazadeh, S. Rasouli, E. Khodadad, E. Borhani, Studying the effect of hydroxyapatite particles in osteoconductivity of Ti-HA bioceramic. J. Aust. Ceram. Soc. 55, (2019), pp. 395–403 https://doi.org/10.1007/s41779-018-0247-7

[39] G.K. Pouroutzidou, G.S. Theodorou, E. Kontonasaki, L. Papadopoulou, N. Kantiranis, D. Patsiaoura, K. Chrissafis, C.B. Lioutas, K.M. Paraskevopoulos, Synthesis of a bioactive nanomaterial in the ternary system SiO2-CaO-MgO doped with CuO: The effect of Ball milling on the particle size, morphology and bioactive behavior. AIP Conf. Proc. 2075, (2019), 200005. https://doi.org/10.1063/1.5091430

[40] D. Angioni, R. Orrù, G. Cao, S. Garroni, A. Iacomini, D. Bellucci, V. Cannillo, Spark Plasma Sintering, Mechanical and In-vitro Behavior of a Novel Sr- and Mg-Containing Bioactive Glass for Biomedical Applications, J. Eur. Ceram. Soc. 42, (2022), pp. 1776–1783 https://doi.org/10.1016/j.jeurceramsoc.2021.11.061

[41] L. Lutterotti, R. Ceccato, R. Dal Maschio, E. Pagani, Quantitative analysis of silicate glass in ceramic materials by the Rietveld method. Mater. Sci. Forum 87, (1998), pp. 278-281. https://doi.org/10.4028/www.scientific.net/MSF.278-281.87

[42] F.L. Matthews, R. Rawlings. Composite Materials: Engineering and Science. Chapman & Hall, Great Britain; 1994.

[43] W. Oliver, G. Pharr, An improved technique for determining hardness and elastic modulus using load and displacement sensing indentation experiments. J. Mater. Res. 7, (1992), pp. 1564–1583. https://doi.org/10.1557/JMR.1992.1564

[44] T. Kokubo, H. Takadama, How useful is SBF in predicting in vivo bone bioactivity? Biomaterials 27, (2006), pp. 2907–2915. https://doi.org/10.1016/j.biomaterials.2006.01.017

[45] A. Cuccu, S. Montinaro, R. Orrù, G. Cao, D. Bellucci, A. Sola, V. Cannillo, Consolidation of different Hydroxyapatite powders by SPS: optimization of the sintering conditions and characterization of the obtained bulk products, Ceram. Int. 41(1), (2015), pp. 725-736. https://doi.org/10.1016/j.ceramint.2014.08.131

[46] M. Baricco, T.A. Baser, S. Enzo, G. Vaughan, A.R. Yavari, Analysis of crystallization behavior of $Fe_{48}Cr_{15}Mo_{14}Y_2C_{15}B_6$ bulk metallic glass by synchrotron radiation. J. Mater. Res. 23, (2008), pp. 2166-2173. https://dx.doi.org/10.1557/JMR.2008.0264

[47] L. Desogus, A. Cuccu, S. Montinaro, G. Cao, D. Bellucci, A. Sola, V. Cannillo, Classical Bioglass® and innovative CaO-rich bioglass powders processed by Spark Plasma Sintering: A comparative study. J. Eur. Ceram. Soc. 5(15), (2015) pp. 4277-4285. https://doi.org/10.1016/j.jeurceramsoc.2015.07.023

[48] G. Kaur, V. Kumar, F. Baino, J.C. Mauro, G. Pickrell, I. Evans, O. Bretcanu, Mechanical properties of bioactive glasses, ceramics, glass-ceramics and composites: State-of-the-art review and future challenges, Mater. Sci. Eng. C 104 (2019), 109895. https://doi.org/10.1016/j.msec.2019.109895

[49] J.K.M.F. Daguano, K. Strecker, E.C. Ziemath, S.O. Rogero, M.H.V. Fernandes, C. Santos, Effect of partial crystallization on the mechanical properties and cytotoxicity of bioactive glass from the 3CaO.P2O5–SiO2–MgO system, J. Mech. Behav. Biomed. Mater. 14, (2012), pp. 78-88, https://doi.org/10.1016/j.jmbbm.2012.04.024

[50] L.A. Núñez-Rodríguez, M.A. Encinas-Romero, A. Gómez-Álvarez, J.L. Valenzuela-García, G.C. Tiburcio-Munive, Evaluation of Bioactive Properties of α and β Wollastonite Bioceramics Soaked in a Simulated Body Fluid, J. Biomater. Nanobiotechnol. 9, (2018), pp. 263-276. https://doi.org/10.4236/jbnb.2018.93015

[51] F.A. Shah, Towards refining Raman spectroscopy-based assessment of bone composition, Sci. Rep. 10, (2020), 16662. https://doi.org/10.1038/s41598-020-73559-2

[52] E. Cañas, M.J. Orts, E. Sánchez, D. Bellucci, V. Cannillo, Deposition of bioactive glass coatings based on a novel composition containing strontium and magnesium, J. Eur. Ceram. Soc. 42, (2022), pp. 6213–6221. https://doi.org/10.1016/j.jeurceramsoc.2022.05.064

[53] J. Liu, U. Glasmacher, M. Lang, C. Trautmann, K.-O. Voss, R. Neumann, G.A. Wagner, R. Miletich, Raman spectroscopy of apatite irradiated with swift heavy ions with and without simultaneous exertion of high pressure, Appl. Phys. A 91, (2008), pp 17–22. https://doi.org/10.1007/s00339-008-4402-9

Bioactivity Enhancement by a Ball Milling Treatment in Novel Bioactive Glass-Hydroxyapatite Composites produced by Spark Plasma Sintering

Damiano Angioni[1], Roberto Orrù[1,*], Giacomo Cao[1],
Sebastiano Garroni[2], Devis Bellucci[3], Valeria Cannillo[3]

[1]*Dipartimento di Ingegneria Meccanica, Chimica, e dei Materiali, Unità di Ricerca del Consorzio Interuniversitario Nazionale per la Scienza e Tecnologia dei Materiali (INSTM), Università degli Studi di Cagliari, via Marengo 2, 09123 Cagliari, Italy*

[2]*Dipartimento di Scienze Chimiche, Fisiche, Matematiche e Naturali, Università degli Studi di Sassari, Via Vienna 2, 07100 Sassari,*

[3]*Dipartimento di Ingegneria "Enzo Ferrari", Università di Modena e Reggio Emilia, Via P. Vivarelli 10, 41125 Modena, Italy*

Corresponding author: Roberto Orrù (roberto.orru@unica.it)

Abstract

Hydroxyapatite (HA) and a lab-made bioactive glass (BGMS10) are combined (50/50 wt.%) in this work, where the effect produced by a ball milling (BM) treatment (0-120 min) prior SPS consolidation on the characteristics of the resulting products is investigated. An extraordinary improvement of the apatite-forming ability during in-vitro test on SPS samples (800°C/70MPa/2min) is obtained using the 30 min BMed mixture. Superior Young's Modulus (122 GPa) and Vickers Hardness (675) were also found compared to unmilled samples (95 GPa and 510, respectively). Microstructural changes induced by BM, with 90 nm HA crystallites size in the bulk composite, and the intimate HA/BGMS10 interfaces established, are the factors mainly responsible for such result. When milling was prolonged to 120 min, samples with relatively lower density, mechanical properties, and in-vitro bioactivity, were produced under the same SPS conditions. The formation of crystalline SiO_2 during SPS might be responsible for such behaviour.

Keywords

Bioactive glass; Hydroxyapatite; Composites; Ball milling; Spark Plasma Sintering (SPS)

1. Introduction

The availability of innovative bioceramics able to ~~properly~~ stimulate the repair of biological tissues, in particular for the treatment of bone defects, ~~is well known to~~ represents a current need in regenerative medicine **[1-4]**. To this aim, a useful contribution could be provided by the combination of Hydroxyapatite (HA) with suitable Bioactive Glass (BG) formulations. Due to its similarity to human bone mineral composition, the related biocompatibility and osteoconductivity, HA is the most widely exploited ceramic for orthopaedic applications **[5-7]**. As a drawback, it displays scarce mechanical strength as well as an excessively slow reactivity and interaction with biological fluids and tissues, so that biodegradability and osteoinductivity properties are not adequate for regenerating tissues at the required rate. The latter characteristics could be improved when HA is coupled with bioactive glasses (BGs), which bond tissue to bone more rapidly than other bioceramics **[8-11]**; specific ~~bioactive glass~~ BG compositions are also able to bond to soft tissues. Moreover, molecular biology studies have demonstrated that ~~bioactive glasses~~ BGs can stimulate new bone formation, i.e., osteogenesis, through the release in the physiological environment of critical concentration of dissolution products, acting as chemical stimuli which activate the osteoprogenitor cells **[12]**. The higher reactivity of such materials, due to their intrinsic amorphous character, is expected to promote both the bioactivity and the biological responsiveness of the resulting composite material and, in turn, the growth rate of the new natural tissue. The use of glasses can be further exploited to introduce specific ions of biological interest – such as strontium, magnesium, or fluorine – into the HA lattice, in order to mimic the composition of the biological apatite, which is characterized by several ion substitutions **[13,14]**. Finally, the addition of suitable amounts of ~~bioactive glass~~ BG also facilitates the consolidation of HA powders, so that the temperature conditions required to obtain bulk products are correspondingly lowered.

Along this line, several studies reported in the literature have been addressed to the fabrication and characterization of HA-BG composites **[15-27]**. In most of these investigations, the two constituents are homogeneously distributed across the volume **[15-**

18,20-25,27]. However, the possibility to combine HA and BG to form Functional Graded Materials was also explored **[19,26]**. For many years, the main focus of these works was the mechanical improvement of HA through the addition of calcium phosphate glasses **[16]**, which were preferred by virtue of their chemical similarity to HA. Only later, the opportunity of tuning the HA degradation or enhance its bone bonding ability have begun to be investigated, together with the production of porous composites (i.e., scaffolds) for bone tissue regeneration and repair. In this context, silicate glasses (in particular, 45S5 Bioglass®, i.e., the first bioactive glass, whose excellent bioactivity was due to its finely tuned composition) were mostly employed on account of their high bioactivity. In fact, silicon seems to be essential for bone formation, as it favours the adhesion, proliferation, and differentiation of osteoblast-like cells; silicon supplementation is reported to reduce bone fragility and to increase bone mineral density in several animal models **[28,29]**. On the other hand, thermal treatments necessary to sinter and properly densify HA/~~bioactive glass~~ BG composites may induce the glassy phase to crystallize, thus slowing down, or even inhibiting, both the bioactivity and ion release of the final system **[30]**. For these reasons, in recent years different works have been devoted to the production of new silicate ~~bioactive glasses~~ BGs with low tendency to crystallize **[31,32]**; such glasses have been combined with HA in order to obtain a new generation of ceramic composites, whose biological responsiveness, degradation and mechanical performance can be designed as a function of the given clinical requirement **[20,21]**.

In this contest, the effect produced by a ball milling (BM) treatment of the composite powder mixture on the densification, mechanical and bioactivity behavior of the resulting bulk product is totally unexplored, to the best of our knowledge. BM is a well-known and versatile mechanical treatment route able to induce structural transformations in the processing powders, thus allowing for the synthesis of non-equilibrium phases, the formation of nanostructured alloys, increasing mixture reactivity, degradation of toxic species, etc. **[33]**. The extent of the produced effects depends on the system, the employed devices (planetary ball mills, attritors, etc.), the related operating conditions (rotational speed, milling time, ball to powder or charge ratio, CR, etc.), and it is basically due to the

combination of impact and attrition actions involving milling tools and processing powders **[33-36].**

Apart from HA-BG composite systems, the influence of a ball milling treatment on ~~bioactive glass~~ BG or other bioceramics was also barely investigated **[37-39]**. Ibrahim et al. **[37]** examined the effect produced when different milling media made of WC or ZrO_2 were used for the treatment of ~~bioactive glass~~ BG powders (Na_2O-CaO-SiO_2-P_2O_5 system) obtained by melt quenching. Milling was carried out for 18 min using a planetary mill at 500 rpm and negligeable effects were correspondingly noted on the amorphous silica network glass structure. Similarly, no beneficial effects were observed with an increase of the milling time from 20 to 50 h (planetary ball mill, 300 rpm, CR=10, Argon) when processing Ti-HA composite powders, based on SBF (Simulated Body Fluid) assay and wettability test results conducted on the corresponding sintered samples **[38]**.

Sol-gel derived bioactive nanomaterials based on the quaternary MgO-CaO-CuO-SiO_2 system were mechanically processed for 6h at different rotational speeds, in the range 300-500 rpm, using a S100 centrifugal ball mill **[39]**. Bioactivity test results in SBF revealed that apatite formation occurred earlier (after 1 day) when using unmilled powders instead of the milled ones (HA was detected after 3 days). No specific explanation was provided by the authors to justify such negative effect of the mechanical treatment on powder bioactivity.

In this work, the effect produced by a ball milling treatment of HA-BG composite powders on the densification, mechanical, and in vitro biological behaviour is investigated for the very first time in the literature. A mixture consisting of commercial HA and a recently developed Sr- and Mg-containing ~~bioactive glass~~ BG named BGMS10, with low tendency to crystallize **[32,40]**, is first ball milled for different times. The resulting powders are consolidated by Spark Plasma Sintering (SPS) to provide bulk samples to be characterized. Composition, microstructure, mechanical properties, and the bioactivity behaviour in a SBF solution of the sintered composite products are analysed and compared.

2. Materials and methods

2.1 Composite powders

Commercial hydroxyapatite (CAPTAL® Hydroxylapatite, Cod. CAPTAL 60-1, Ca/P ratio equal to 1.67, 99% purity, 99% crystallinity) supplied by Plasma Biotal Ltd. (UK) was selected as one of the composite constituents. The second one is the lab-made BGMS10 bioactive glass with nominal composition (mol%): 2.3% Na_2O, 2.3% K_2O, 25.6% CaO, 10.0% MgO, 10.0% SrO, 2.6% P_2O_5, and 47.2% SiO_2. The glass has been prepared according to a melt-quenching procedure and subsequently ground to obtain powders with grain size < 63 μm, as described elsewhere **[32]**.

50 wt.% HA and 50 wt.% BGMS10 powders (about 16 g total) were mildly mixed in a SPEX 8000 (SPEX CertiPrep, USA) shaker mill using plastic vials and small agata balls (7 mm diam.). The corresponding ball-to-powder weight or charge ratio (CR) was maintained very low, about 0.2. The obtained powders will be considered as unmilled (t_{BM} = 0 min).

Approximately 2.4 g of the latter composite mixture was subsequently mechanically treated at different times (t_{BM}= 30 and 120 min) still using the SPEX 8000 device, but with agata vial and two larger agata balls (12 mm diam.) as milling tools, and by setting a CR value equal to 2.

Particle size distribution was measured using a laser light scattering analyser (CILAS 1180, France).

N_2 sorption isotherms were collected with a Sorptomatic 1990 instrument (Fisons Instruments, Milan, Italy) and the corresponding superficial areas were calculated according to the BET method. 800 mg of each sample were placed in a quartz tube and degassed under mild conditions (100 Pa at 180 °C for 24 h) to prevent any structural evolution. The dead volume of the quartz tube was evaluated through helium adsorption measurements.

Phases identification and structural characteristics of mixed and milled powders were first investigated by X-ray diffraction analysis (Philips PW 1830, Netherlands) using Cu Kα radiation, over a range of scattering angles 2ϑ from 20 to 130, in steps of 0.05° with 15 s acquisition time per angle. The Rietveld method (MAUD program) was used for the

analysis of XRD patterns to determine phases amount and the corresponding microstructural parameters **[41]**.

For TEM observations, a FEI TECNAI 200 operating at 200 kV was used, while samples were prepared by dispersing a few milligrams in absolute ethanol using an ultrasonic bath. Finally, one or two drops of the as-obtained suspension were dispersed on a holey carbon supported grid.

2.2 Bulk composite samples

About 1.56 g of either the unmilled (t_{BM}=0 min) or milled (t_{BM}=30 and 120 min) composite mixture were first placed inside a die cylinder (35 mm external diameter; 15 mm inside diameter; 40 mm height) equipped with two plungers (14.7 mm diameter, 30 mm height), consisting of AT101 graphite (ATAL Srl., Italy). The die was then inserted in the sintering chamber of the SPS equipment (515S model, Fuji Electronic Industrial Co., Ltd., Kanagawa, Japan) which was properly evacuated down to about 20 Pa before electric current application. This apparatus was set to operate with a current sequence of 12 ON pulses followed by 2 OFF pulses, and 3.3 ms as characteristic time of single pulse. Temperature was measured using a K-type thermocouple (TC Misure e Controlli S.R.L., Italy) introduced in a small hole drilled on the external surface of graphite dies, about 1-2 mm far from the processing powders. To make sample release easier after SPS, a graphite foil (0.13 mm thick, Alfa Aesar, Karlsruhe, Germany) was placed between the powders and the inner walls of die/plungers. In addition, thermal losses from the die were limited by covering it with a graphite felt (3 mm thick, Atal s.r.l., Italy).

As reported in Supplementary **Fig. S1**, the temperature was firstly increased at a rate of 50°C/min from the room value to 100°C below the maximum level (T_D). Subsequently, to avoid or reduce possible overshooting problems, the final T_D value was reached at a lower rate (10°C/min). The sample was isothermally heated for 2 min at T_D, then the temperature was decreased at a rate of 50°C/min down to 300°C, followed by a natural cooling step. The applied pressure (P) was suddenly raised to the maximum value in about 1 min, then

maintained constant during the non-isothermal and isothermal heating steps, whereas this parameter was gradually reduced during sample cooling (**Fig. S1**).

Bulk composite samples were produced at different dwell temperature and pressure conditions, in the ranges 750-900°C and 16-70 MPa, respectively. Before their subsequent characterization, the opposite sides of the sintered specimens were accurately ground/polished using abrasive paper to remove residual impurities from the graphite tools. Cylindrical samples with approximately 14.7 mm diameter and 2.5-3 mm height were finally obtained. For the sake of reproducibility, each experimental condition was replicated at least twice.

In what follows, sintered samples to be characterized will be also referred to as t_{BM}/T_D-P, to differentiate them depending on the milling (t_{BM}) and sintering (T_D and P) conditions adopted.

The relative density (ϱ) of bulk samples was determined by the Archimedes' method using ethanol as immersing medium. Sintered disks were weighted using a Ohaus Explorer Pro (Ohaus Corporation, NJ, USA) analytical balance (± 0.0005 g precision). Relative densities were calculated by considering 3.062 g/cm^3 as theoretical value of the composite system, determined by means of a rule of mixture **[42],** and using the values of 3.16 and 2.97 g/cm^3 **[40]** for HA and BGMS10, respectively.

2.3 Microstructural characterization and Mechanical testing

Scanning electron microscopy (ESEM – Quanta 2000, FEI Co., Eindhoven, The Netherlands) was employed to investigate the microstructure of the sintered disks. Additional studies were also conducted using a high-resolution scanning electron microscopy (HR-SEM, mod. S4000, Hitachi, Tokyo, Japan) equipped with a UltraDry EDS detector (Thermo Fisher Scientific, Wal-tham, MA, USA).

The mechanical properties of the samples, embedded into resin and mirror polished, were evaluated by micro-indentation technique. Open Platform equipment, with Vickers indenter tip, (CSM Instruments, Peseux, Switzerland) was employed to measure both the hardness and the Young's modulus of the composites. A load of 500 mN was used during

the indentation process, with 1.5 N/min as loading/unloading rate (loading time at maximum load: 15 s). At least fifteen measurements for each sintered disk were obtained. For each indentation, the load–penetration depth curve was automatically recorded. The elastic modulus was then calculated from the indentation load-unloading curves, according to the Oliver and Pharr method **[43]**.

2.4 *In vitro* bioactivity tests

The bioactivity of the obtained composites was investigated by soaking them in a Simulated Body Fluid solution (SBF), according to the Kokubo protocol **[44]**. Before using it, the pH of the solution was adjusted to 7.4, as recommended **[44]**. Each sample was immersed in 25 ml of SBF and stored in plastic flasks at 37 °C; SBF was refreshed every 48 h. The samples were removed from the solution after 7 and 14 days, carefully washed with distilled water and left to dry at room temperature for 24 h. The possible precipitation of HA on the samples' surface was evaluated by means of both ESEM and micro-Raman spectroscopy. The ESEM was equipped with an Energy Dispersive X-ray microanalysis (INCA, Oxford Instruments, U.K) and used in low-vacuum conditions, i.e. ~0.5 Torr. Raman spectra were acquired by using a LabRAM HR Evolution spectrometer (Horiba, France) with a diode laser source emitting at 632.8 nm (output power: 21 mW at the sample). Photons scattered by each sample were dispersed by a 1800 lines/mm grating monochromator and then collected by on a CCD camera (a 100x objective was employed as collection optic). A spectra collection setup of ten acquisitions, each of them taking 30 s, was used.

3 Results and discussion

3.1 Composite powders

First, it should be specified that, as reported in previous studies, particles of commercial HA powders are relatively coarser (d10, d50, d90, and d43: 8.80, 34.0, 52.0, and 32.7 μm, respectively) **[45]** compared to those ones of the glass constituent (d10, d50, d90, and d43: 0.8, 4.9, 26.2, and 9.4 μm, respectively) **[40]**.

As for the HA-BGMS10 system investigated in this work, the effect produced by the ball milling treatment on particle size of the resulting mixture can be deduced from **Fig. 1**. The corresponding d10, d50, d90, and d43 are reported in supplementary **Table S1**.

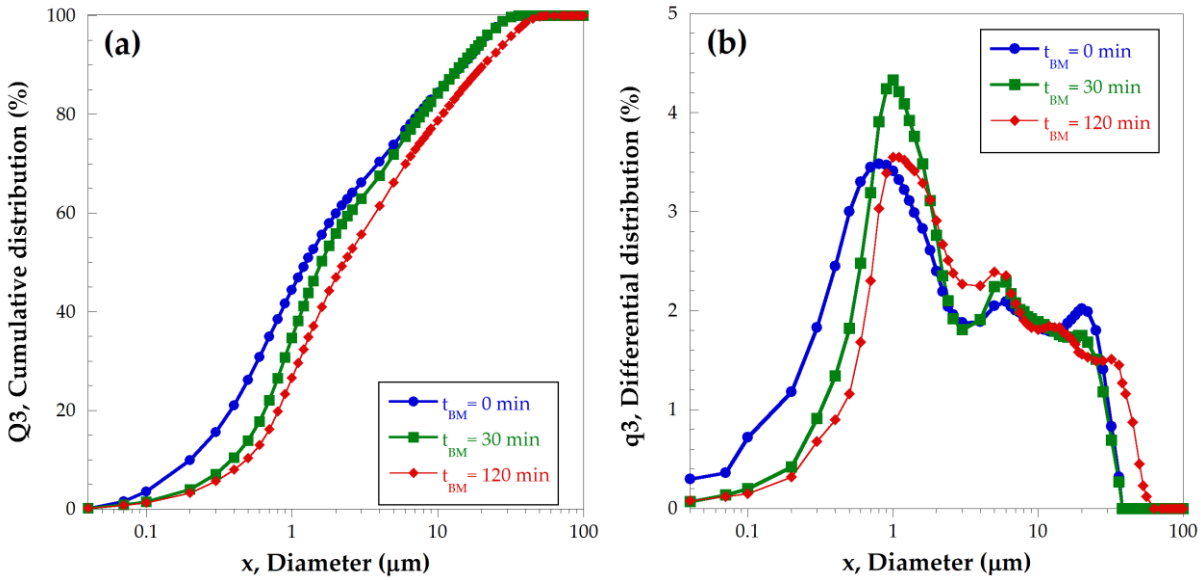

Figure 1 Particles size distribution of unmilled (t_{BM} = 0 min) and milled HA-BGMS10 composite powders: cumulative (a) and differential (b) curves

Both cumulative and differential curves evidence that particles progressively increase their size during milling, to indicate the occurrence of powder agglomeration phenomena. It is likely that the softer HA particles incorporate the glass ones. In addition, the results of this analysis suggest that, when the mechanical treatment is conducted up to 30 min, most of the changes are confined to the lower range of particles size (< 2.5 μm). This is supported by the fact that, the maximum value of the q3 curve at about 1 μm, which represents the higher percent of particles at that size, markedly increases. On the other hands, only small changes in the cumulative and differential curves, compared to the unmilled (t_{BM} = 0 min) mixture, can be observed when considering the larger particles size range. Moreover, the measured average size (d43=4.6 μm) did not vary compared to that of untreated powders (see supplementary **Table S1**).

In contrast, when the milling treatment is prolonged to 2 h, powder agglomeration leads to the formation of coarser particles, as manifested by the shifting of both Q3 and q3 curves on the right side as well as by the decreased intensity of the q3 curve maximum.

Textural properties of the unmilled (t_{BM} = 0 min) and milled (t_{BM} = 30 and 120 min) samples have been then investigated by N_2 physisorption. The isotherms of all the samples are depicted in **Figs. 2(a)-2(c)**. BET (Brunauer, Emmett, Teller) surface areas vary from 5.0 m^2g^{-1} for the unmilled (t_{BM} = 0 min) to 11.7 and 11.1 m^2g^{-1} for the systems milled at 30 and 120 minutes, respectively (see **Table 1**).

Table 1. B.E.T surface area values estimated for the unmilled (t_{BM} = 0 min) and milled (t_{BM} = 30 and 120 min) samples. HA have been measured for comparison.

Sample	**B.E.T Surface Area [m^2g^{-1}]**
HA (commercial)	5.5
t_{BM} = 0 min ~~Unmilled~~	5.0
t_{BM} = 30 min	11.7
t_{BM} = 120 min	11.1

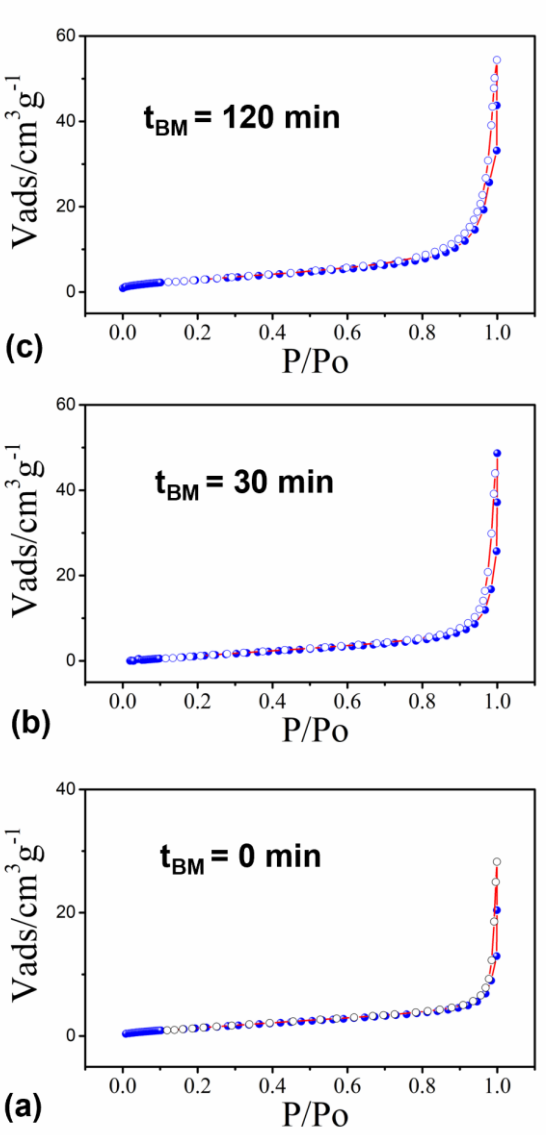

Figure 2. N_2 physisorption isotherms of the (a) unmilled (t_{BM} = 0 min) sample and, milled for 30 (b) and 120 minutes (c) samples.

All the samples show a type II isotherm with a H3 type hysteresis loop typical of macroporous materials. The mechanical processing acts significantly by increasing the specific surface area of the system, thus reaching the maximum value after 30 minutes. The increase of the specific surface area during the first period of milling is the result of the new exposed surfaces correspondingly formed, together with the desorption of physisorbed gases, which typically occlude nanopores. With the extension of the milling treatment, particle fracturing is balanced by the formation of agglomerates, and only minor changes in the specific surface area are observed.

Structural and microstructural characteristics of the three batches of powders are then investigated by XRD analysis (**Fig. 3**).

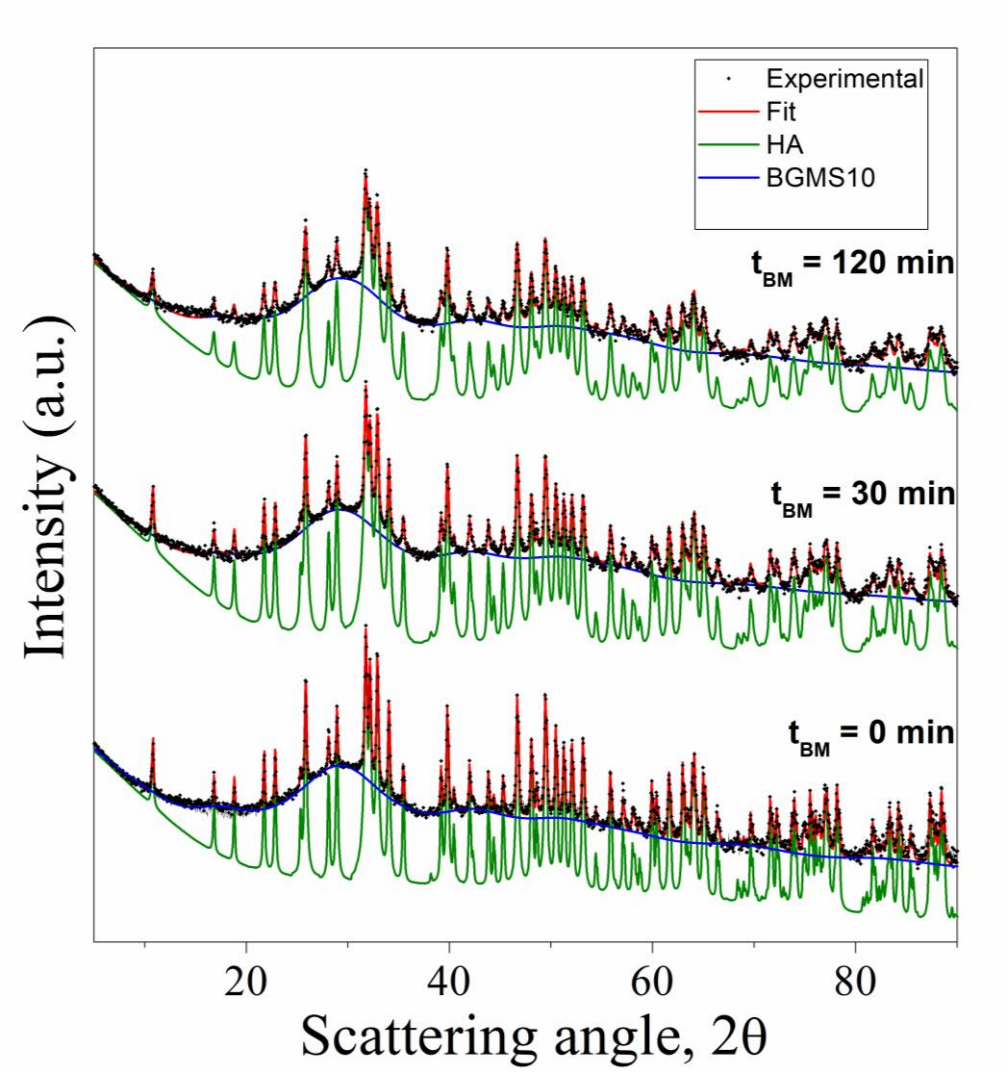

Figure 3. XRD patterns of unmilled (t_{BM} = 0 min) and milled HA-BGMS10 samples. Black dots are experimental data, and the red line is the calculated fit. Deconvoluted amorphous BGMS10 and hydroxyapatite phases are indicated by blue and green full line.

The pattern referred to the unmilled system shows Bragg reflections ascribable to the hydroxyapatite phase (S.G. *P63/m*) together with a typical shape of an amorphous glass related with the BGMS10. The phase, named as $Ca_{1.5}Na_{2.64}Si_9O_3$, has been computed using a pseudo-crystalline structure factor ($Ca_{1.5}Na_{2.64}Si_9O_3$ phase; symmetry: trigonal; space group: R-3 m; crystallite size: 20 Å; microstrain: 0.03) according to the LeBail approach **[46]**.

Relative amount of each phase and microstructural parameters determined by Rietveld refinement, are reported in supplementary **Table S2**. The relative amount of each phase contained in the unmilled (t_{BM} = 0 min) composite (46/54 wt.% - HA/BGMS10) is rather consistent with the initial nominal mixture. This holds also true when considering the milled powders. **Fig. 3** also highlights that the XRD pattern of the sample milled for 30 minutes is still characterized by the halo peak ascribable to the amorphous phase. However, as expected, the hydroxyapatite crystallites size decreased significantly from > 2000 Å to 700 Å (**Table S2**), as a consequence of the mechanical processing. Increasing the milling time up to 120 minutes, both crystalline and amorphous phases are still observed, while the crystallite dimensions of the hydroxyapatite phase further decreased down to 470 Å (**Table S2**). Interestingly, as emerged from the microstructural parameters here estimated, the cell volume associated with the hydroxyapatite phase increases as the milling time was augmented.

The microstructure of unmilled and milled powders was further characterized by TEM. The corresponding images presented in **Fig. 4** suggest that all the three systems analysed are characterized by agglomerates of particles with different shapes which confirms the formation of an intimate mixture already when HA and BGMS10 were just mixed. Crystalline domains decreased, accordingly to the XRD analysis, when the powders were subject to mechanical milling. No new phase emerged both from TEM and XRD characterization, at least up to this stage of milling.

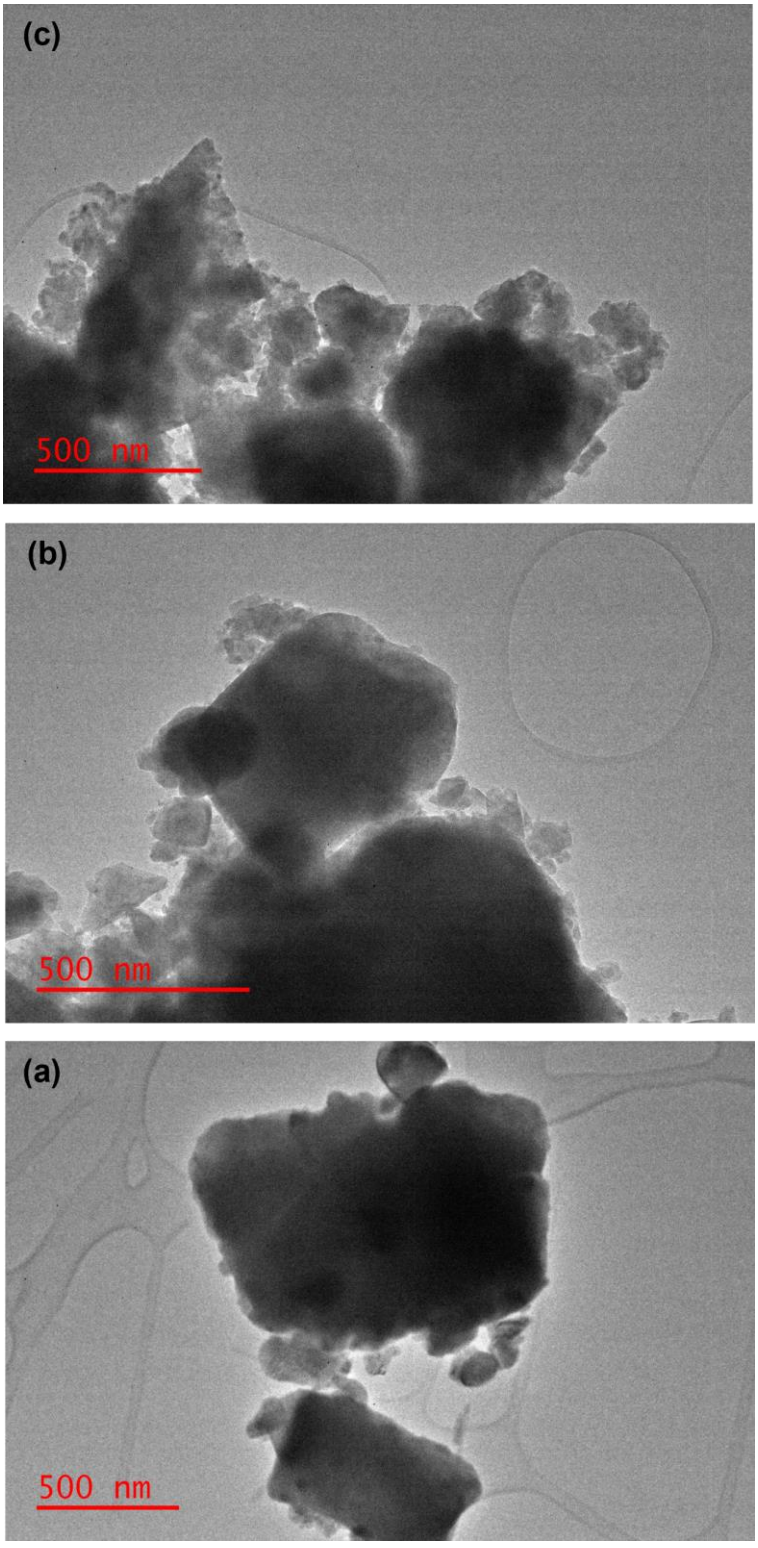

Figure 4. Representative TEM images at comparable magnifications of the (a) unmilled (t_{BM} = 0 min), (b) 30, and (c) 120 min milled powders.

3.2 *Bulk samples*

The effect of the holding temperature (P=16 MPa) and the applied pressure (T_D=800°C) on the densification of the sintered products was investigated for the case of t_{BM} = 0 min, i.e. unmilled composite powders. The obtained results are reported in **Fig. 5a-5b**. **Fig. 6** shows the corresponding compositional/structural changes.

Powders are scarcely consolidated at 750°C (about 88.4 % relative density). No evidence of glass crystallization arises from the resulting XRD analysis on the bulk products. The latter statement holds also true when T_D was increased to 800°C, which determined an improvement in sample densification (93%). On the other hand, new peaks ascribed to α- and β-$CaSiO_3$ are detected in the pattern at 850°C, corresponding to a 95.9% dense product. The two crystalline phases formed from the glass are also observed when the holding temperature was raised to 900°C, which also led to a slight decrease in product density (95.6%). The latter feature could be due to the progress of glass crystallization and grain growth caused by the temperature increase.

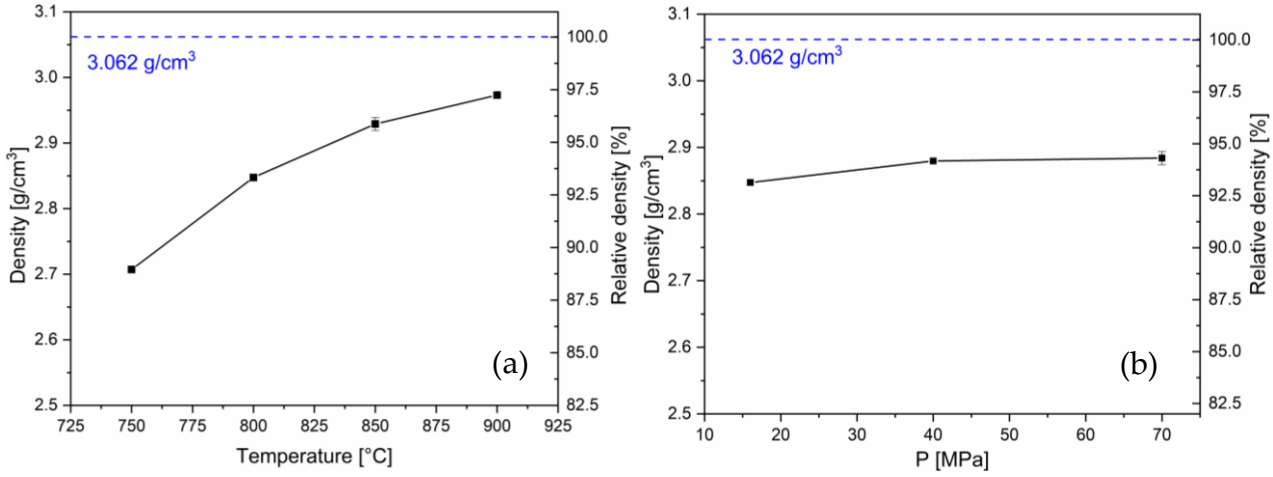

Figure 5. Density of SPS products from unmilled (t_{BM} = 0 min) composite HA-BGMS10 powders as a function of (a) the holding temperature (P=16 MPa) and (b) the applied pressure (T_D=800°C).

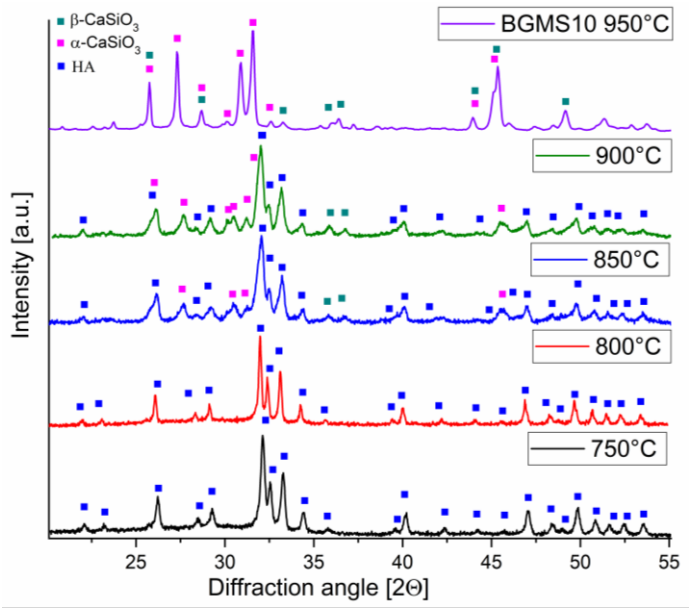

Figure 6. XRD patterns of dense composite samples obtained at different temperatures by SPS from unmilled powders (t_{BM} = 0 min). The pattern corresponding to the sintered glass-ceramic product obtained at 950°C from pure BGMS10 **[40]** is also reported for comparison.

Fig. 5(b) shows that an increase of the mechanical pressure from 16 to 40 MPa at T_D=800°C provided an improvement of sample density from 93 to 94%, whereas only modest changes (94.2%) were observed when this processing parameter was further raised to 70 MPa. No modifications in product composition were correspondingly obtained (supplementary **Fig. S2**), being hydroxyapatite the only crystalline phase detected under such conditions.

The effect produced by a mechanical treatment of the composite powders before their consolidation by SPS was then investigated. As evidenced in **Fig. 7**, a beneficial outcome was obtained after 30 min ball milling, with an increase of the relative density from 94.2 to 94.7%. The interfaces between the two constituents are enhanced by ball milling, so that sintering phenomena are promoted. In contrast, when such treatment was extended to 2h, sintered sample were relatively less dense (92.4%). A possible motivation for such outcome could be that, is spite of the beneficial effect produced by the interface formation, particles become considerable coarser for t_{BM}=120 min (**Figure 1 and Table S1**), which is expected to hinder powder consolidation. Another supplementary plausible explanation will be provided afterwards, after examining the composition of SPS product.

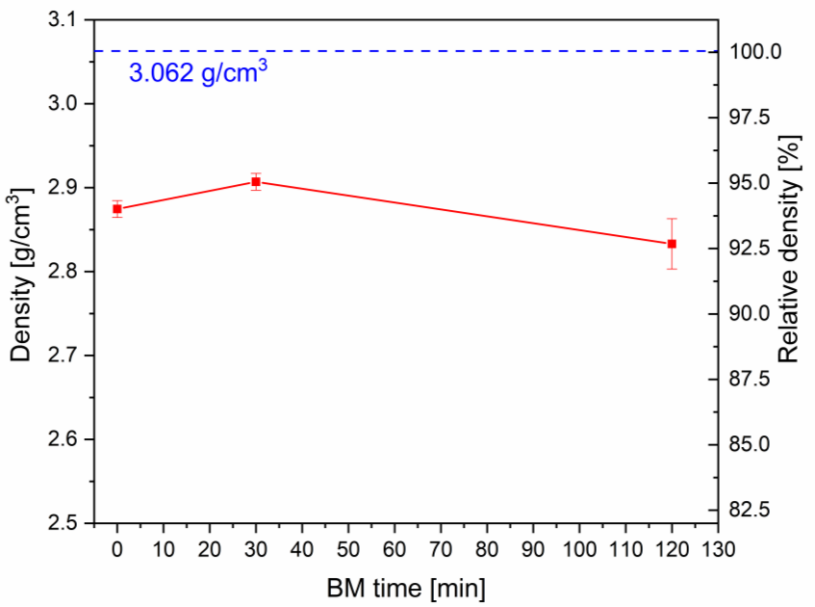

Figure 7. Effect of the milling time (t_{BM}) on the density of products obtained by SPS (T_D=800°C, P=70 MPa).

The XRD experimental patterns (black rhombohedral) and the best fit (red line) relative to the SPS products obtained from unmilled (t_{BM} = 0 min) and milled powders are shown, on a log scale, in **Fig. 8**. Supplementary **Table S3** summarizes the structural and microstructural parameters evaluated from the Rietveld analysis applied to these patterns. The 0/800-70 sample obtained starting from the unmilled powders consists of the amorphous glass and crystalline hydroxyapatite phases, with an estimated relative amount of 53 and 47 wt.%, respectively. Similar values for the HA/BGMS10 weight ratio were also obtained for the milled systems processed by SPS (supplementary **Table S3**). Moreover, when t_{BM}=30 min (sample 30/800-70), the crystallite sizes of HA keep within nanostructured conditions of 900 Å, just slightly higher than those relative to the starting milled powders, i.e. 709 Å (supplementary **Table S2**). Interestingly, similar crystallite dimensions (850 Å) can be achieved for the sintered sample 120/800-70 obtained from the powders milled for 2 hours. This value corresponds roughly twice those of the original milled powders, i.e. 472 Å (supplementary **Table S2**). Along to this significant result, which can be linked to the higher reactivity of this set of mechanically processed powders, it is important to highlight

that the corresponding XRD pattern presents a second crystalline phase ascribable to SiO_2 (5 wt.%). In this regard, it can be postulated that the prolonged ball milling enhanced the reactivity of BGMS10 powders, thus favoring the nucleation and segregation of quartz from the glass phase. This is in accordance with the trend observed for the volume dimension of the hydroxyapatite crystal lattice which can be distorted by the diffusion of alkali metal cations.

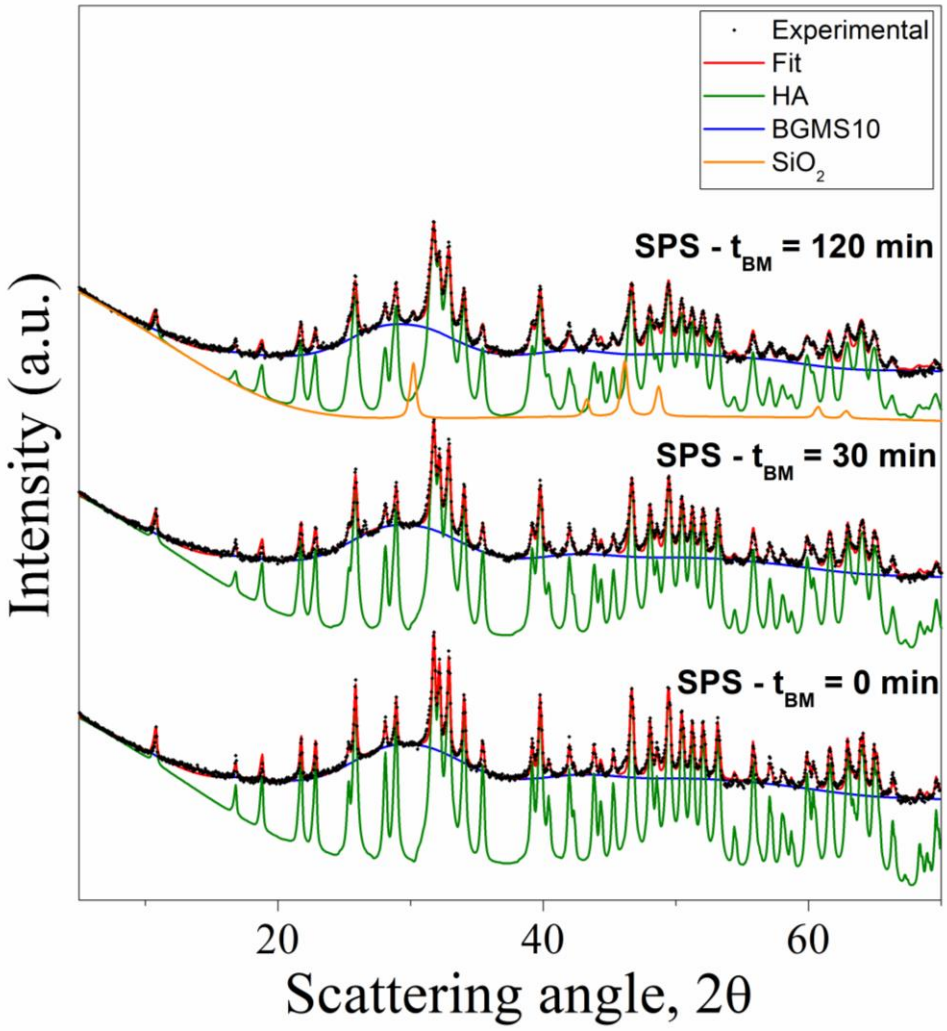

Figure 8. XRD patterns of dense composite samples obtained from the unmilled (t_{BM} = 0 min) and milled powders. Black dots are experimental data, and the red line is the calculated fit. Deconvoluted amorphous BGMS10, hydroxyapatite, and quartz (SiO_2) phases are indicated by blue, green, and orange full lines, respectively.

The formation of a crystalline phase during SPS likely provides a further explanation for justifying the sample density decrease when the milling treatment was extended from 30 to

120 min (**Fig. 7**). Indeed, the occurrence of crystallization phenomena during consolidation of BGMS10 and other glass powders by SPS was found to correspond to relatively less dense products **[40,47]**.

3.3 Microstructural and Mechanical characterization

SEM images of the surface of the sintered composites are shown in **Fig. 9**. The samples appear very similar one to each other, are adequately consolidated, and possess a dense microstructure, apart from some local defects and residual microporosity. This fact confirms the effectiveness of the sintering protocol and is in accordance with the results of the density measurements **(Table 2)**. The more detailed SEM-EDS analysis conducted on the 0/850-16 sample (supplementary **Fig. S3**) evidenced that residual porosity is confined to rounded regions corresponding to the HA constituent. On the other hand, the glassy counterpart in the composite appears to be fully consolidated.

The mechanical properties of the composites (Young's modulus and hardness), as measured by micro-indentation tests, are reported in **Table 2**. In general, the obtained results are analogous or even slightly better than those recently obtained for BGMS10 powders sintered by SPS **[40]**, in particular for 0/850-16 and 30/800-70 samples. This demonstrates the beneficial contribution exerted by the HA phase in the composite; it should be stressed that pure HA, when consolidated by SPS, tends to have better mechanical properties than BGMS10 products obtained by the same technique **[45]**, although it is not straightforward to compare the performance of such samples, given the different processing parameters employed to sinter them, i.e. T_D=1200°C (HA) **[45]**, and T_D=750-950 °C (BGMS10) **[40]**. In addition, it should be also noted that the composite samples investigated in this work possess lower relative densities (in the range 92.4-95.9) compared to those resulting from pure HA (fully dense) **[45]**, and BGMS10 (in the range 98.6-99.6%) **[40]**

The results reported in **Table 2** reveal an increment of both the local elastic modulus and hardness with increasing holding temperature in the set of samples obtained from unmilled powders (i.e., 0/800-70 and 0/850-16). This fact can be ascribed to the increased density of

the samples treated at higher temperature and to the progressive crystallization of their glassy phase, with the concurrent formation of α- and β-$CaSiO_3$ (see **Fig. 6**); in fact, a slight devitrification of the glass phase is expected to increase the mechanical performance of HA/BG composites, as crystalline phases are usually mechanically stronger than their parent glass **[48,49]**. On the other hand, a too wide crystallization should be avoided in this kind of samples, as the development of new phases may also imply non-trivial changes in specific volumes, with a reduction in the final density and compactness of the sintered composite **[40,47]**; in turn, a density reduction is typically associated to a decrease of the mechanical performance. The differences in the Young's modulus of the samples prepared at the same holding temperature (i.e., 800 °C), but with increasing milling times of the starting powders (i.e., ~~unmilled~~ 0 min, 30 min and 120 min ball milling), may be also explained in terms of the different degree of density and compactness achieved after sintering (see **Figs. 5** and **7, Table 2**).

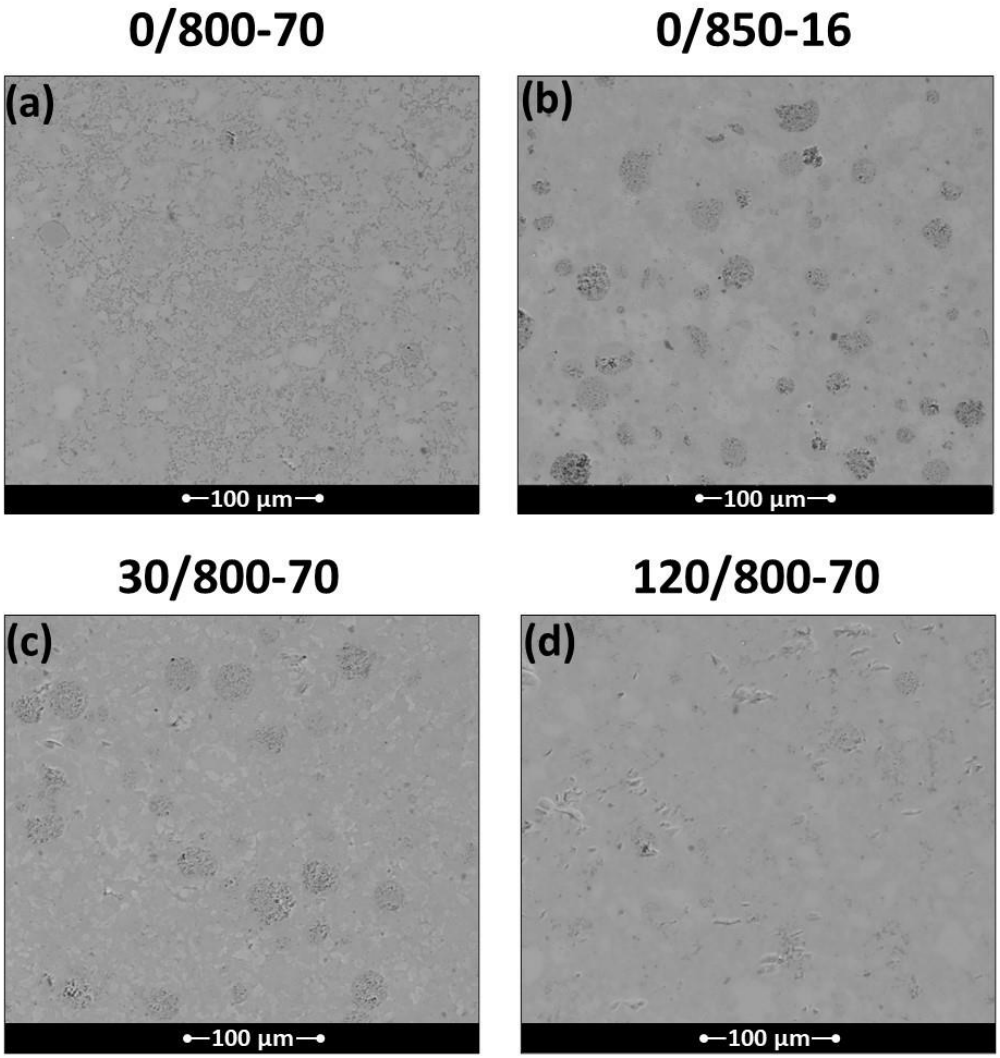

Figure 9. The surface of the sintered disks, showing an excellent densification.

Table 2 Young's modulus and hardness of the investigated samples, as determined by micro-indentation tests. The corresponding relative density values are also reported.

Sample	Relative density (%)	Young's Modulus (GPa)	Hardness (Vickers)
0/800-70	94.2	95.24 ± 2.47	509.88 ± 34.29
0/850-16	95.9	116.39 ± 4.49	697.61 ± 26.89
30/800-70	94.7	122.33 ± 3.58	675.32 ± 38.45
120/800-70	92.4	98.01 ± 4.55	683.22 ± 42.21

3.4 *In vitro* bioactivity

The bioactivity of the produced composites has been evaluated *in vitro* by immersing them in a Simulated Body Fluid solution, which contains an ionic concentration similar to that of human plasma **[44]**. As BGs bond to bone through the formation of a superficial HA film, which mimics the mineral phase of bone tissue, the bone-bonding aptitude of bioactive glasses and bioactive glass-based composites can be easily estimated by studying the ability of HA to form on the samples' surface during their immersion in SBF for different periods of time. These findings are widely employed to preliminary check the reactivity of a potential bioactive material in physiological environment.

The results of the SEM analysis performed on HA/BGMS10 disks after 7 and 14 days in SBF are shown in **Fig. 10**. It is evident that the process parameters – in particular, the milling time of the starting powders and the holding temperature – influence the bioactivity of the samples in a non-trivial way. After one week, the surface of all the produced composites appeared highly degraded, with a widespread porosity due to the dissolution of the samples and their ionic release. After 14 days in SBF, the composites were characterized by different degree of bioactivity; in particular, the sample 0/850-16 showed an almost absence of surface precipitates ascribable to HA. This behaviour can be partially attributed to the crystallization of the glass phase with the concurrent formation of α- and β-$CaSiO_3$, two phases characterized by a slower in vitro reactivity and, therefore, by a less marked bioactivity compared to that of the parent glass **[50]**. All the samples produced with a lower holding temperature (i.e., 800 °C) appeared bioactive after two weeks of soaking, with different degree of reactivity depending on the milling time. It should be noted the extraordinary bioactivity of the 30/800-70 samples, whose surface, already after a week, is highly degraded and completely covered by white precipitates with the typical morphology of *in vitro* formed HA. The X-EDS analysis reported in **Fig. 11** confirms the presence of precipitates rich in calcium and phosphorus, with a Ca/P ratio which gradually approaches that of stoichiometric HA.

The chemical nature of the globular precipitates formed on the sintered disks after immersion in SBF has been further investigated by means of a Raman microscope. In fact,

such technique can be used to locally identify the presence of HA, as the main Raman peaks of the P–O vibrational modes are particularly intense; moreover, since the in vitro grown HA is typically carbonated and the Raman spectroscopy is sensitive to the C–O vibrational modes, the presence of carbonated groups was also verified. **Fig. 12** reports the Raman spectra acquired on the phosphorus and calcium rich precipitates which formed on the 30/800-70 samples after 7 and 14 days in SBF (since the spectra obtained from the other samples are very similar, they are not reported for the sake of brevity). Already after 7 days in SBF, the Raman spectra are dominated by the characteristic peaks of carbonated HA, as reported by the literature [51–53]:

- a very sharp peak at ~960 cm^{-1}, which is related to the symmetric stretching mode of the PO_4 groups;
- two broad peaks at ~430 cm^{-1} and ~590 cm^{-1}, ascribable to the bending modes of the same group;
- a broad peak at about 1070 cm^{-1}, which is imputable to the symmetric stretching mode of the CO_3 groups.

It is then possible to conclude that the precipitates are mainly composed of carbonated HA, thus confirming the marked bioactivity of the produced samples.

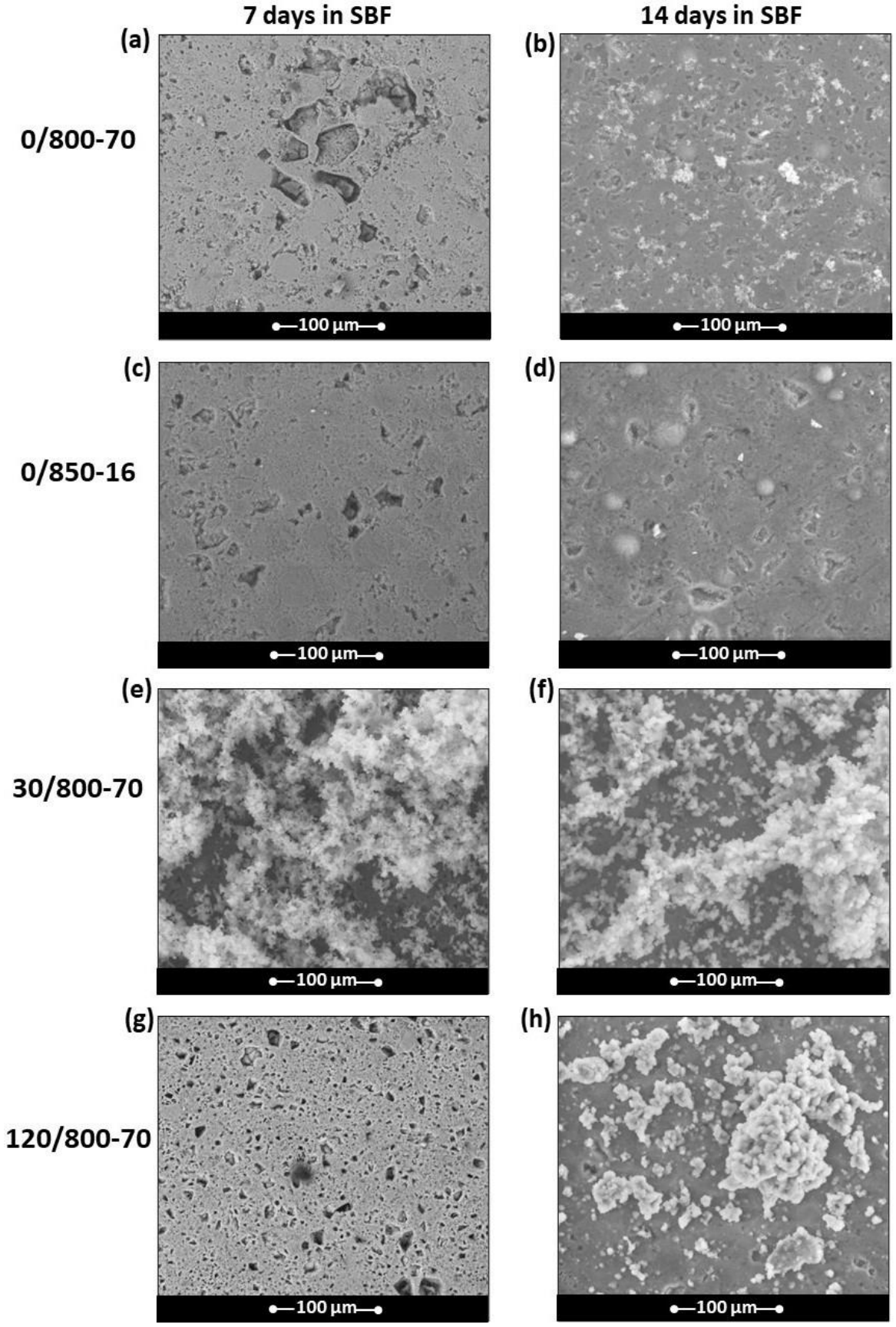

Figure 10. SEM images of the sintered samples after soaking them in SBF for 7 and 14 days. It should be noted the marked HA precipitation on the 30/800-70 samples already after 7 days of immersion.

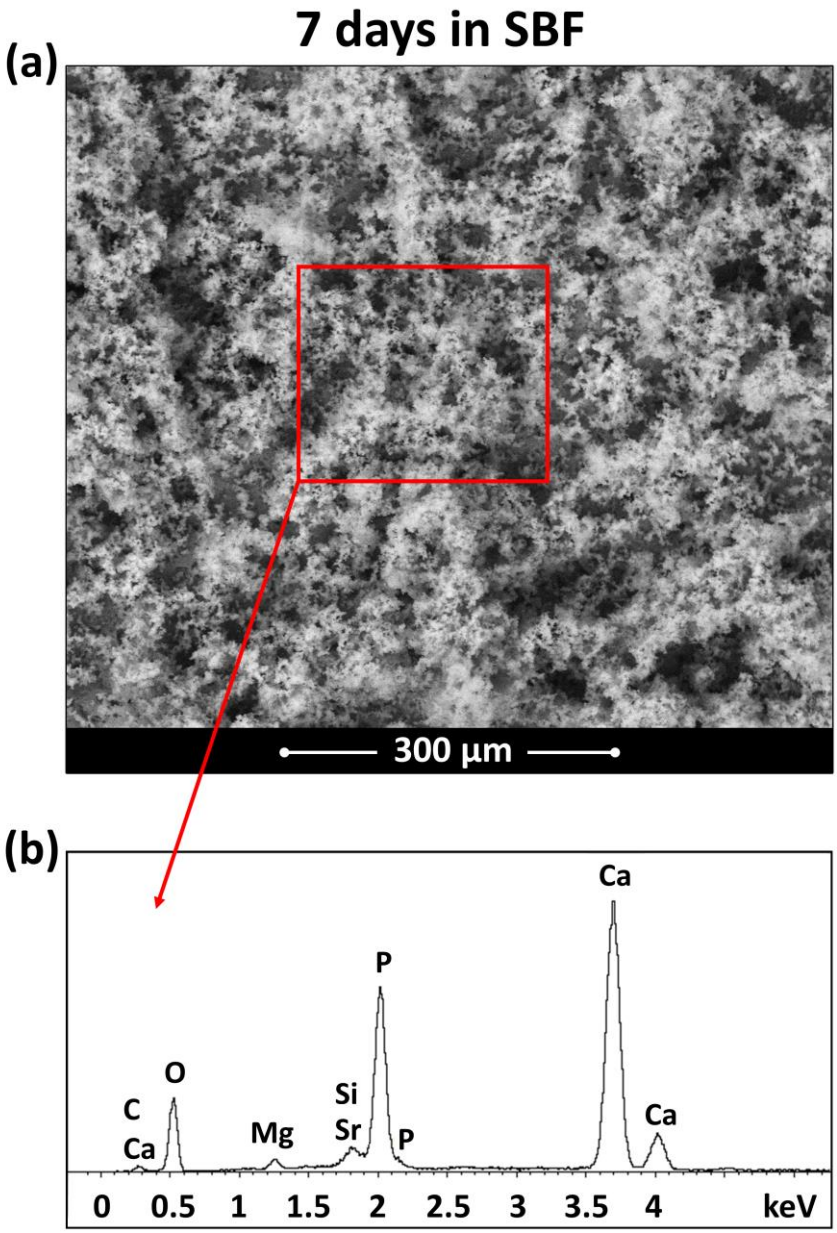

Figure 11. (a) HA formed on the 30/800-70 sample after 7 days in SBF and (b) results of the X-EDS analysis performed on the area shown in (a).

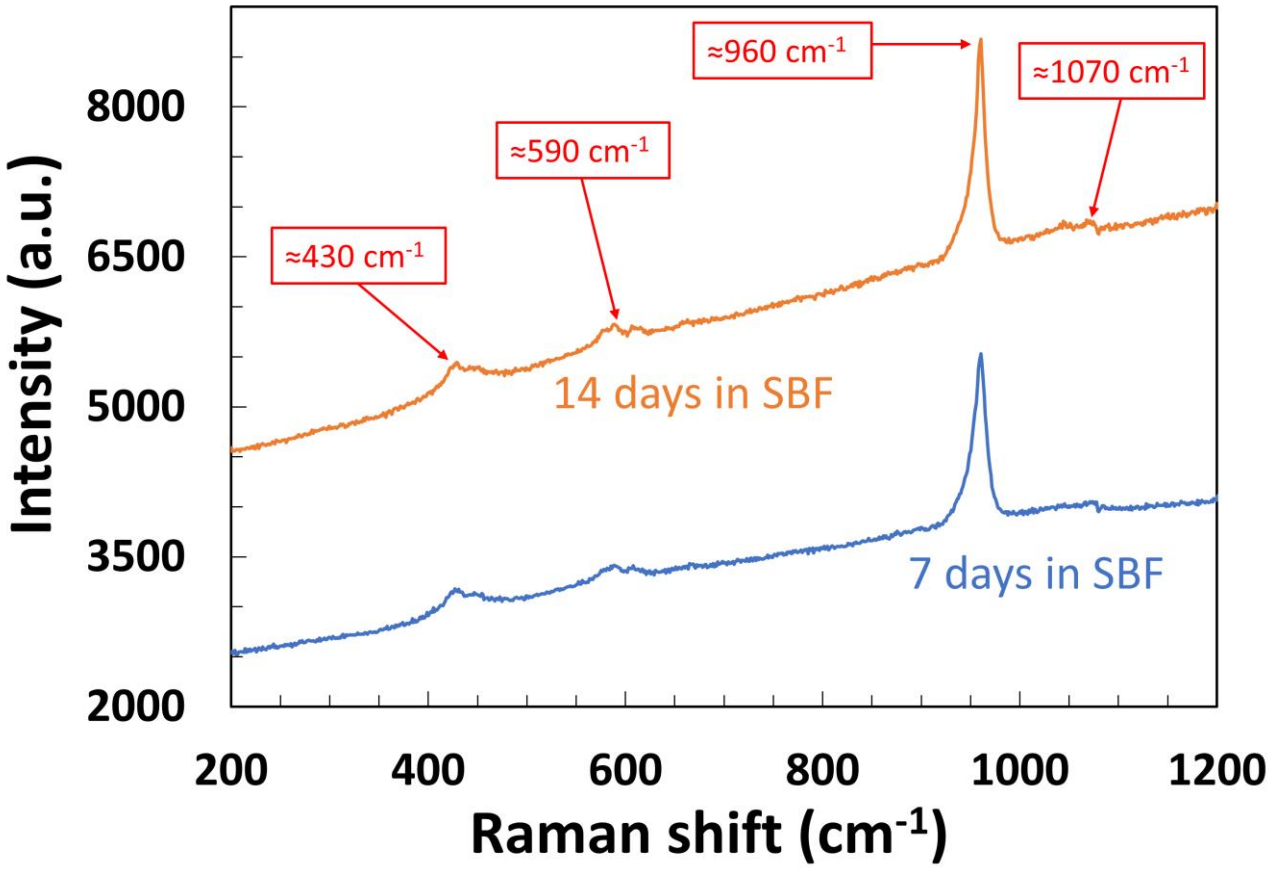

Figure 12. Raman spectra acquired on the calcium and phosphorus rich precipitates formed on the 30/800-70 samples after 7 and 14 days in SBF.

To justify the surprisingly different bioactivity behavior exhibited during in-vitro test by HA/BGMS10 sintered samples when the starting composite powders are mechanically treated prior to SPS, some considerations will be made in what follows. First, as mentioned in the introduction, structural changes, as well as the formation of intimate interfaces among the different processed constituents, are induced by BM. This feature also emerges in this work from the analysis of the three sets of powders. A progressive crystallite size refinement of the HA phase from > 2000 Å (untreated) to 700 Å (t_{BM}=30 min), and 470 Å (t_{BM}=120 min), was correspondingly achieved. Although an unavoidable crystallites growth occurred during their heat treatment by SPS, the samples corresponding to milled powders were still nanostructured, with crystallite size in the range 85-90 nm. Such fine microstructure corresponds to a broader grain boundary area compared to the unmilled sample, so that

composite reactivity, dissolution, and ion-exchange phenomena, as well as the nucleation of the new apatite phase, during SBF test, are expected to be highly promoted.

The formation of intimate composite mixtures induced by the BM treatment, as evidenced by particle size analysis and TEM observation, could also have played a role for the observed enhancement of SPS samples reactivity. The features above could be considered the main factors responsible for the marked bioactivity improvement which came out from SBF test results involving sintered samples prepared using 30 min milled powders. Such considerations are also valid when considering the 2h milled specimen, since the latter one also displays improved HA-forming ability (**Fig.10 (g)-(h)**) with respect to the unmilled (t_{BM} = 0 min) sample (**Fig.10 (a)-(b)**). Nonetheless, product bioactivity was relatively reduced with a prolonged milling treatment. The main structural/compositional difference observed when t_{BM} was increased from 30 to 120 min was the formation of SiO_2 in the bulk SPS products, while very similar HA crystallites size were obtained (90 or 85 nm, respectively). Therefore, the presence of crystalline SiO_2, which is certainly less bioactive than the original glass phase, apparently slows down the apatite-forming ability of the composite.

4 Summary and concluding remarks

The densification behaviour, mechanical properties, and biological response in SBF, of four groups of samples obtained by SPS from unmilled and ball milled (30 and 120 min, CR=2) composite mixture (50/50 wt.%) consisting of HA and BGMS10 glass powders ~~was investigated in detail.~~ can be briefly summarized in what follows.

a) No crystallization from the glassy phase is observed in bulk samples (93-94.2% dense) obtained by SPS at 800°C from unmilled powders; samples density is improved at 850°C, α- and β-$CaSiO_3$ are formed, Young modulus and Vickers Hardness are higher (from 95 to 116 GPa and from 510 to 698, respectively), whereas the related HA-forming ability during 14 days SBF test is very scarce.

b) HA crystallites size growth is highly retained (from 70 to 90 nm) during SPS of 30 min milled powders; the obtained samples show superior Young's Modulus (122 GPa),

Vickers Hardness (675) and, above all, an extraordinary biological response, being their surface completely covered by HA precipitates just after 7 days immersion in SBF. These findings can be explained by the increased surface area and the significant reduction of HA crystallites size (from above 200 to 70 nm) induced in the powders by the mechanical treatment.

c) The extension to 120 min of the BM process is self-defeating, as it results in less dense products with poorer mechanical properties and lower in-vitro bioactivity. The formation of crystalline SiO_2 during SPS is postulated to be responsible for such outcome.

~~The mechanical treatment was found to produce progressively larger composite agglomerates, an increase of the surface area, and a significantly reduction of HA crystallites size, from the micrometer-submicrometer range, i.e. >200 nm (unmilled), to the nanometer range, i.e. about 70 and 47 nm, for 30 and 120 min milled powders, respectively. As for the fabrication of bulk composites, the optimal temperature to avoid crystallization from the glass phase using unmilled powders was found to be 800°C and the resulting composites were 93.0 (P=16 MPa) or 94.2 % (P=70 MPa) dense. When the holding temperature was raised to 850°C, relative density increased to 95.9% (P=16 MPa) but α- and β-$CaSiO_3$ crystalline phases were also formed. The latter samples displayed higher mechanical properties (Young modulus and Vickers Hardness equal to 116 GPa and 698, respectively) compared to the composite products where the amorphous nature of the glass was fully preserved (95 GPa and 510, respectively). However, the related HA-forming ability up to 14 days during SBF test was very scarce.~~

~~A slight densification improvement (from 94.2 to 94.7%) was obtained by SPS (800°C/70MPa) when the composite powders were subjected to a milling treatment of 30 min duration. In addition, HA crystallites size growth was highly retained during SPS (from 70 to 90 nm) while the glass phase entirely maintained its original character. Superior Young's Modulus (122 GPa) and Vickers Hardness (675) were correspondingly measured compared to samples obtained from untreated powders. Very interesting and unexpected was the extraordinary biological response induced by the 30 min BM treatment, being the~~

~~corresponding SPS samples completely covered on their surface by HA precipitates just after 7 days immersion in SBF.~~

~~In contrast, when the 2h milled batch of powders was used, less dense samples with poorer mechanical properties and lower in-vitro bioactivity, compared to the case of t_{BM}=30 min, were obtained under the same SPS conditions. All these outcomes can be ascribed to the formation of crystalline SiO_2 during sintering. The microstructural changes induced by the prolonged BM treatment are expected to be responsible for the nucleation and segregation of this new phase from the glass, whose presence, apparently, plays a negative role on the performances of the resulting bulk composite.~~

Based on the results above, it is expected that BM could represent a promising tool, if utilized under proper conditions, for improving the bioactivity of composite systems of potential interest in regenerative medicine.

Future work will be devoted to a comprehensive biological characterization, to further corroborate the findings of this work; specifically other in-vitro tests will be carried out, such as cellular direct and indirect tests. Moreover, an in vivo study will be performed on the most promising products.

Acknowledgements

Damiano Angioni performed his activity in the framework of the International PhD in Innovation Sciences and Technologies at the University of Cagliari, Italy. The authors acknowledge the GAUSS-CeSAR (Centro Servizi d'Ateneo per la Ricerca) of the University of Sassari for TEM analyses. Thanks are due to Dr. Francesco Loy (University of Cagliari) for his technical assistance during SEM-EDS analysis. The authors acknowledge the funding FAR 2021 (Dipartimento di Ingegneria "Enzo Ferrari", Università degli Studi di Modena e Reggio Emilia, Italy).

5 References

[1] Bone Repair Biomaterials. In Woodhead Publishing Series in Biomaterials Editors: J.A. Planell, S.M. Best, D. Lacroix, A. Merolli, Woodhead Publishing, (2009) ISBN 978-1845693855.

[2] A.S. Mao, D.J. Mooney, Regenerative medicine: Current therapies and future directions Proc. Natl. Acad. Sci. U.S.A. 112(47), (2015) pp. 14452-14459 https://doi.org/10.1073/pnas.1508520112

[3] R. Comesaña, F. Lusquiños, J. Del Val, F. Quintero, A. Riveiro, M. Boutinguiza, J.R. Jones, R.G. Hill, J. Pou, Toward smart implant synthesis: Bonding bioceramics of different resorbability to match bone growth rates. Sci. Rep. 5, (2015) 10677 https://doi.org/10.1038/srep10677

[4] E. Saiz, A.R. Boccaccini, J. Chevalier, M. Peroglio, Editorial on Bioceramics for Bone Repair. J. Eur. Ceram. Soc. 38(3), (2018), pp. 821-822. https://doi.org/10.1016/j.jeurceramsoc.2017.11.036

[5] Bioceramics and their Clinical Applications. In Woodhead Publishing Series in Biomaterials, Editor: Tadashi Kokubo, Woodhead Publishing, 2008, ISBN 978-1845692049

[6] S.V. Dorozhkin, Calcium orthophosphate bioceramics Ceram. Int. 41(10), (2015), pp. 13913–13966. https://doi.org/10.1016/j.ceramint.2015.08.004

[7] N.C. Paxton, S.K. Powell, M.A. Woodruff, Biofabrication: The future of regenerative medicine. Tech. Orthop. 31(3), (2016), pp. 190-203 https://doi.org/10.1097/BTO.0000000000000184

[8] A.R. Boccaccini, Q. Chen, L. Lefebvre, L. Gremillard, J. Chevalier, Sintering, crystallization and biodegradation behaviour of bioglass®-derived glass–ceramics, Faraday Discuss. 136, (2007), pp. 27–44. https://doi.org/10.1039/b616539g

[9] L.C. Gerhardt, A.R. Boccaccini, Bioactive Glass and Glass-Ceramic Scaffolds for Bone Tissue Engineering, Materials 3, (2010), 3867. https://doi.org/10.3390/ma3073867

[10] S. Grasso, R.K. Chinnam, H. Porwal, A.R. Boccaccini, M.J. Reece, Low temperature spark plasma sintering of 45S5 Bioglass®, J. Non-Cryst. Solids. 362, (2013), pp. 25-29. https://doi.org/10.1016/j.jnoncrysol.2012.11.009

[11] J.R. Jones Review of bioactive glass: from Hench to hybrids. Acta Biomater. 9, (2013) pp. 4457-4486. https://doi.org/10.1016/j.actbio.2012.08.023

[12] L.L. Hench, Genetic design of bioactive glass. J. Eur. Ceram. Soc. 9, (2009), pp. 1257–1265. https://doi.org/10.1016/j.jeurceramsoc.2008.08.002

[13] J. Kolmas, A. Jaklewicz, A. Zima, M. Bućko, Z. Paszkiewicz, J. Lis, A. Slósarczyk, W. Kolodziejski, Incorporation of carbonate and magnesium ions into synthetic hydroxyapatite: the effect on physicochemical properties, J. Mol. Struct. 987, (2011), pp. 40–50. https://doi.org/10.1016/j.molstruc.2010.11.058

[14] S. Von Euw, Y. Wang, G. Laurent, C. Drouet, F. Babonneau, N. Nassif, T. Azaïs, Bone mineral: new insights into its chemical composition. Sci. Rep. 9(1), (2019), 8456 https://doi.org/10.1038/s41598-019-44620-6

[15] J.C. Knowles, W. Bonfield. Development of a glass reinforced hydroxyapatite with enhanced mechanical properties. The effect of glass composition on mechanical properties and its relationship to phase changes. J. Biomed. Mater. Res. 27 (1993), pp. 1591–1598. https://doi.org/10.1002/jbm.820271217

[16] L.J. Jha, J.D. Santos, J.C. Knowles, Characterization of apatite layer formation on P_2O_5-CaO, P_2O_5-CaO-Na_2O, and P_2O_5-CaO-$Na_2OAl_2O_3$ glass hydroxyapatite composites. J Biomed Mater Res. 31, (1996). pp. 481–486. https://doi.org/10.1002/(sici)1097-4636(199608)31:4%3C481::aid-jbm7%3E3.0.co;2-h

[17] J.D. Santos, R.L. Reis, F.J. Monteiro, J.C. Knowles, G.W. Hastings. Liquid phase sintering of hydroxyapatite by phosphate and silicate glass additions: Structure and properties of the composites. J. Mater. Sci. Mater. Med. 6, (1995), pp. 348–352. https://doi.org/10.1007/BF00120303

[18] J.D. Santos, P.L. Silva, J.C. Knowles, S. Talal, F.J. Monteiro. Reinforcement of hydroxyapatite by adding P2O5-CaO glasses with Na2O, K2O and MgO. J. Mater. Sci. Mater. Med. 7, (1996), pp. 187–189. https://doi.org/10.1007/BF00121259

[19] D. Tanaskovic, B. Jokic, G. Socol, A. Popescu, I.N. Mihailescu, R. Petrovic, Dj. Janackovic, Synthesis of functionally graded bioactive glass-apatite multistructures

on Ti substrates by pulsed laser deposition. Appl. Surf. Sci. 254(4), (2007), pp. 1279-1282. https://doi.org/10.1016/j.apsusc.2007.08.009

[20] D. Bellucci, A. Sola, V. Cannillo. Bioactive glass-based composites for the production of dense sintered bodies and porous scaffolds. Mater. Sci. Eng. C 33, (2013), pp. 2138–2151. https://doi.org/10.1016/j.msec.2013.01.029

[21] D. Bellucci, A. Sola, A. Anesi, R. Salvatori, L. Chiarini, V. Cannillo, Bioactive glass/hydroxyapatite composites: Mechanical properties and biological evaluation, Mater. Sci. Eng. C 51, (2015), pp. 196–205. https://doi.org/10.1016/j.msec.2015.02.041

[22] D. Bellucci, L. Desogus, S. Montinaro, R. Orrù, G. Cao, V. Cannillo, Innovative hydroxyapatite/bioactive glass composites processed by spark plasma sintering for bone tissue repair. J. Eur. Ceram. Soc. 37(4), (2017), pp. 1723–1733 https://doi.org/10.1016/j.jeurceramsoc.2016.11.012

[23] D. Bellucci, R. Salvatori, A. Anesi, L. Chiarini, V. Cannillo, SBF assays, direct and indirect cell culture tests to evaluate the biological performance of bioglasses and bioglass-based composites: Three paradigmatic cases. Mater. Sci. Eng. C 96, (2019) pp. 757–764 https://doi.org/10.1016/j.msec.2018.12.006

[24] S. Mondal, G. Hoang, P. Manivasagan, M.S. Moorthy, T.P. Nguyen, T.T. Vy Phan, H.H. Kim, M.H.; Kim, S.Y., Nam, J. Oh, Nano-hydroxyapatite bioactive glass composite scaffold with enhanced mechanical and biological performance for tissue engineering application. Ceram. Int. 44(13), (2018), pp. 15735-15746 https://doi.org/10.1016/j.ceramint.2018.05.248

[25] J.A. Rincón-López, J.A. Hermann-Muñoz, D.A. Fernández-Benavides, A. David, A.L. Giraldo-Betancur, J.M.,Alvarado-Orozco, J. Muñoz-Saldaña, Isothermal phase transformations of bovine-derived hydroxyapatite/bioactive glass: A study by design of experiments. J. Eur. Ceram. Soc. 39(4), (2019), pp. 1613-1624 https://doi.org/10.1016/j.jeurceramsoc.2018.11.021

[26] M. Luginina, D. Angioni, S. Montinaro, R. Orrù, G. Cao, R. Sergi, D. Bellucci, V. Cannillo, Hydroxyapatite/bioactive glass functionally graded materials (FGM) for

bone tissue engineering, J. Eur. Ceram. Soc. 40, (2020), pp. 4623-4634. https://doi.org/10.1016/j.jeurceramsoc.2020.05.061

[27] M. Lakrat, M. Jabri, M. Alves, M.H. Fernandes, L.L. Ansari, C. Santos, E.M. Mejdoubi, Three-dimensional nano-hydroxyapatite sodium silicate glass composite scaffold for bone tissue engineering - A new fabrication process at a near-room temperature Mater. Chem. Phys. 260, (2021), 124185 https://doi.org/10.1016/j.matchemphys.2020.124185

[28] D. Reffitt, N. Ogston, R. Jugdaohsingh, H. Cheung, B. Evans, R. Thompson, J.J. Powell, G.N. Hampson, Orthosilicic acid stimulates collagen type I synthesis and osteoblastic differentiation in human osteoblastlike cells in vitro. Bone 32, (2003), pp 127–135. https://doi.org/10.1016/s8756-3282(02)00950-x

[29] M. Dong, G. Jiao, H. Liu, W. Wu, S. Li, Q. Wang, D. Xu, X. Li, H. Liu, Y. Chen, Biological Silicon Stimulates Collagen Type 1 and Osteocalcin Synthesis in Human Osteoblast-Like Cells Through the BMP-2/Smad/RUNX2 Signaling Pathway. Biol Trace Elem Res. 173, (2016), pp. 306-15. https://doi.org/10.1007/s12011-016-0686-3

[30] O. Bretcanu, X. Chatzistavrou, K. Paraskevopoulos, R. Conradt, I. Thompson, A.R. Boccaccini, Sintering and crystallization of 45S5 bioglass® powder, J. Eur. Ceram. Soc. 29, (2009), pp. 3299–3306. https://doi.org/10.1016/j.jeurceramsoc.2009.06.035

[31] D. Bellucci, A. Sola, V. Cannillo, Low temperature sintering of innovative bioactive glasses. J. A. Ceram. Soc. 95 (2012) pp. 1313–1319. https://doi.org/10.1111/j.1551-2916.2012.05100.x

[32] D. Bellucci, V. Cannillo, A novel bioactive glass containing strontium and magnesium with ultra-high crystallization temperature, Mater. Lett. 213, (2018), pp. 67-70. https://dx.doi.org/10.1016/j.matlet.2017.11.020

[33] C. Suryanarayana, Mechanical alloying and milling. Prog. Mater. Sci. 46(1-2), (2001), pp. 1-184. https://doi.org/10.1016/S0079-6425(99)00010-9

[34] D. Maurice, T.H. Courtney, Milling dynamics: Part. II. dynamics of a SPEX mill and a one-dimensional mill. Metall. Mater. Trans. A: Phys. Metall. Mater. Sci. 27(7), (1996), pp. 1973–1979 https://doi.org/10.1007/BF02651947

[35] F. Delogu, M. Monagheddu, G. Mulas, L. Schiffini, G. Cocco, Impact characteristics and mechanical alloying processes by ball milling: experimental evaluation and modelling outcomes. Int. J. Non-Equilib. Process. 11(3), (2000), pp. 235–269

[36] High-Energy Ball Milling, Editor(s): Małgorzata Sopicka-Lizer, Woodhead Publishing, (2010) ISBN 978-1845695316

[37] N.F. Ibrahim, H. Mohamad, S.N.F.M. Noor, Effects of milling media on the fabrication of melt-derived bioactive glass powder for biomaterial application. AIP Conf. Proc. 1791, (2016), 010011. https://doi.org/10.1063/1.4968865

[38] D. Bovand, M. R. Allazadeh, S. Rasouli, E. Khodadad, E. Borhani, Studying the effect of hydroxyapatite particles in osteoconductivity of Ti-HA bioceramic. J. Aust. Ceram. Soc. 55, (2019), pp. 395–403 https://doi.org/10.1007/s41779-018-0247-7

[39] G.K. Pouroutzidou, G.S. Theodorou, E. Kontonasaki, L. Papadopoulou, N. Kantiranis, D. Patsiaoura, K. Chrissafis, C.B. Lioutas, K.M. Paraskevopoulos, Synthesis of a bioactive nanomaterial in the ternary system SiO2-CaO-MgO doped with CuO: The effect of Ball milling on the particle size, morphology and bioactive behavior. AIP Conf. Proc. 2075, (2019), 200005. https://doi.org/10.1063/1.5091430

[40] D. Angioni, R. Orrù, G. Cao, S. Garroni, A. Iacomini, D. Bellucci, V. Cannillo, Spark Plasma Sintering, Mechanical and In-vitro Behavior of a Novel Sr- and Mg-Containing Bioactive Glass for Biomedical Applications, J. Eur. Ceram. Soc. 42, (2022), pp. 1776–1783 https://doi.org/10.1016/j.jeurceramsoc.2021.11.061

[41] L. Lutterotti, R. Ceccato, R. Dal Maschio, E. Pagani, Quantitative analysis of silicate glass in ceramic materials by the Rietveld method. Mater. Sci. Forum 87, (1998), pp. 278-281. https://doi.org/10.4028/www.scientific.net/MSF.278-281.87

[42] F.L. Matthews, R. Rawlings. Composite Materials: Engineering and Science. Chapman & Hall, Great Britain; 1994.

[43] W. Oliver, G. Pharr, An improved technique for determining hardness and elastic modulus using load and displacement sensing indentation experiments. J. Mater. Res. 7, (1992), pp. 1564–1583. https://doi.org/10.1557/JMR.1992.1564

[44] T. Kokubo, H. Takadama, How useful is SBF in predicting in vivo bone bioactivity? Biomaterials 27, (2006), pp. 2907–2915. https://doi.org/10.1016/j.biomaterials.2006.01.017

[45] A. Cuccu, S. Montinaro, R. Orrù, G. Cao, D. Bellucci, A. Sola, V. Cannillo, Consolidation of different Hydroxyapatite powders by SPS: optimization of the sintering conditions and characterization of the obtained bulk products, Ceram. Int. 41(1), (2015), pp. 725-736. https://doi.org/10.1016/j.ceramint.2014.08.131

[46] M. Baricco, T.A. Baser, S. Enzo, G. Vaughan, A.R. Yavari, Analysis of crystallization behavior of $Fe_{48}Cr_{15}Mo_{14}Y_2C_{15}B_6$ bulk metallic glass by synchrotron radiation. J. Mater. Res. 23, (2008), pp. 2166-2173. https://dx.doi.org/10.1557/JMR.2008.0264

[47] L. Desogus, A. Cuccu, S. Montinaro, G. Cao, D. Bellucci, A. Sola, V. Cannillo, Classical Bioglass® and innovative CaO-rich bioglass powders processed by Spark Plasma Sintering: A comparative study. J. Eur. Ceram. Soc. 5(15), (2015) pp. 4277-4285. https://doi.org/10.1016/j.jeurceramsoc.2015.07.023

[48] G. Kaur, V. Kumar, F. Baino, J.C. Mauro, G. Pickrell, I. Evans, O. Bretcanu, Mechanical properties of bioactive glasses, ceramics, glass-ceramics and composites: State-of-the-art review and future challenges, Mater. Sci. Eng. C 104 (2019), 109895. https://doi.org/10.1016/j.msec.2019.109895

[49] J.K.M.F. Daguano, K. Strecker, E.C. Ziemath, S.O. Rogero, M.H.V. Fernandes, C. Santos, Effect of partial crystallization on the mechanical properties and cytotoxicity of bioactive glass from the 3CaO.P2O5–SiO2–MgO system, J. Mech. Behav. Biomed. Mater. 14, (2012), pp. 78-88, https://doi.org/10.1016/j.jmbbm.2012.04.024

[50] L.A. Núñez-Rodríguez, M.A. Encinas-Romero, A. Gómez-Álvarez, J.L. Valenzuela-García, G.C. Tiburcio-Munive, Evaluation of Bioactive Properties of α and β Wollastonite Bioceramics Soaked in a Simulated Body Fluid, J. Biomater. Nanobiotechnol. 9, (2018), pp. 263-276. https://doi.org/10.4236/jbnb.2018.93015

[51] F.A. Shah, Towards refining Raman spectroscopy-based assessment of bone composition, Sci. Rep. 10, (2020), 16662. https://doi.org/10.1038/s41598-020-73559-2

[52] E. Cañas, M.J. Orts, E. Sánchez, D. Bellucci, V. Cannillo, Deposition of bioactive glass coatings based on a novel composition containing strontium and magnesium, J. Eur. Ceram. Soc. 42, (2022), pp. 6213–6221. https://doi.org/10.1016/j.jeurceramsoc.2022.05.064

[53] J. Liu, U. Glasmacher, M. Lang, C. Trautmann, K.-O. Voss, R. Neumann, G.A. Wagner, R. Miletich, Raman spectroscopy of apatite irradiated with swift heavy ions with and without simultaneous exertion of high pressure, Appl. Phys. A 91, (2008), pp 17–22. https://doi.org/10.1007/s00339-008-4402-9

Figure 1a

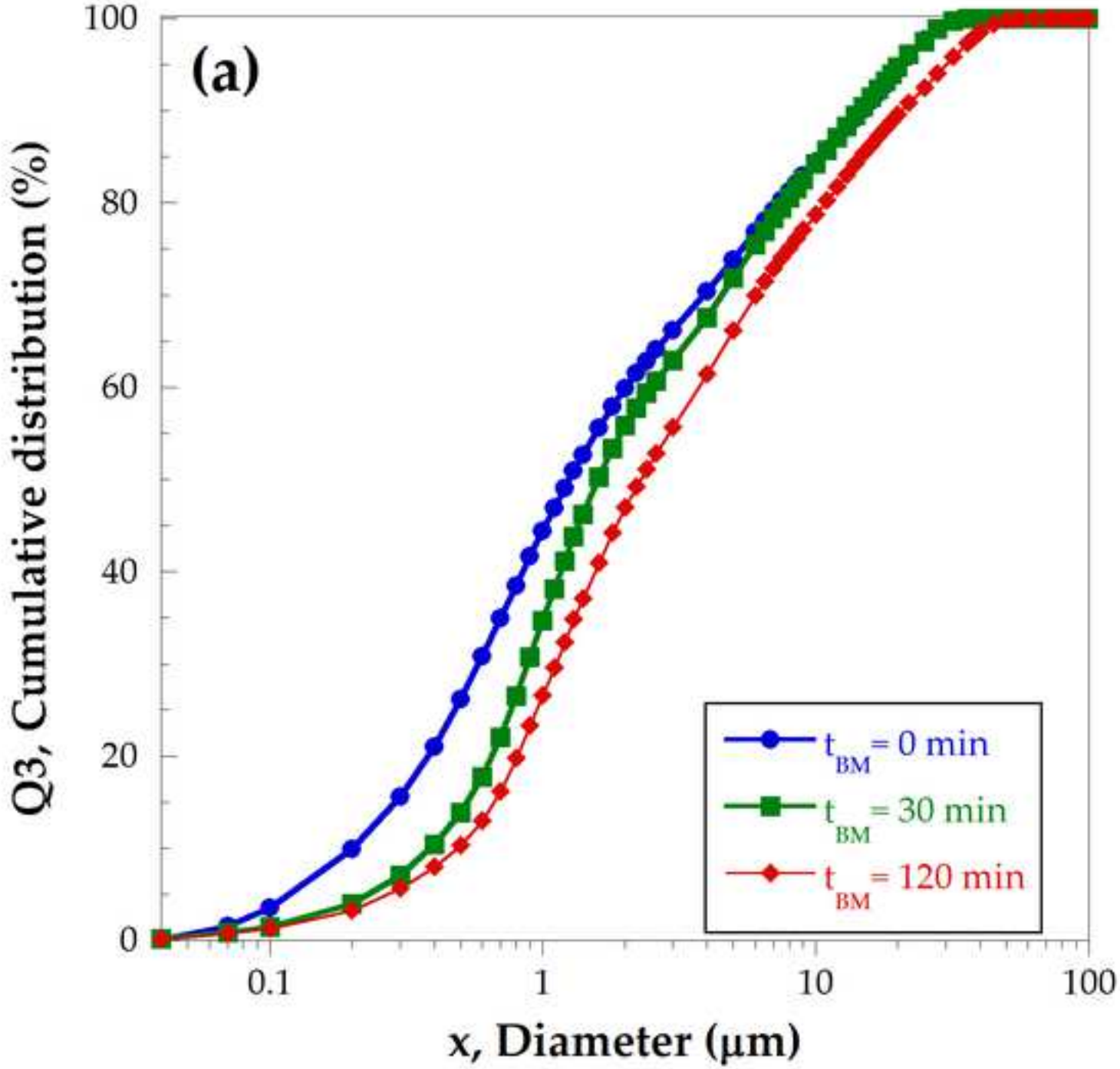

Figure 1b

Click here to access/download;Figure;Figure 1b.tif

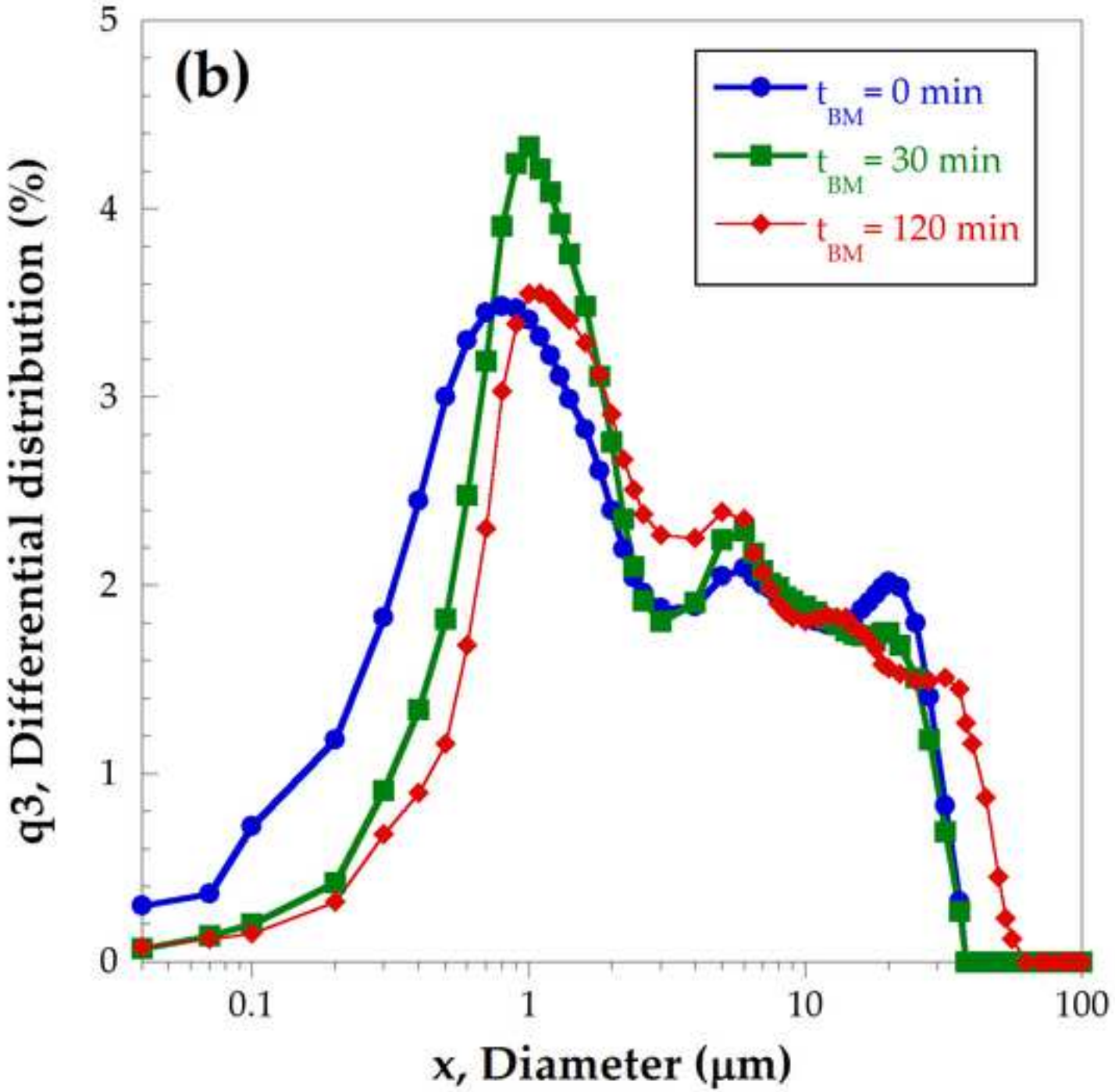

Figure 2

Click here to access/download;Figure;Figure 2.tif

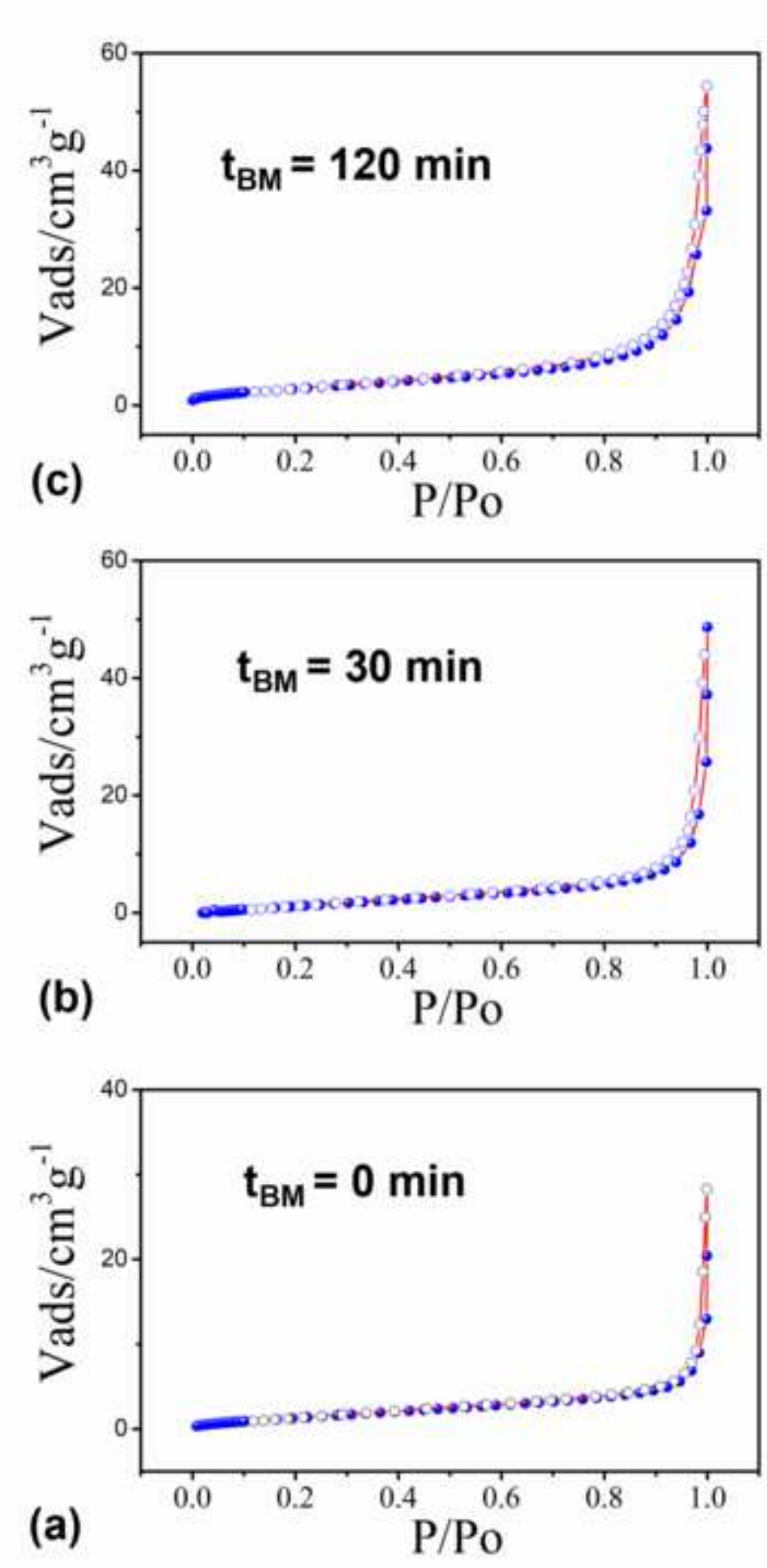

Figure 3

Click here to access/download;Figure;Figure 3.tif

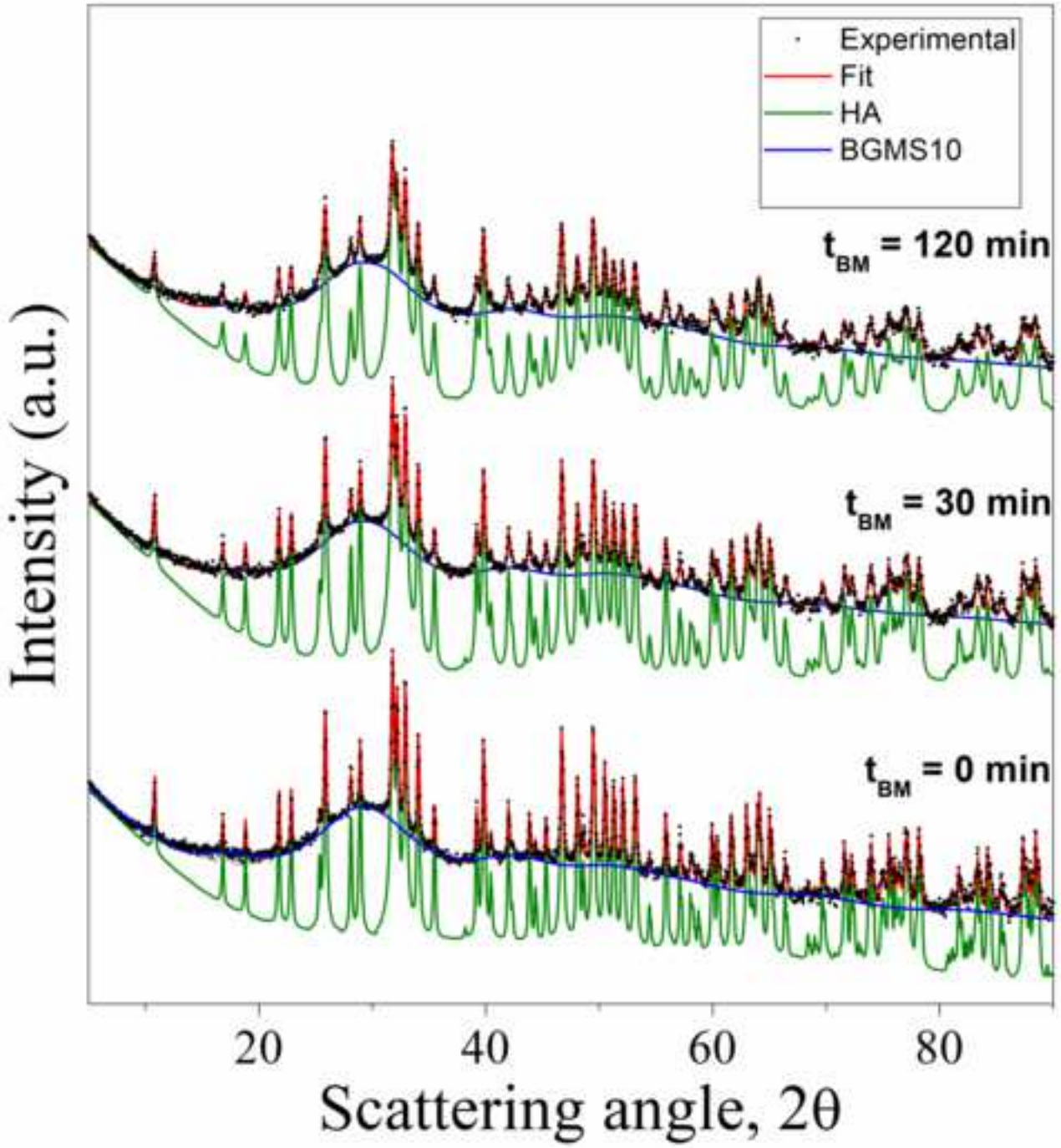

Figure 4

Click here to access/download;Figure;Figure 4.tif

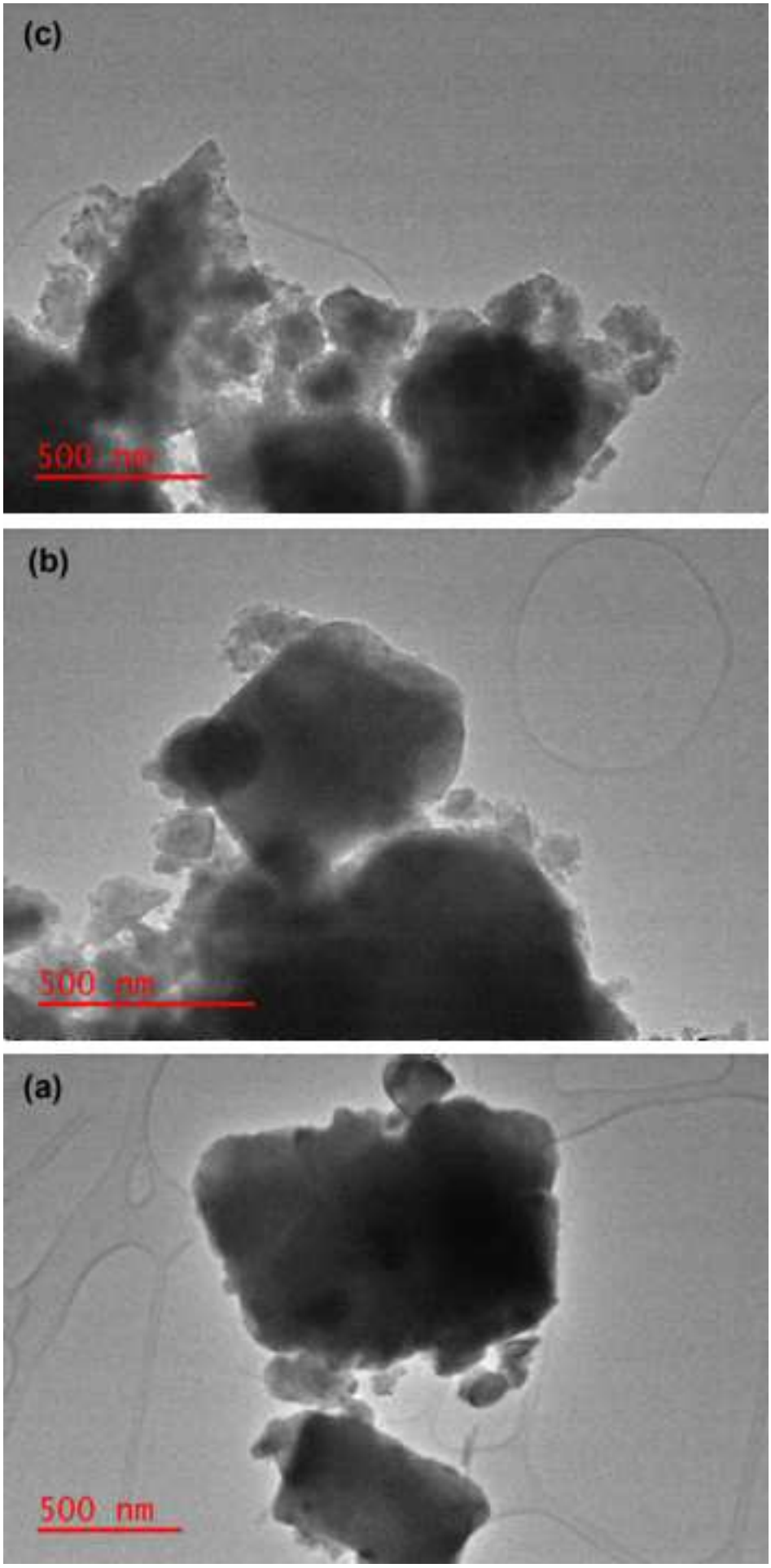

Figure 5a

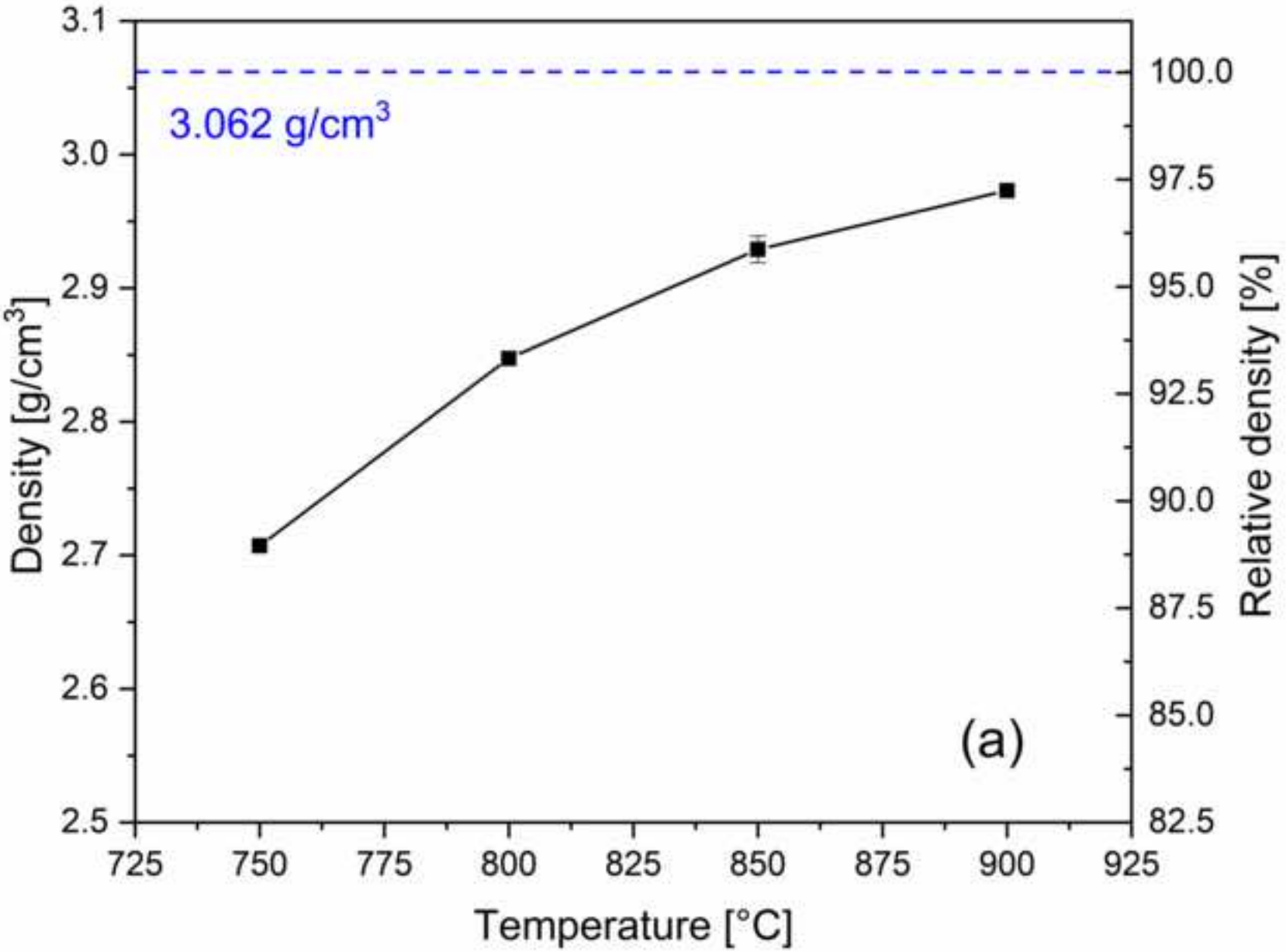

Figure 5b

Click here to access/download;Figure;Figure 5b.tif

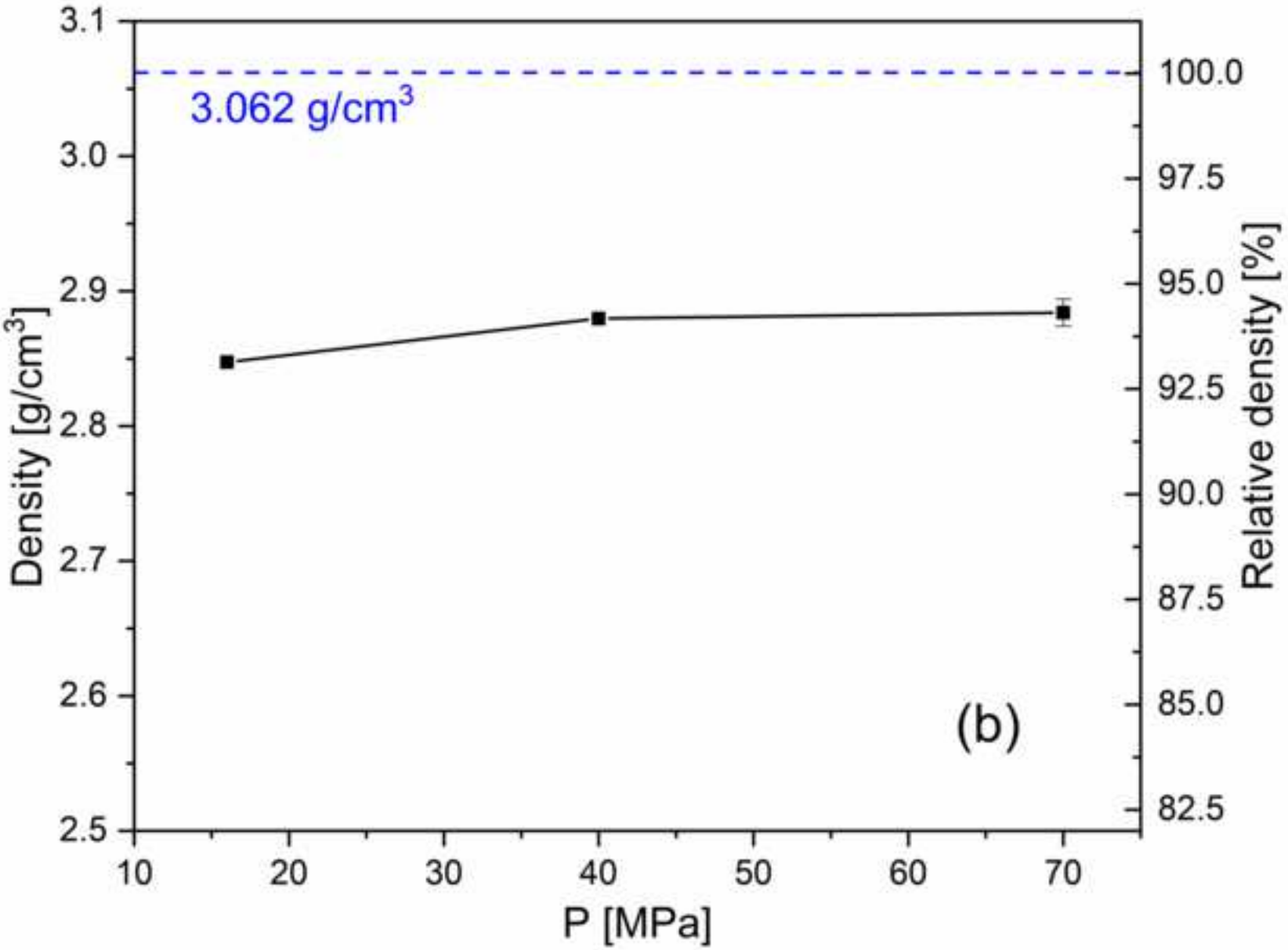

Figure 6

Click here to access/download;Figure;Figure 6.tif

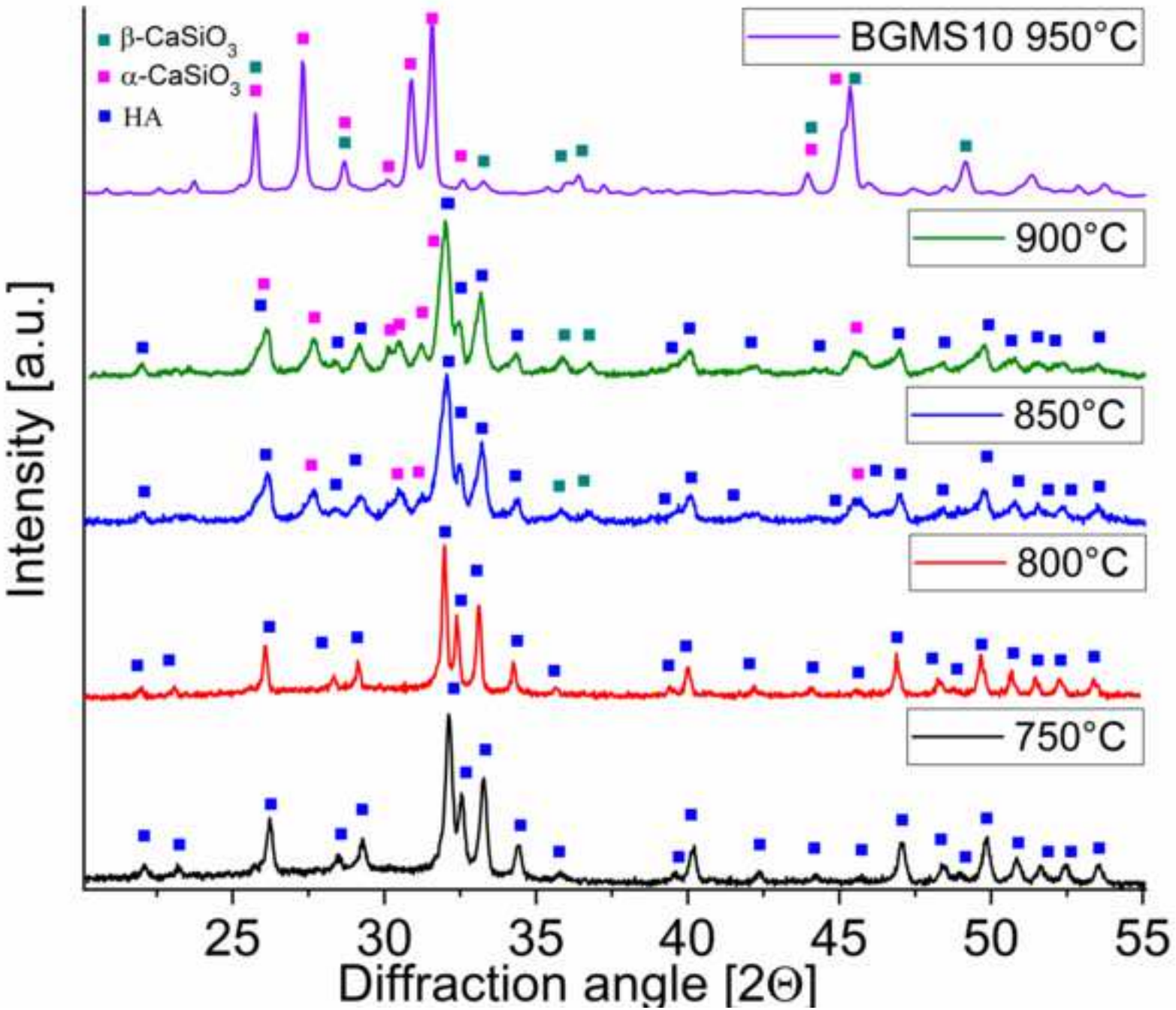

Figure 7

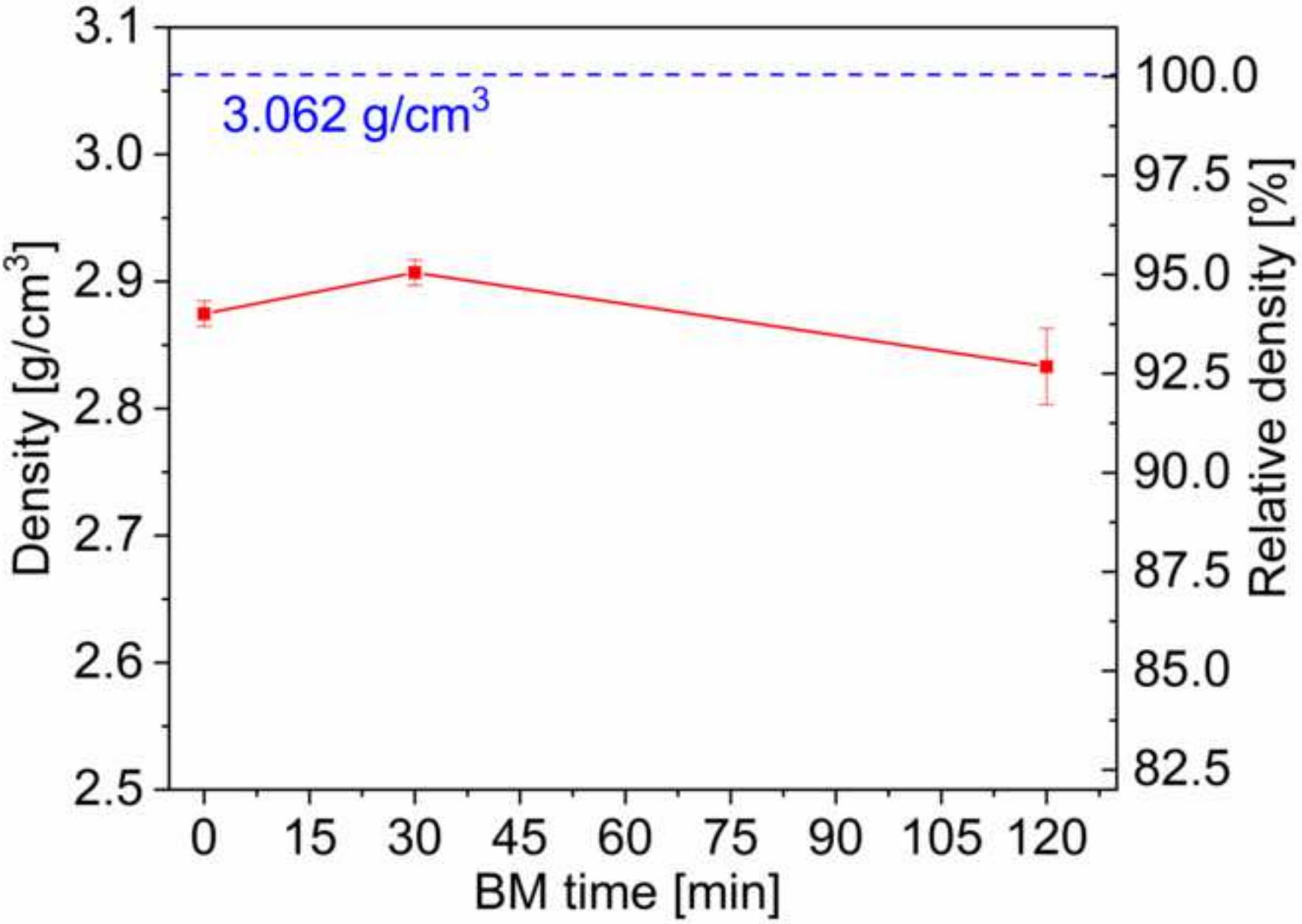

Figure 8

Click here to access/download;Figure;Figure 8.tif

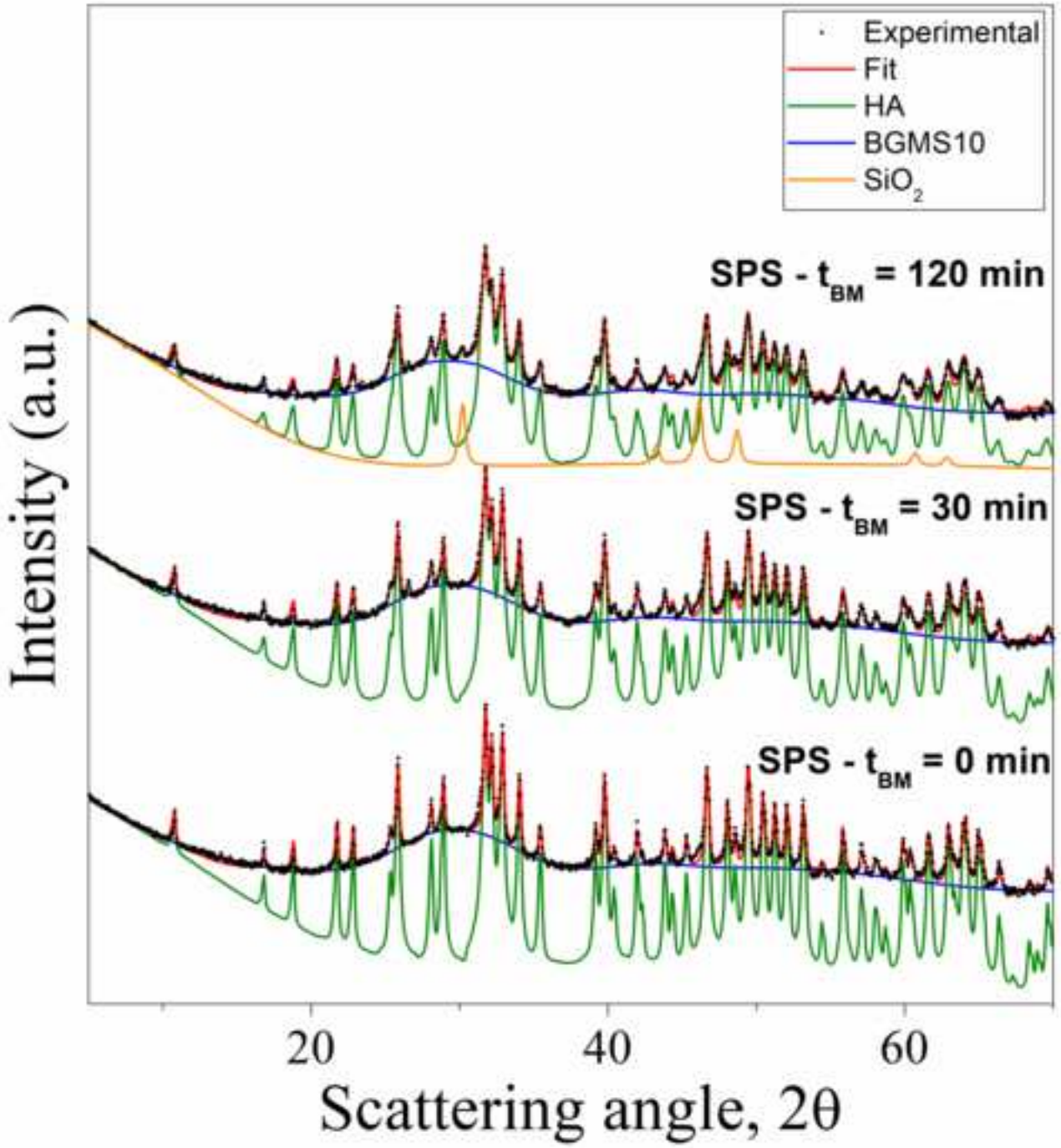

Figure 9

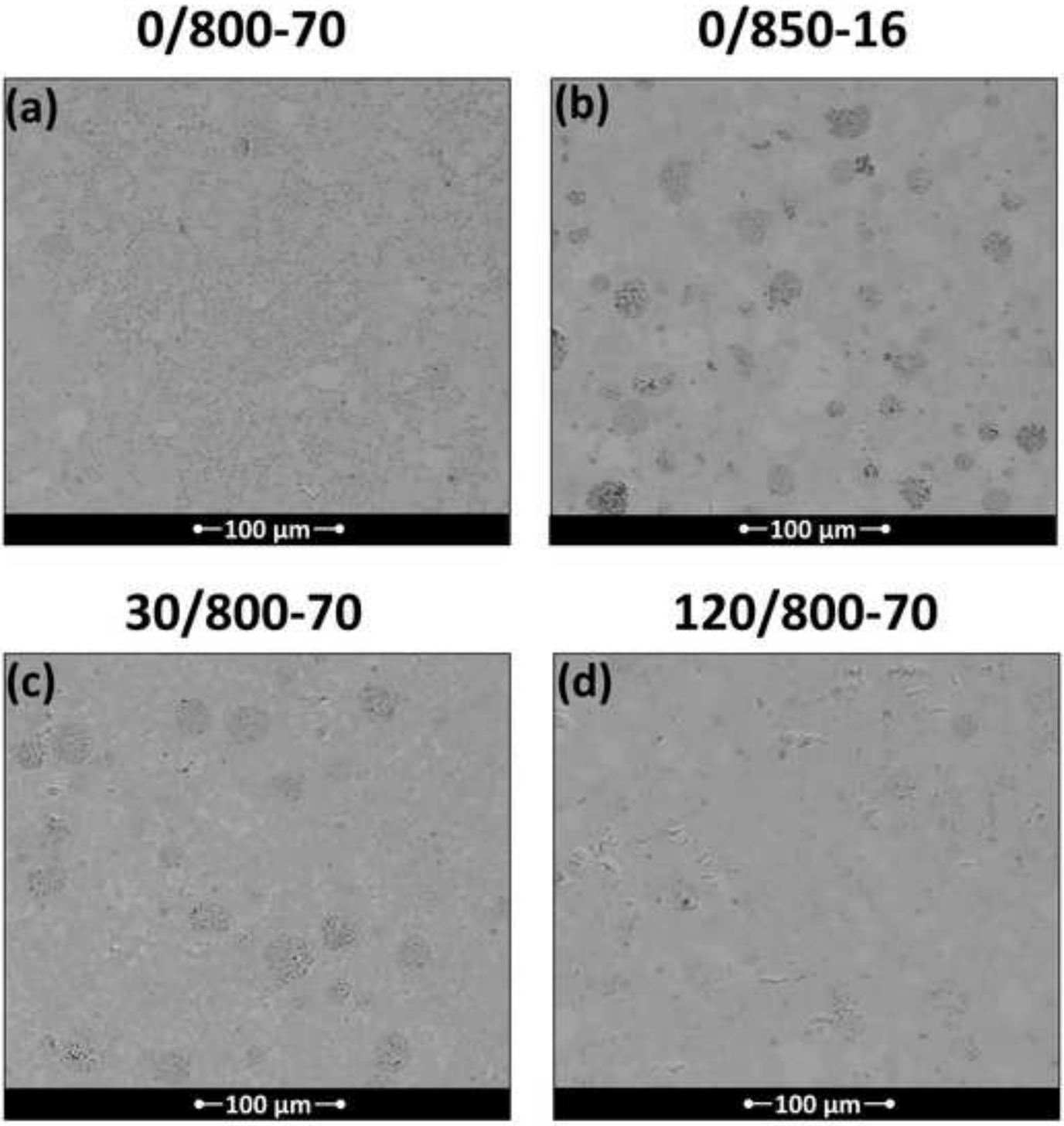

Figure 10

Click here to access/download;Figure;Figure 10.tif

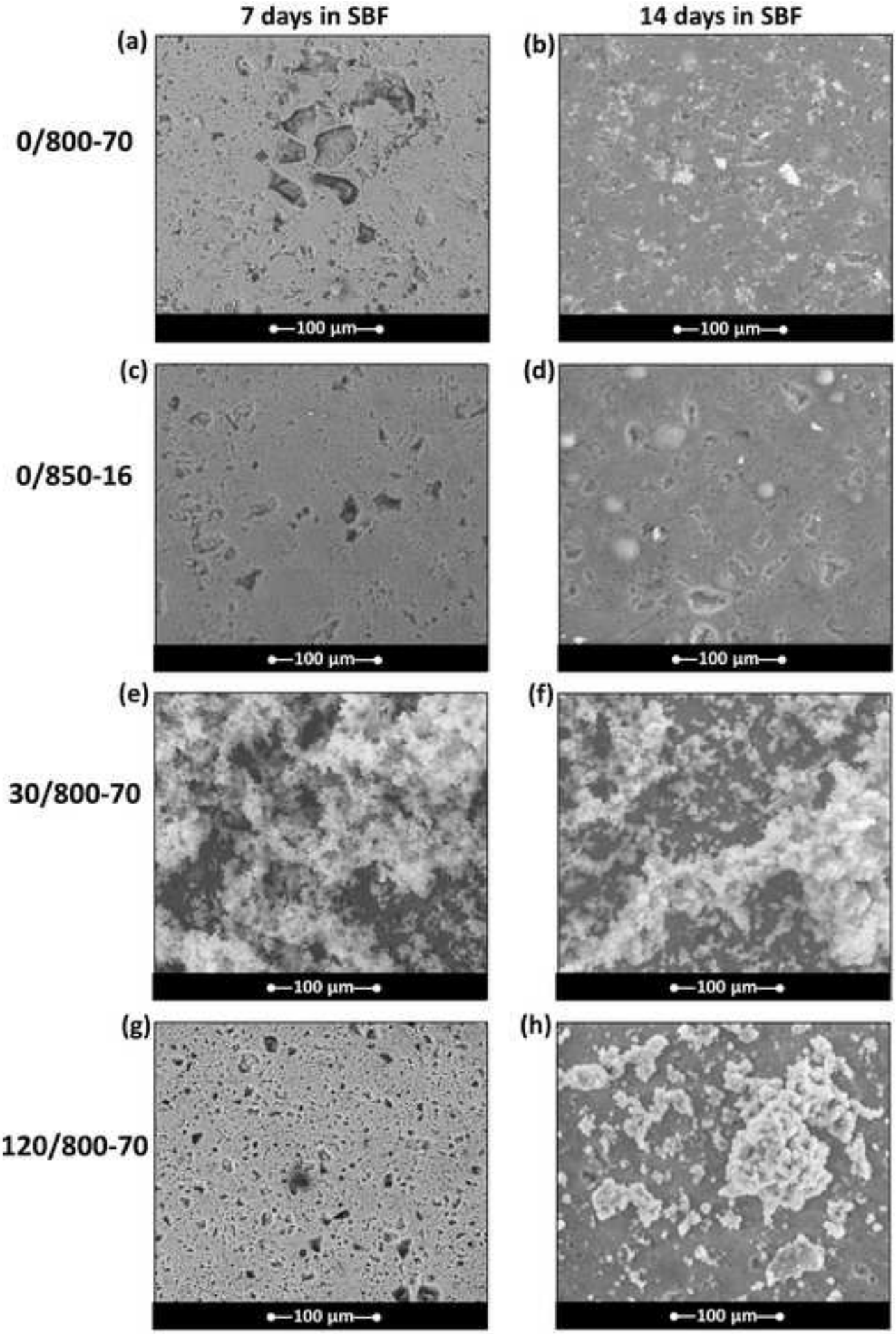

Figure 11

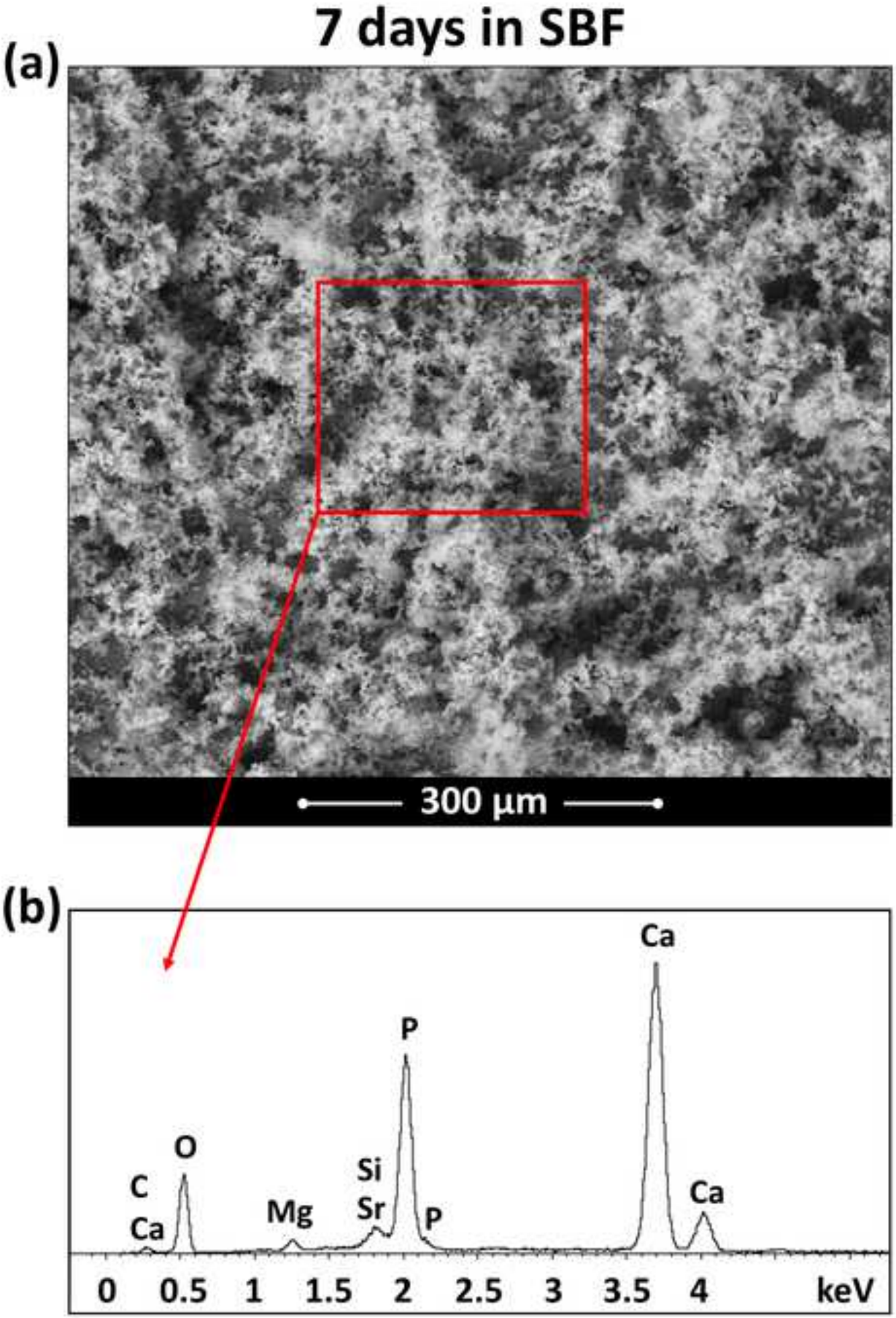

Figure 12

Click here to access/download;Figure;Figure 12.tif

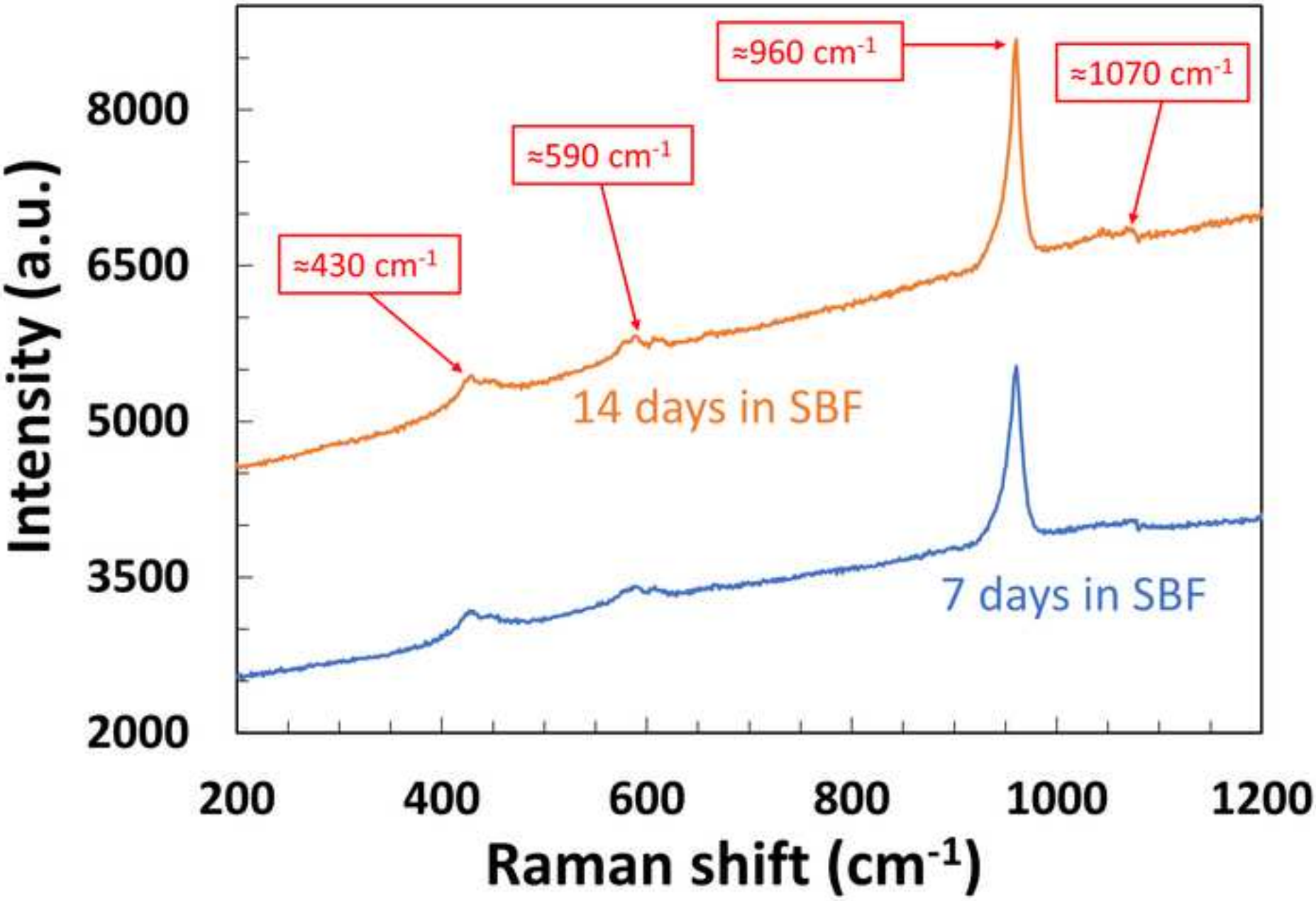

Supplementary Figure S1

Click here to access/download;Figure;Figure S1.TIF

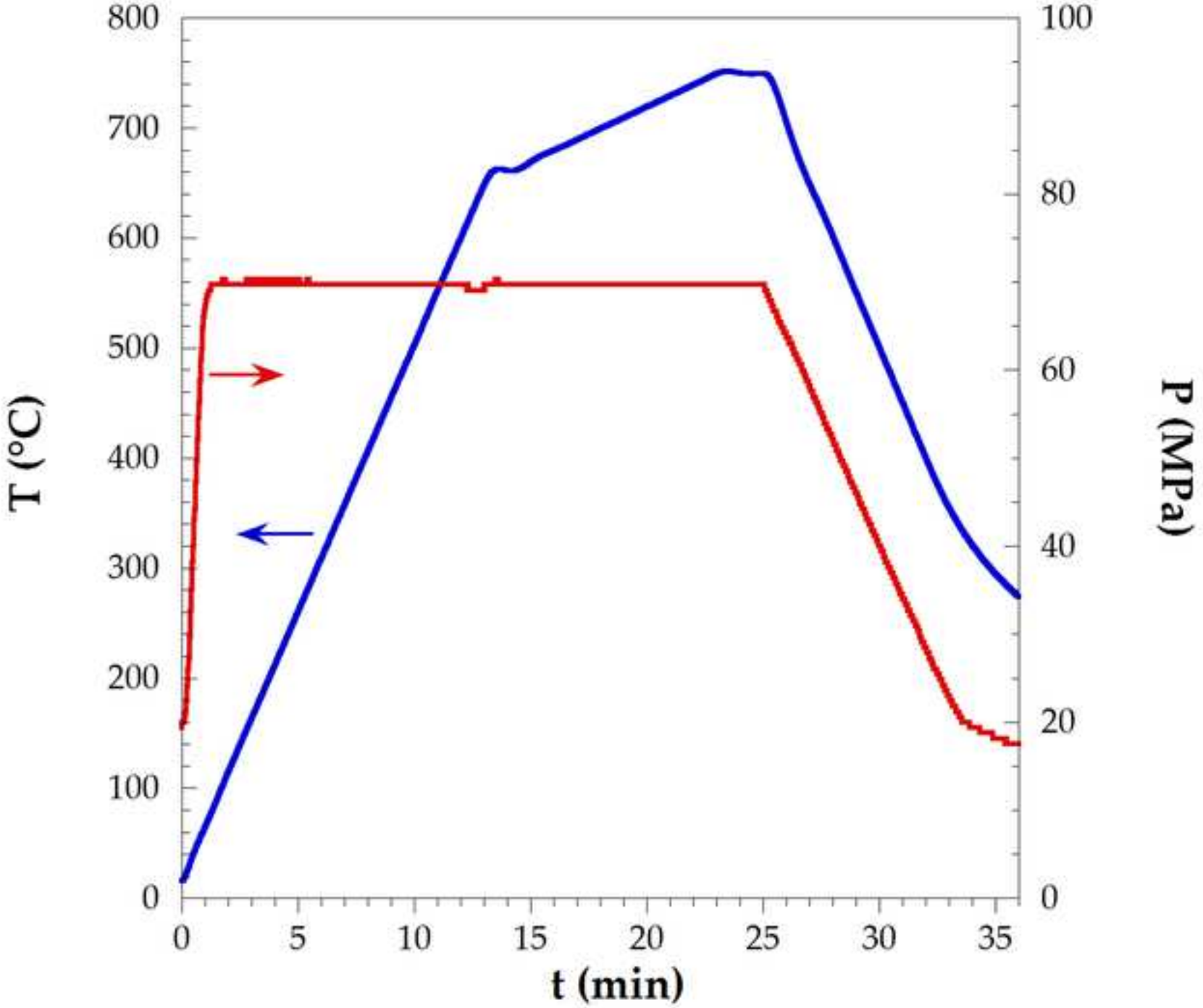

Supplementary Figure S2

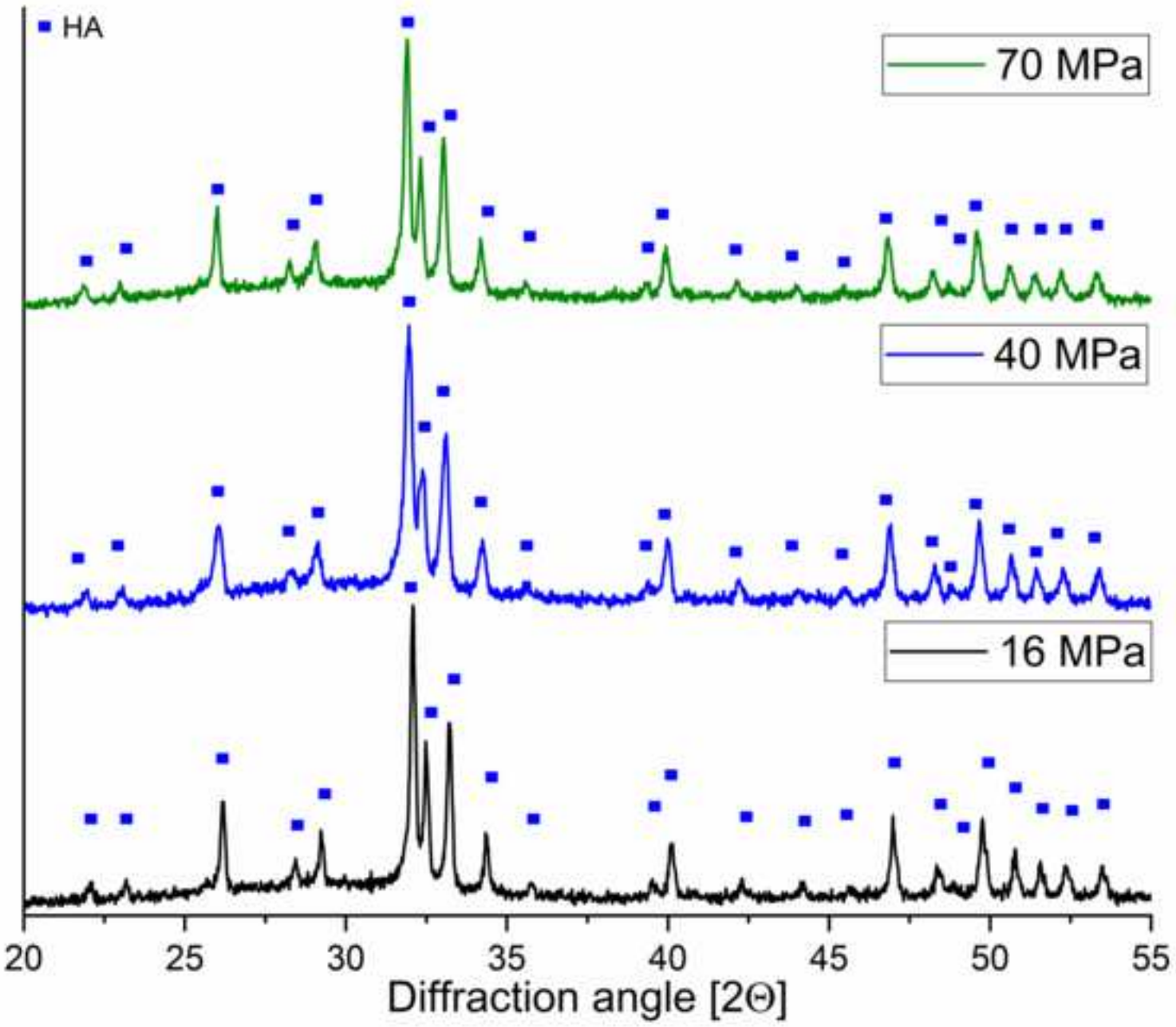

Supplementary Figure S3

Click here to access/download;Figure;Figure S3.tif

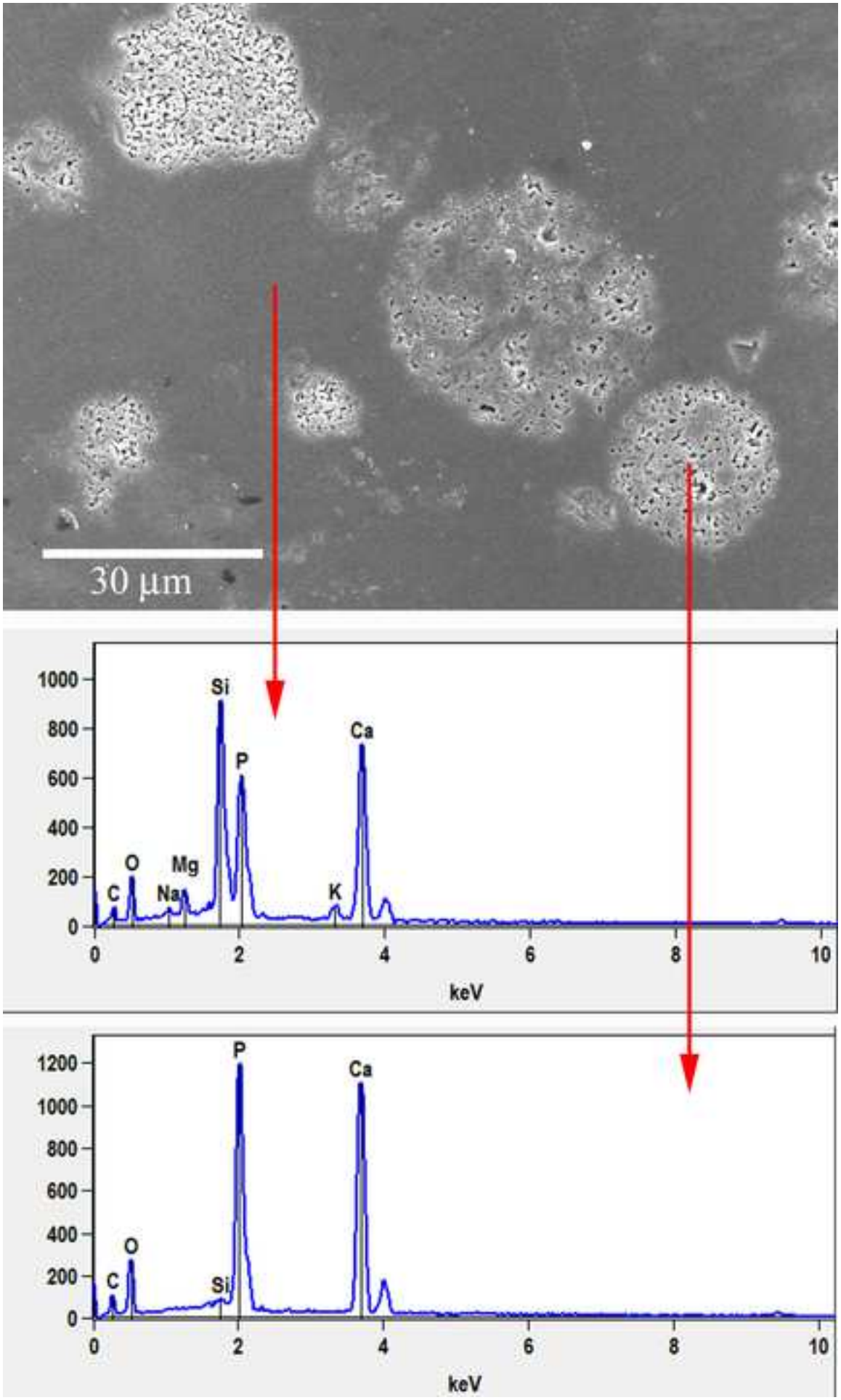

Captions for figures

Figure 1 Particles size distribution of unmilled (t_{BM} = 0 min) and milled HA-BGMS10 composite powders: cumulative (a) and differential (b) curves

Figure 2. N_2 physisorption isotherms of the (a) unmilled (t_{BM} = 0 min) sample and, milled for 30 (b) and 120 minutes (c) samples.

Figure 3. XRD patterns of unmilled (t_{BM} = 0 min) and milled HA-BGMS10 samples. Black dots are experimental data, and the red line is the calculated fit. Deconvoluted amorphous BGMS10 and hydroxyapatite phases are indicated by blue and green full line.

Figure 4. Representative TEM images at comparable magnifications of the (a) unmilled (t_{BM} = 0 min), (b) 30, and (c) 120 min milled powders.

Figure 5. Density of SPS products from unmilled (t_{BM} = 0 min) composite HA-BGMS10 powders as a function of (a) the holding temperature (P=16 MPa) and (b) the applied pressure (T_D=800°C).

Figure 6. XRD patterns of dense composite samples obtained at different temperatures by SPS from unmilled powders (t_{BM} = 0 min). The pattern corresponding to the sintered glass-ceramic product obtained at 950°C from pure BGMS10 **[40]** is also reported for comparison.

Figure 7. Effect of the milling time (t_{BM}) on the density of products obtained by SPS (T_D=800°C, P=70 MPa).

Figure 8. XRD patterns of dense composite samples obtained from the unmilled (t_{BM} = 0 min) and milled powders. Black dots are experimental data, and the red line is the calculated fit. Deconvoluted amorphous BGMS10, hydroxyapatite, and quartz (SiO_2) phases are indicated by blue, green, and orange full lines, respectively.

Figure 9. The surface of the sintered disks, showing an excellent densification.

Figure 10. SEM images of the sintered samples after soaking them in SBF for 7 and 14 days. It should be noted the marked HA precipitation on the 30/800-70 samples already after 7 days of immersion.

Figure 11. (a) HA formed on the 30/800-70 sample after 7 days in SBF and (b) results of the X-EDS analysis performed on the area shown in (a).

Figure 12. Raman spectra acquired on the calcium and phosphorus rich precipitates formed on the 30/800-70 samples after 7 and 14 days in SBF.

Declaration of interests

☒ The authors declare that they have no known competing financial interests or personal relationships that could have appeared to influence the work reported in this paper.

☐The authors declare the following financial interests/personal relationships which may be considered as potential competing interests: